

https://dspace.org/

Titanates and titania coated titanates as supports in the Fischer-Tropsch synthesis

Phadi, Thabiso Terence

2009-02-02T08:42:30Z
http://hdl.handle.net/10539/5989

Downloaded from a DSpace repository. https://dspace.org/

Titanates and titania coated titanates as supports in the Fischer-Tropsch synthesis

By

Thabiso Terence Phadi

Titanates and titania coated titanates as supports in the Fischer-Tropsch synthesis

By

Thabiso Terence Phadi

A dissertation submitted to the Faculty of Science at The University of the Witwatersrand, Johannesburg

In fulfillment of the requirements for the degree of

Masters of Science

Johannesburg, 2008

Declaration

I know the meaning of plagiarism and I declare that all the work in this dissertation is my own, unaided work. It is being submitted for the degree of Masters of Science in the University of the Witwatersrand, Johannesburg. It has not been submitted before for any degree or examination in any other body or organization or person outside the University of the Witwatersrand, Johannesburg.

(Signed) Thabiso Terence Phadi

-----------Day of ---------- 2008

Dedicated to my grandparents
ntate Maboya le nkgono Maboya

"The only time when success comes before work is in the dictionary."
"Nobody who ever gives his best regrets it." *E. M. Zondi*

In memory of my colleague and friend,

Mluleki Sitoza

My friend may your soul rest in eternal peace.

Acknowledgements

This thesis would not be complete if the people who contributed in making this work a success are not acknowledged. This science would not have been possible without the kind and unwavering support of you all. Thank you very much for the love and support.

Firstly, I fully acknowledge Centre of Excellence in Catalysis (*c**change), The University of the Witwatersrand, Bradlows Trust, THRIP and Sasol for all the financial assistance.

A big THANK YOU goes to Professor Neil Coville, my supervisor, for simplifying all the "horrible" aspects, the scientific input, all the bright ideas, teaching, and the proof reading of the insensible manuscripts of this thesis without making fun about them. Most importantly I would like to thank your hospitality, support and caring which was made available to me over the two years I spent with you. I thoroughly enjoyed working with you and loved the atmosphere in the group. I especially enjoyed the tone of our meetings which allowed me to express my views openly.

Basil Chassoulas "The intellect", without you I would not know the basics of FT. I enjoyed spending all those long stressing afternoons and evenings with you in Lab 113, while we were trying to overcome the reaction's thermal runaways (for more than 8 months without getting it right). However, you always came up with helpful suggestions. Most of all, the jokes that you always cracked kept me overcoming those *riotous* stress levels.

Big ups to the following four doctors; Lucky Sikhwivhilu, Itai Mabaso, Kalala Jalama, Munga Bahome, for defining all the principles behind this work.

CAT-OM-MAT group. Life in the department would be boring without you all.

Lebohang Petronella Mokoena, Zweli Mabaso, Taelo Kotsi, Lennox Masangane, Walter Ngobeni, you have always been very special in my life. I can't imagine life without you.

Gents, I'm proud to say that West Campus Village would have not been alive without all of you. The year 2007 was my best year ever at the University. Iyoooo!!! I would like to acknowledge all you clowns for that: Judges Modikwa, Winston Nxumalo, The late Mluleki Sitoza, Siyanda Mthembu, Robson Lokothwayo, Lindani Ngidi, Ofentse Gumede, Thabang Ntho and Nkosana Khumalo. Thato Sello I will also put you in this list for obvious reasons.

Finally, and most importantly I would like to thank my family, Aus Mapule, Abuti Freddy, Cynthia and Ian. You have always been my pillar of strength, you have shared my tears when tough times stroke, you have given me your full support and above all you have always put your trust in me. Without doubt, life for me would have been meaningless without all of you in my life. I wholeheartedly love you all. Thank you so very much for everything…….……..."*Mom I made it*"

Publications and Poster presentations arising from this work

Publications

- Titanates and titania coated titanates as supports for catalysts used in Fischer-Tropsch synthesis (To be published)

Poster presentations

- The effect of metal-support interactions on the catalytic activity and selectivity in the Fischer-Tropsch synthesis, CATSA conference, *Mossel Bay*, (2006)

- Titania coated potassium titanates as supports for catalysts used in Fischer-Tropsch synthesis, CATSA conference, *Richards Bay*, (2007)

Abstract

A titanate nanotube (TNT) material with a high surface area of 231 m^2/g was prepared by reacting TiO_2 with KOH in an autoclave for 24 hours. This surface area was about five times higher than that of the commercial TiO_2 nanoparticles (TN) (or P25 Degussa) with a BET surface area of 47 m^2/g. TEM images revealed that the TNT material consisted of clean tubular materials made up of coiled TiO_2 sheets. The diameters of the tubes ranged from tens to hundreds of nanometers, while the lengths of these tubes varied from 60 to about 200 nm. Prolonged washing of this TNT material for about 3 weeks with deionised water was required to obtain pure tubular materials.

Cobalt catalysts with loadings of 10 and 20% were prepared by impregnating a cobalt nitrate solution onto the TNT support using a pH controlled precipitation methodology. A range of techniques was used to characterize these catalysts and their catalytic performance was investigated in a plug flow reactor in the Fischer-Tropsch (FT) synthesis at 230, 250 and 280 ^oC with a syn-gas ($H_2/CO = 2$) flowrate of 12 ml/min under a total pressure of 8 bar. The obtained FT results were compared with those obtained for cobalt loaded on TN. A low CO conversion of 2.2% was achieved when 10%Co/TNT was used at 230 ^oC while a higher CO conversion of 22.4% was achieved when 10%Co/TN was used at the same temperature. The reason for the low FT activity obtained with the tubular TNT based catalyst was partly due to the presence of potassium ions which poisoned cobalt active sites. TPR studies also revealed that it was more difficult to reduce 10%Co/TNT than it was for 10%Co/TN since its cobalt reduction peaks occurred at temperatures higher than those for the TN based catalysts.

A titania coated titanate nanotube (TC-TNT) material was prepared by a sol-gel method so that a titania "protective" layer was created over the potassium TNT surface. This material was achieved by dispersing a TNT material in the solution of $Ti[O(CH_2)_3CH_3]_4$. The ratio of TNT to $Ti[O(CH_2)_3CH_3]_4$ was 1:5 and the reaction was hydrolyzed with HNO_3. The surface area for this material was measured as 222 m^2/g when the sol-gel preparation solution was heated at 35 ^oC. TEM revealed that the preparation of TC-TNT was successful and this was confirmed by the appearance of a TiO_2 coating and the

formation of small black particles representing the sol-gel derived TiO_2 on the surface of the TNT. The evaluation of 10%Co/TC-TNT in the FT reaction at 230 ^{o}C improved the CO conversion to 9.4%. However, this conversion was still lower than that obtained for 10%Co/TN. This low conversion was due to the formation of SMSI between cobalt and the TC-TNT support.

Contents

Dedications ..... **i**

Acknowledgements ..... **iii**

Publications and poster presentations arising from this work ..... **iv**

Abstract ..... **v**

Contents ..... **vii**

List of Figures ..... **x**

List of Tables ..... **xiii**

Nomenclature ..... **xv**

Dissertation synopsis ..... **xvii**

1. Literature Overview *1*

1.1 History and background **1**

1.2 The Fischer-Tropsch synthesis **5**

1.3 The Fischer-Tropsch reaction **7**

1.3.1 Other reactions taking place 7

1.4 Fischer-Tropsch product spectrum **8**

1.5 Factors influencing product selectivity **10**

1.5.1 Operating conditions 10

1.6 Fischer-Tropsch reactors **11**

1.7 Catalysts for Fischer-Tropsch synthesis **13**

1.7.1 Active metals 13

1.7.2 Catalyst supports and promoters 15

1.7.3 Catalyst activation and deactivation 17

1.8 Synthesis of Fischer-Tropsch catalysts **19**

1.8.1 Incipient wetness impregnation method 20

1.8.2 pH-controlled precipitation method 21

1.9 Novel routes to the preparation of Fischer-Tropsch supports **22**

1.9.1 Titanate nanotubes 22

1.9.2 Sol-gel and titania coating....25
1.10 References....27

2. Scope of this work....32
2.1 Summary of the main aims of the study:....33
2.2 References....35

3. Experimental Methods....36
3.1 Introduction....36
3.2 Preparation of catalyst and support materials....37
3.2.1 Preparation of titania nanoparticles support....37
3.2.2 Preparation of titanate nanotubes support....37
3.2.3 Preparation of titania coated titanate nanotubes support....38
3.2.4 Catalyzed preparation of 10%Co/support by a pH-controlled precipitation method....40
3.2.5 Catalyzed preparation of 20%Co/supports by an incipient wetness impregnation method....41
3.3 Characterization of catalysts and supports....41
3.3.1 Brunauer-Emmett-Teller method (BET)....42
3.3.2 Thermogravimetric analysis (TGA)....42
3.3.3 Transmission Electron Microscopy (TEM)....42
3.3.4 X-ray diffraction spectroscopy (XRD)....42
3.3.5 X-ray Fluorescence (XRF) spectroscopy....43
3.3.6 Temperature-Programmed Reduction (TPR)....43
3.3.7 H_2 chemisorption and O_2 titration analysis....43
3.4 Fischer-Tropsch Synthesis experiments....47
3.4.1 Reactor system and experimental setup....47
3.4.2 Reactor and catalyst packing....49
3.4.3 Experimental procedure for catalyst evaluations....51
3.5 Product analysis....51
3.5.1 Gas chromatographic analysis....51
3.5.2 Data work-up....53
3.6 References....58
4. Results and discussion....58
4.1 Characterization of support materials....58

4.1.1 TEM analysis of support materials....58
4.1.2 Porosity and surface area analysis of support materials....61
4.1.3 A thermal analysis of support materials using TPR and TGA....63
4.1.4 XRD analysis of support materials....64
4.2 Catalyst characterization....66
4.2.1 Porosity and surface area analysis of catalyst....66
4.2.2 Metal loading by XRF spectroscopy....67
4.2.3 XRD analysis of catalysts....68
4.2.4 A thermal analysis of catalysts using TPR and TGA....70
4.2.5 Chemisorption analysis for catalysts....74
4.3 Reactor studies for catalyst evaluation....76
4.3.1 FTS for 10% cobalt loaded catalysts....76
4.3.2 FTS for 20% cobalt loaded catalysts....81
4.3.3 Schulz-Flory distribution on the cobalt loaded catalysts....85
4.3.4 Comparison of catalyst activities at *iso*-conversions....88
4.4 References....92

5. Conclusions and Recommendations....94

List of Figures

Chapter 1

Figure 1.1 Simple FT stepwise growth process (where ≷ = surface).....6

Figure 1.2 FTS product distributions by Anderson-Schulz-Flory model 9

Figure 1.3 Deactivation mechanisms: (A) coke formation, (B) poisoning, (C) sintering of active metal particles and (D) sintering and solid-solid phase transitions and encapsulation of active metal particles [45] 18

Figure 1.4 Schematic representation of experimental set up for incipient wetness impregnation [1].....21

Figure 1.5 Schematic representation of (a) the formation pathway of titanate nanotubes [80], (b) the structure of the titanate nanotube and (c) the three-dimentional drawing of a titanate nanotube [81] 24

Figure 1.6 Postulated mechanism for the sol-gel polymerization of $Ti(O^iPr)_4$ using an organogel as a template: (a) gelator, (b) gelation, (c) sol-gel polymerization of TEOS and adsorption onto the gelator, (d) hollow helical-ribbon (upper) and hollow double-layered nanotube (low) of the TiO_2 formed after calcinations [90].....26

Chapter 2

Figure 2.1 A diagrammatic representation of (a) TiO_2 nanoparticles (TN), (b) Co/TN, (c) Titanate nanotubes (TNT), (d) Co/TNT, (e) Titania coated titanate nanotubes (TC-TNT) and (f) Co/TC-TNT 34

Chapter 3

Figure 3.1 Flow chart of the preparation of titania coated titanate nanotubes by sol-gel method...39

Figure 3.2 A schematic representation of the set up for the preparation of coated titanate nanotubes by the sol-gel method 40

Figure 3.3 A schematic diagram for the reactor system 48

Figure 3.4 A diagrammatic representation (top) and a digital image (bottom) of a stainless-steel fixed bed reactor that has been used 50

Figure 3.5 A typical FT spectrum for gaseous products obtained from an FID GC.....53

Chapter 4

Figure 4.1 Low resolution TEM micrographs of titania nanoparticles (TN).....59

Figure 4.2 Low resolution TEM micrographs of tinanate nanotubes (TNT) and titania coated titanate nanotubes (TC-TNT) prepared by different methodologies 60

Figure 4.3 Low resolution TEM micrograph of titania coated titanate nanotubes (TC-TNT) (The dashed circles show that the sol-gel derived TiO_2 particle sizes are not uniform) 61

Figure 4.4 TPR profiles of calcined TN, uncalcined TNT and uncalcined TC-TNT support materials 63

Figure 4.5 TGA plots of calcined and uncalcined TC-TNT support 64

Figure 4.6 Powder XRD patterns of calcined support materials (TN, TNT and TC-TNT), where A = anatase phase and R = rutile phase 65

Figure 4.7 XRD patterns of calcined unsupported Co_3O_4 and 10% cobalt loaded catalysts, where * = Co_3O_4 phase.....68

Figure 4.8 XRD patterns of calcined unsupported Co_3O_4, 20%Co/TN and 20%Co/TNT, where * = Co_3O_4 phase.....70

Figure 4.9 TPR of calcined unsupported cobalt oxide precursor.....71

Figure 4.10 TPR profiles of calcined 10% cobalt loaded catalysts 72

Figure 4.11 TPR of calcined 20% cobalt loaded catalysts 72

Figure 4.12 TGA plots of calcined and uncalcined 10%Co/TC-TNT catalyst sample 74

Figure 4.13 Effect of temperature on CO conversion in the Fischer-Tropsch synthesis as a function of time on stream for 10%Co/TN.....77

Figure 4.14 Effect of temperature on CO conversion in the Fischer-Tropsch synthesis as a function of time on stream for 10%Co/TNT 78

Figure 4.15 Effect of temperature on CO conversion in the Fischer-Tropsch synthesis as a function of time on stream for 10%Co/TC-TNT.....78

Figure 4.16 Effect of temperature in %CO conversion in the Fischer-Tropsch synthesis as a function of time on stream for 20%Co/TN.....82

Figure 4.17 Effect of temperature in CO conversion in the Fischer-Tropsch synthesis as a function of time on stream for 20%Co/TNT 82

Figure 4.18 Effect of temperature in CO conversion in the Fischer-Tropsch synthesis as a function of time on stream for 20%Co/TCNT.....83

Figure 4.19 Typical overall hydrocarbon distribution on (a) 10%Co/TN, (b) 20%Co/TN, (c) 10%Co/TNT, (d) 20%Co/TNT, (e) 10%Co/TC-TNT and (f) 20%Co/TC-TNT catalysts 87

List of Tables

Chapter 1

Table 1.1 Summary of dominant plants that produced liquid products by FTS since the early 1950s....3
Table 1.2 An overview of Fischer-Tropsch reactor developments....12
Table 1.3 Comparison of reactor types - 1980 [26]....13
Table 1.4 Temperature values of metals that are relevant for FTS and support material similar to those used in this work [47, 48]....19

Chapter 3

Table 3.1 The effect of washing by monitoring pH, conductivity and the surface area....38
Table 3.2 H_2 analysis and O_2 titration conditions for cobalt containing catalysts....45
Table 3.3 A dialog program used in TCD and FID analysis....48
Table 3.4 Conditions for gas chromatographic analyses....52

Chapter 4

Table 4.1 Porosity measurements of support materials....62
Table 4.2 XRD data of the most intense planes for the calcined support materials (TN, TNT and TC-TNT)....66
Table 4.3 Porosity measurements of catalysts....66
Table 4.4 XRF analysis for the %Co loading on support materials....67
Table 4.5 XRD data of the most intense planes for calcined unsupported Co_3O_4 and 10% cobalt loaded catalysts....69
Table 4.6 XRD data of the most intense planes for calcined unsupported Co_3O_4, 20%Co/TN and 20%Co/TNT....70
Table 4.7 H_2-Chemisorption results for all calcined catalysts....75
Table 4.8 FTS data for the catalytic performance of 10%Co/TN catalyst....79
Table 4.9 FTS data for the catalytic performance of 10%Co/TNT catalyst....80
Table 4.10 FTS data for the catalytic performance of 10%Co/TC-TNT catalyst....80

Table 4.11 FTS data for the catalytic performance of 20%Co/TN catalyst.....84

Table 4.12 FTS data for the catalytic performance of 20%Co/TNT catalyst 84

Table 4.13 FTS data for the catalytic performance of 20%Co/TC-TNT catalyst.....85

Table 4.14 Comparison of product selectivity data for Co/TN and Co/TNT at iso-conversion.....88

Table 4.15 Comparison of product selectivity data for Co/TNT and Co/TC-TNT at iso-conversion.....89

Table 4.16 Comparison of product selectivity data for Co/TN and Co/TC-TNT at iso-conversion 90

Nomenclature

Abbreviation	Description
ASF	Anderson-Schulz-Flory
BASF	Badische Anilin und Soda Fabrik
BET	Brunauer-Emmett-Teller
CFB	Circulating-fludized-bed
CH_4	Methane/Natural gas
%Conv.	Percentage conversion
d_p	Crystallite diameters
D%	Percentage dispersion
FBR	Fixed bed reactor
FID	Flame Ionization Detector
FT	Fischer-Tropsch
FTS	Fischer-Tropsch synthesis
GC	Gas Chromatography
GTL	Gas-to-liquid
HTFT	High Temperature Fischer-Tropsch synthesis
HNO_3	Nitric Acid
h	Hours
$ID_{reactor}$	Internal diameter of a reactor
KOH	Potassium hydroxide
LTFT	Low Temperature Fischer-Tropsch synthesis
UHP	Ultra high pressure
N_s	Number of active metal sites
NTP	Normal Temperature and Pressure
r_{FTS}	Rate of Fischer-Tropsch Synthesis reaction
r_{WGS}	Rate of water gas shift reaction
TEM	Transmission Electron Microscope
TCD	Thermal Conductivity Detector
TC-TNT	Titania coated titanate nanotubes
$TC\text{-}TNT_{35^oC}$	Titania coated titanate nanotubes prepared at 35oC
TGA	Therogravimetric Analysis
$Ti[O(CH_2)_3CH_3]_4$	Titanium (IV) butoxide
TN	Titania nanomaterials
TNT	Titanate nanotubes
TOF	Turnover frequency
TOS	Time on stream

TPR	Temperature Programmed Reduction
SA	Surface Area
SAS	Sasol Advanced Synthol
S_i	Selectivity of species i
SMDS	Shell Middle Distillate Synthesis
SMSI	Strong Metal Support Interactions
Syn-gas	Synthesis gas
WGS	Water gas shift
wt/wt	Weight by weight
XRF	Xray-Fluorescence
XRD	X-Ray Diffraction

Dissertation synopsis

The Fischer-Tropsch synthesis is a reaction which entails the conversion of synthesis gas (H_2 and CO mixture) into liquid hydrocarbons. This reaction was first carried out in the early 20th century. The synthesis gas mixture can be obtained either from coal, biomass, natural gas and even from organic wastes. Subsequently work in the literature revealed that both cobalt and iron catalysts were excellent for the production of higher hydrocarbons. However these metals have different characteristics. In this thesis a study of cobalt-based catalysts was undertaken.

To ensure that the active metal maintains stability a catalyst support is normally required as a metal carrier. The active metal particles (i.e. cobalt or iron) are then dispersed on the support and stable catalysts particles are achieved. If the highest possible amount of metal atoms is aimed to be exposed to gaseous reactants during Fischer-Tropsch synthesis, then the metal catalyst must be deposited on a high-surface area support to obtain a high metal dispersion. When this high dispersion is achieved an improvement of the catalyst activity can be achieved due to an improved amount of active metal sites.

In this study the preparation of a novel high surface-area titanate nanotube (TNT) support was produced by treating titania (TiO_2) with a base (i.e. KOH). The preparation of a high surface-area titania coated titanate nanotube (TCNT) support was prepared by addition of a sol-gel derived titania made by hydrolyzing titanium butoxide, $Ti[O(CH_2)_3CH_3]_4$ in the presence of titanate nanotubes (TNT). Cobalt particles were impregnated onto each of these supports using a pH controlled methodology.

Preparation of this high surface area TNT support and catalysts was achieved. When these high surface area TNT-based catalysts were evaluated for activity during the Fischer-Tropsch synthesis they did not form a better support for cobalt than their "low" surface area TiO_2 counterparts. The reason for this poor catalytic activity exhibited by this material might be due to the presence of the potassium ions in the TNT sample. When the TNT supports were coated with the sol-gel derived TiO_2 to form the TCNT support for cobalt in the Fischer-Tropsch synthesis the activity improved, but the improved activity was still lower than that obtained when "low" surface area TiO_2 was

used as a support. This was due to the strong-metal-support-interactions (SMSI) which occurred in this catalyst. These species were more difficult to reduce.

Chapter 1

1. Literature Overview

1.1 History and background

A reaction which entails the conversion of synthesis gas or syn-gas (H_2 and CO mixture) to liquid hydrocarbon fuels is known as the Fischer-Tropsch synthesis (FTS). This syn-gas mixture is obtained from natural gas (CH_4), coal, petroleum, biomass or even from organic wastes. The first FTS experiments were carried out at the beginning of the 20th century [1]. It was in 1902 that Sabatier and Senderens discovered that methane could be synthesised from a mixture of CO and H_2 over nickel or cobalt catalysts at atmospheric pressure [2]. In 1913 Badische Anilin und Soda Fabrik (BASF) reported the production of liquid products by using cobalt catalysts [3]. A decade later, in 1923, after a patent from BASF, Hans Fischer and Franz Tropsch proposed the Synthol process, which gave a mixture of aliphatic oxygenated compounds through the reaction of CO with H_2 over iron chips at 400 ^{o}C under high pressures, of 10 to 15 MPa [4]. This product was transformed into a mixture of hydrocarbons after heating under pressure and this mixture was known as “Synthine”.

In 1936 Pichler made an important discovery that when the syn-gas pressure was increased from atmospheric to 15 bar the life of an iron catalyst was markedly improved. It was also discovered that even at lower pressures (≈7 bar) hydrocarbons could be produced, but it was found that the iron catalysts deactivated rapidly at this pressure. A lot of work was then focused on the use of nickel and cobalt as catalysts at low pressures, but nickel too had to be discarded due to its high tendency to produce methane and also

because its activity deteriorated due to loss of nickel from the reactor in the form of $Ni(CO)_4$ [5]. Ruthenium has also been found to be capable of achieving the required activity for a commercial Fischer-Tropsch (FT) application, but unfortunately it is more costly and the amount of ruthenium that is available on earth is insufficient for large scale application [6]. Subsequently, early work in the literature revealed that both cobalt and iron catalysts were excellent for the production of higher hydrocarbons. It is now generally accepted that most group 8-10 metals have measurable CO hydrogenation activity with the distinguishing factor being the product distribution [7, 8]. Iron catalysts have advantages over cobalt catalysts in the conversion of coal or biomass to liquid fuels because of their low cost, low methane selectivity, flexible product slate and robustness in converting coal- or biomass-derived syn-gas at a low H_2/CO ratio [9]. However, in general cobalt catalysts are more active, more stable and a better match for converting natural gas-derived syn-gas to hydrocarbon liquids.

All FT plants built in Germany during World War II employed a cobalt based catalyst in fixed-bed reactors. In the 1950s USA scientists attempted to employ fluidized-bed reactors to convert syn-gas from natural gas into petrol, but they were largely unsuccessful. In 1951 five offers were received by Sasol for the design and expansion of a coal-to-oil plant they wished to commission. Sasol decided to take two of the offers; one from M.W. Kellogg relating to the design of a circulating fluidized-bed (CFB) reactor and one from Arbeit-Gemeinschaft Lurgie and Ruhrchemie relating to construction of Arge fixed-bed reactors. In 1955 the first commercial FT plant, Sasol I, was commissioned in South Africa (Sasolburg) and the driving force for this plant was the large coal reserves in South Africa and the need to reduce the country's dependence on imported oil. This proved to be successful and the result was that South Africa managed to reduce its imports from about 100% of crude to about 50%. Today Sasol operates at a profit without government support and it appears that it maintain a larger staff than other international companies of a similar size [10].

Since the 1960s other plants and developments in FT have been made (Table 1.1). In 1980 and 1982, the Sasol II and Sasol III plants were conceived in Secunda, South Africa. These plants used entrained CFB reactors and produced mainly gasoline and

diesel fuels. Hydrocarbon selectivities of up to 70% C_5-C_{10} olefin and up to 60% olefin selectivity for C_{11}-C_{18} hydrocarbons were achieved at these plants. These plants were later scaled up to what is known today as the commercial Sasol Advanced Synthol (SAS) reactor plants with a capacity of 11 000 bbl/day (barrels per day). Since then and particularly in the early 1990's Sasol has replaced their sixteen CFB reactors with eight SAS reactors and four of these have capacities of 20 000 bbl/day. A summary of these (and future) developments is given in Table 1.1.

Table 1.1 Summary of dominant plants that produced liquid products by FTS since the early 1950s

Year	Company	Production /barrels per day
1955	Sasol I	500
1980	Sasol II	11 000 (later 20 000)
1982	Sasol III	11 000 (later 20 000)
1989	Shell	12 500
1993	PetroSA	14 000
1990's	BP	70
1990's	Conoco-Phillips	400
1994	Exxon Mobil	200
2006	Oryx	34 000
2009	Oryx-Chevron	100 000
2015	Oryx-Chevron	450 000

In June 1992 the onshore plant construction of the Mossgas (currently known as PetroSA) facility in South Africa was completed and went into full production in January 1993. This plant utilized Sasol's CFB reactor technology and was constructed with three 14 000 bbl/day reactors. Unlike Sasol, PetroSA uses natural gas as its feedstock. Even though PetroSA experienced problems with natural gas supply and shutdowns due to an explosion and corrosion in the reformers, they have been operating for more than 10 years at near capacity levels with an on stream factor above 90%. Currently they are joining with Statoil to operate a 1000 bbl/day slurry bubble column reactor at their gas-to-liquid (GTL) plant.

Shell started designing a 12 500 bbl/day plant in 1989 at Malaysia using the so-called Shell Middle Distillate Synthesis (SMDS). The facility started operating in 1993. It was only at the end of 1996 that Shell reported they could produce 98% capacity in their operation for sale to the market. Shell has since divulged little specific information about the details of their fixed-bed FTS unit as it is operated in the SMDS process. In 2000 the SMDS plant improved their cobalt based catalysts and their capacity increased by 25%.

Other companies that were linked to the construction of FT pilot plants in the 1990's era include Exxon (now Exxon Mobil), BP and Conoco-Phillips. All of these pilot plants used the abundant natural gas reserves in other parts of the world. Exxon Mobil developed a slurry reactor which operated at 200 bbl/day, BP's fixed-bed reactor operated at 70 bbl/day while the Conoco-Phillips plant produced 400 bbl/day.

Recently in 2003 Oryx, which is a joint venture between Qatar Petroleum and Sasol has constructed a second-generation GTL complex in the Ras Laffan industrial city complex in Qatar. This location was chosen as it is close to the large natural gas reserves (proven to be over 260 000 billion liters per day) in the North of Qatar. The $900 million plant's construction was completed by December 2005 and the operations officially started in late June 2006 after a stringent commissioning and validation process was made. This plant is able to produce 34 000 bbl/day of liquids. Plans to evaluate the expansion of this plant to produce 100 000 bbl/day of liquids were made between Qatar Petroleum and Sasol in conjunction with Chevron. However, if this plant is built it will require the construction of a three-train facility that can handle a capacity of about 65 000 bbl/day. The expected start-up date of the fist train is 2009 while that of the subsequent trains is set to commence in 2011. In addition to this, plans to build a 10 000 bbl/day upstream/downstream integrated GTL facility based upon the Sasol slurry phase distillate process which will also exploit the reserves of the Qatar North gas field had been proposed. A tentative start-date for this is set to be 2010. Sasol and Qatar Petroleum hope to be producing 450 000 bbl/day of liquids in 2015 with several other new facilities planned in the years ahead [11].

1.2 The Fischer-Tropsch synthesis

Fischer-Tropsch synthesis (FTS) is possibly the most promising source of chemicals and fuels from a non-petroleum based supply such as natural gas and coal [8]. Ever since Fischer, Tropsch and co-workers [4, 12, 13] developed this work on cobalt and iron-based catalysts, there has been a tremendous interest and dedication towards the commercialization of this synthesis technology. This process is a promising option for environmentally sound production of chemicals and fuels from coal since the reserves of crude oil are being depleted and the price of crude oil continues to rise [4]. Significant advances in coal gasification technology for production of syn-gas suggest that the Fischer-Tropsch (FT) process will be a major contender on the energy scene.

In this FT process a wide range of high molecular weight hydrocarbons and oxygenated hydrocarbons are produced from smaller starting materials (i.e. H_2/CO) irrespective of operating conditions. This has consequently been likened to a polymerisation reaction since analogous steps are followed during the formation of polymers. Dry [14] illustrated a simple stepwise growth process of FT products, similar to that shown in Figure 1.1. It is however to be noted that this is not an actual FT mechanism but detailed mechanisms have been proposed in the literature. Although there are controversies about the actual mechanism for the FTS process all of those proposed models assume that the growth of the hydrocarbon chains is a stepwise process [5, 13, 15-17].

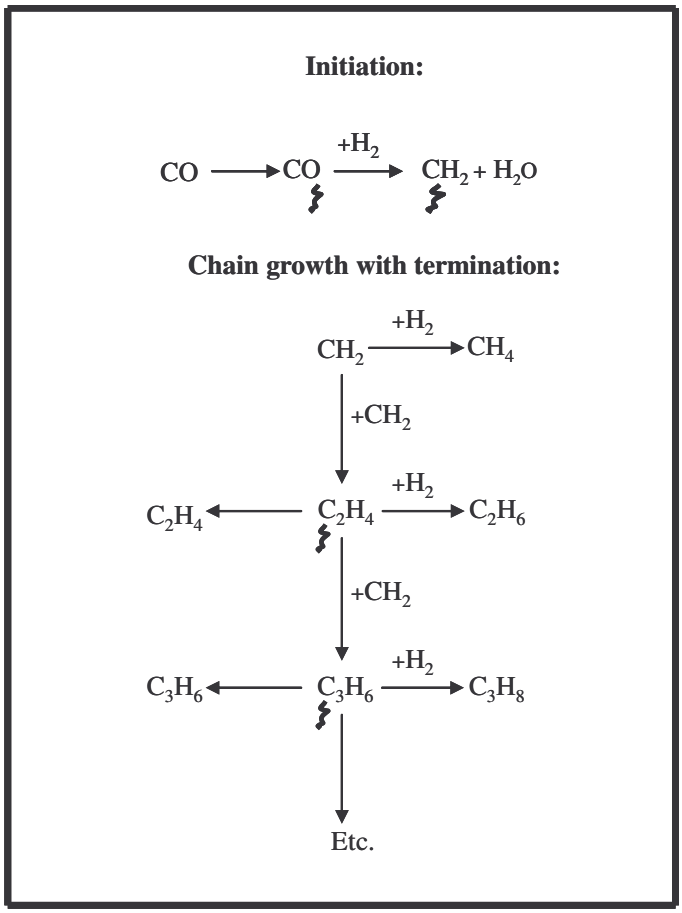

Figure 1.1 Simple FT stepwise growth process (where ⚡ = surface)

The stepwise growth process occurs at the surface of the catalyst and when CO is hydrogenated the CH_2 units are formed and these are taken as the "monomers" in a stepwise oligomerization process. These adsorbed units can either desorb or be hydrogenated further to form primary FT products or another monomer unit can add to the chain to continue the chain growth. This process can take place at each stage of growth. Principally two termination reactions are possible, namely α-hydrogenation, yielding a paraffin, or β-dehydrogenation, producing an α-olefin as primary products. Chain termination can occur at any time during the chain growth process to yield an α-olefins or an n-paraffin once the product desorbs. Large amounts of alcohols and aldehydes are also formed and these appear to be some of primary products involving insertion of some form of oxygenated species into a metal alkyl group on the catalyst surface (CO insertion mechanism) [18, 19]. The formation of these functional groups is considered to be a termination step because it occurs at the end of the growing chain by

inserting a CO molecule in some of the alkyl chains that have previously been formed during the FT growth process [20]. In this process the majority of the products are α-olefins and n-paraffins. Regardless of the product type, they are predominantly linear with high olefinicity.

1.3 The Fischer-Tropsch reaction

The Fischer-Tropsch (FT) reaction (1.1 below) is defined as the hydrogenation of carbon monoxide over transition metals to form a wide range of hydrocarbons and oxygenated hydrocarbons. This reaction is the chemical heart of GTL technology. Water is a primary product, whilst the main products are α-olefins and n-paraffins.

FT reaction: $2H_2 + CO \rightarrow -(CH_2)- + H_2O$, $\Delta H_{r,\,270^oC} = -151.9 kJ/mol$ (1.1)

The FT reaction is highly exothermic ($\Delta H_{r,\,270^oC}$ = -151.9kJ/mol) and an extremely large amount of heat is produced during the reaction.

1.3.1 Other reactions taking place

The produced water can react further via the water gas shift (WGS) reaction as represented in equation (1.2):

WGS reaction: $H_2O + CO \leftrightarrow CO_2 + H_2$, $\Delta H_{r,\,270^oC} = -39.3$ kJ/mol (1.2)

The WGS has been known since the 19th century and was noted to occur during the production of domestic and industrial fuel from the pyrolysis of coals. It is mainly catalyzed by iron catalysts whilst with cobalt catalysts this can only be achieved at high temperatures. One advantage of this side reaction is that it can adjust the H_2:CO feed ratio of the syn-gas if it is lower than stoichiometrically required. However, the WGS reaction is undesirable for FTS with hydrogen-rich syn-gas produced from natural gas as it results in low carbon efficiency in gas-to-liquid process since carbon is lost in the form of CO_2.

The other side reaction taking place during a FT reaction is the known as the Boudouard reaction (1.3). This reaction involves the disproportionation of CO and leads to the formation of CO_2 and carbon [20]. The produced carbon can cause catalyst deactivation.

Boudouard reaction: $2CO \leftrightarrow C + CO_2$, $\Delta H_{r,\,270^oC} = -172.4$ kJ/mol (1.3)

1.4 Fischer-Tropsch product spectrum

Figure 1.2 is a graphic representation of the product distribution that occurs during the FTS process. This plot is known as the Anderson-Schulz-Flory (ASF) model and is represented by the following equation (1.4):

$$W_n = n(1-\alpha)^2\alpha^{n-1} \quad (1.4)$$

where *Wn* is the weight percent of a product containing *n* carbon atoms and, α (or p_g), is the chain growth probability. This model suggests that the probabilities of chain growth and chain termination are independent of the chain length. The selectivities of various hydrocarbons can therefore be predicted based on simple statistical distributions calculated from chain growth probabilities and carbon numbers. The model clearly evaluates the predicted distributions for several products and product ranges of particular interest.

The FTS is unquestionably not a selective process in terms of its product spectrum since the achievement of selectivity to a single organic product, except for production of the C_1 products (methane and methanol), has not yet been possible. Senden and co-workers also showed that only methane can be produced with a selectivity of 100% [21]. This observation agrees with the ASF model as depicted in Figure 1.2.

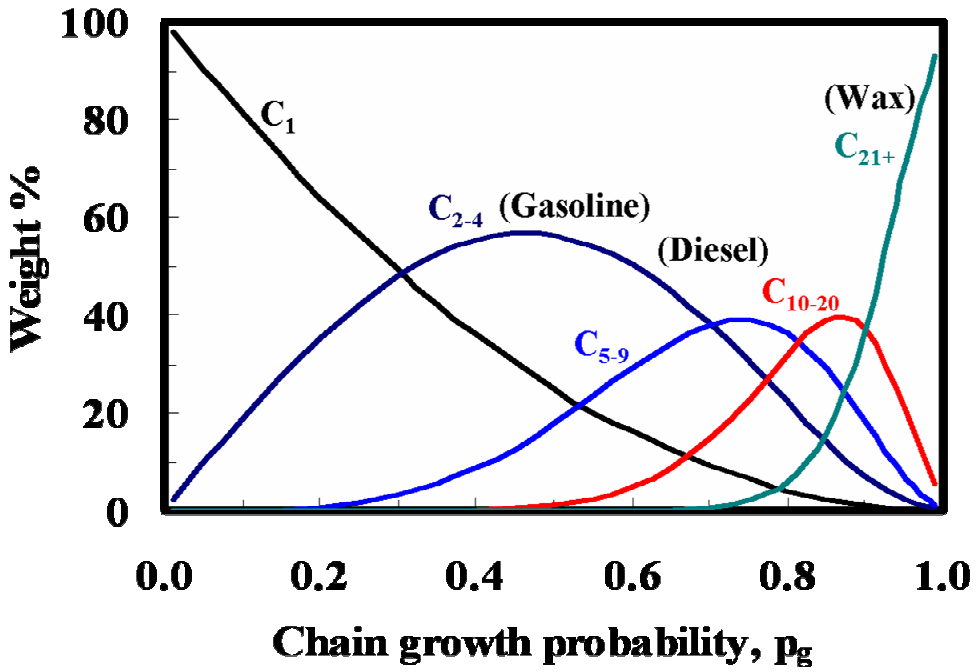

Figure 1.2 FTS product distributions by Anderson-Schulz-Flory model

The only other product that can be produced with high selectivity is heavy paraffin wax. The selectivity of the gasoline product fraction has a maximum selectivity of 48% while that of the diesel product fraction is closer to 40%. However, it has to be noted that the selectivity for the diesel product fraction varies depending on the range of carbon numbers in the product cut. The variables that influence the product distribution are the process operating conditions, the reactor type and the catalyst properties.

1.5 Factors influencing product selectivity

1.5.1 Operating conditions

The cost of producing syn-gas is high and it is therefore important that the maximum amount used is converted in the downstream reactors. It is required that the composition of the syn-gas matches the overall usage. For the cobalt based catalysts a ratio of 2.15:1 for a H_2 to CO mixture is normally used since the dominant reaction is FTS. The ratio for the syn-gas when iron is used changes due to the WGS side reaction that takes place. For the low-temperature FT (LTFT, 200-240 ^{o}C) process using iron the ratio is typically 1.7:1, while for the high-temperature FT (HTFT, 250-350 ^{o}C) it is 1.05:1 since the WGS is rapid and the produced CO_2 is allowed to be converted into FT products via the reverse WGS followed by the FT reaction [14].

The industrial reaction conditions used in the FT reaction range between 200-350 ^{o}C and 25-40 bar. It is difficult to operate at high temperatures (e.g. above 350 ^{o}C) because most of the catalysts that are used degrade or deactivate at high temperatures. Cobalt for instance is known as a LTFT catalyst since it performs well at temperatures between 220-250 ^{o}C for the production of long chain products mainly diesel and wax. If it is used at high temperatures, methane will be the abundant product formed. Iron on the other hand performs well at higher temperatures 250-350 ^{o}C in the production of light products, petrol and chemicals [20]. In the last two decades the development of most FT technologies has been based on LTFT processes. These processes use natural gas as the feed stock for the syn-gas which is generated by vapour reforming, auto-thermal reforming or partial oxidation.

Too much heat produced in the FT reaction can “kill” the catalyst performance because the reaction temperature can be exceeded by an extreme temperature overshoot caused by the exothermic behavior of the reaction. It is crucial that the generated heat be removed or minimized during the reaction. Appropriate reactors that can assist in the rapid heat removal are carefully designed and selected for specific reactions. Also, slow temperature

heating/ramping rates are normally applied during catalyst pretreatments and during the reaction to assist in the minimization of the unwanted exothermic behavior.

1.6 Fischer-Tropsch reactors

The governing factors in the control of product distribution include the reactor type that is used and the type of operation used during FTS. The efficient and speedy removal of the accompanying large heat of reaction is a major consideration since high temperatures lead to excessive methane yields, carbon deposition, particle fragmentation and the catalysts experienced an increased rate of deactivation due to sintering and fouling [8, 14].

After the discovery of FTS, rapid developments and construction of commercial plants took place in Germany. Badger outlined the prospects for these developments and indicated that these are usually carried out in more or less market shift vessels [22]. Ever since then attempts at the invention of new FT reactors continued because principles that defined a unit operation were understood.

Reactors used in the laboratory by Fischer and Tropsch were glass tubes of about 5 mm internal diameter with the catalyst held in a fixed position [5]. For larger reactors the reactor design is of great importance since it is essential to obtain optimum product selectivity and long catalyst life by effectively removing the exothermic heat of reaction.

Recently Davis outlined a brief overview of FT reactors in the periods between 1924 and the future development [10]. This overview is hereby summarized in Table 1.2.

Table 1.2 An overview of Fischer-Tropsch reactor developments

Period	Reactor developments and potentialities
1924 – 1945	Models of temperature profile in a double tube reactor were made. Trial-and-error techniques were used to design reactors. Limitations of reactor modeling due to the pre-computer age.
1945	Introduction of high-pressure reactors for lab use [23]. Utilization of high-pressure autoclaves, fixed-bed and slurry phase reactors. Reactors were then classified into 2 categories: LTFT and HTFT reactors.
1945 – 1970 *(Golden Age)*	Approaches to achieve optimum operating temperatures for stirred reactors were defined. Sasol utilized fluid bed reactors for FTS. M.W. Kellogg company developed a CFB reactor In 1950's Sasol upgraded the Kellogg reactors into the synthol process reactors. Kölbel and co-workers developed a slurry phase reactor that produced gasoline as the dominant liquid product [24]. By 1980, sufficient data existed for comparisons between fixed bed, fluid bed and slurry reactors (see Table 1.3).
1970 till date	Major advance has been the introduction of computers into FTS reactor modeling. In early 1990's Sasol developed a slurry bubble column reactor technology. PetroSA utilized Sasol's CFB reactor technology and had a turnover of 14000 barrels/day During the past 50 years attention has been directed toward bubble column reactors due to its potential to maximize reactor productivity [25].
The future	Interest is now in the development of micro reactors. Microchannel reactors - replacements of one large reactors with many smaller reactors that provide improved control of operating conditions Adaptation of monolith reactor technology. Fixed-bed reactor still attractive - highest catalyst loading and hence the highest potential productivity reactor volume. *Problems that need to be overcome:* 1) Diffusion limitations within the catalyst particle. 2) Decreasing the temperature exotherm. 3) Eliminating the reduced conversion due to accumulation of heavy products inside the catalyst pellet.

Table 1.3 below shows a comparison between the fixed-bed, fluid bed and slurry reactors [26]. Depending on the process involved and the type of products required an appropriate reactor that takes into account the details given in Table 1.3 will achieve optimum FT results.

Table 1.3 Comparison of reactor types - 1980 [26]

Feature	Fixed bed	Fluid bed /circulating	Slurry
Temp. control	Poor	Good	Good
Heat exchanger surface per feed	240 m^2 per 1000 m^3	15-30 m^2 per 2000 m^3	50 m^2 per 1000 m^3
Max. reactor diameter	<0.08 m	Large	Large
CH_4 formation	Low	High	As fixed bed/lower
Product	Full range	Low mol. weight	Full range
Space-time yield (C_2+) in a day	>1000 kg/m^3	4000-12000 kg/m^3	1000 kg/m^3
Cat. effectivity	Lowest	Highest	Intermediate
Back-mixing	Little	Intermediate	Large
Min. H_2/CO feed	As slurry or higher	Highest	Lowest
Construction			Simplest

1.7 Catalysts for Fischer-Tropsch synthesis

1.7.1 Active metals

It is generally accepted that most group 8-10 metals are able to catalyse the FT reaction to liquid hydrocarbons since they can dissociatively adsorb H_2 and CO. Ruthenium followed by iron, nickel, and cobalt are known to be the most active metals for the hydrogenation of CO. It has been shown in the literature (Vannice *et al.*) that the average molecular weight of the hydrocarbons produced by FTS decreases in the following sequence [27]:

Ru > **Fe** > **Co** > Rh > Ni > Ir > Pt > Pd

Thus, only ruthenium, iron, cobalt, and nickel have the required activity for commercial production [14]. Ruthenium is the most active catalyst and shows high selectivity to high molecular weight products at low temperatures. Unfortunately it is too expensive to use commercially. Furthermore, reserves of ruthenium are insufficient for large-scale application. Nickel catalysts under practical operating conditions produce too much methane and do not have the broad selectivity for producing high molecular weight products. This metal is basically a methanation catalyst.

Fischer and Tropsch initially proposed cobalt and iron as the first catalysts for syn-gas conversion [4]. Both cobalt and iron catalysts have been used in industry for the synthesis of hydrocarbons. Cobalt catalysts are more expensive that iron catalysts, but are more resistant to deactivation. Whilst the activity of these two metals is comparable, the productivity at higher conversion is more significant with cobalt catalysts even at lower synthesis pressures. So a higher catalyst cost can be offset by lower operating costs. Iron has a stronger tendency than both nickel and cobalt to produce carbon that deposits on the surface and deactivates the catalyst. Iron readily forms carbides, nitrides and carbonitrides with metallic character that also have FT activity. Iron catalysts also favour the WGS reaction while cobalt catalysts do not have WGS activity (except at high temperatures), which leads to improved carbon conversion to products because CO_2 is not formed. Chain growth probabilities of about 0.95 for iron and 0.94 for cobalt have been reported at relatively low temperature (200-250 ^{o}C) [28-30]. Cobalt catalysts yield mainly straight chain hydrocarbons and very few oxygenates in contrast to iron which produce huge amounts of oxygenates. Iron catalysts produce hydrocarbons and oxygenates under different pressures, temperatures (up to 350 ^{o}C) and H_2/CO ratios while cobalt catalysts operate with a very narrow range of temperatures and pressures. An increase in temperature leads to a spectacular methane selectivity. Iron catalysts usually produce more olefins than do cobalt catalysts. Both cobalt and iron catalysts can be used in the LTFT process for the synthesis of linear long-chain hydrocarbon waxes and paraffins [29, 30]. Cobalt catalysts represent the optimal choice for synthesis of long-chain hydrocarbons in the LTFT because of their stability, higher per pass conversion and

high hydrocarbon productivity. Besides the active catalytic agent, FT catalysts often contain supports and promoters.

1.7.2 Catalyst supports and promoters

The principal function of the catalyst support in FT catalysts is to disperse the active metal and produce stable metal catalyst particles after reduction. The porous structure of the support could control the sizes of supported metal particles. Supported catalysts exhibit better characteristics than unsupported ones. Some of these characteristics include an improved catalyst texture and porosity, controlled particle size, an increased metal dispersion, reduction in the formation of hardly reducible active metal oxides, facilitation of the reducibility and enhancement of mechanical properties and attrition resistance of active metals [31-33]. The effects of different supports used in FTS have been extensively studied and the support is an important component affecting the properties of the catalysts [32, 34-36]. Among the supports, Al_2O_3, SiO_2 and TiO_2 have been most often employed for FTS. This is due to the high surface areas that they possess. Recently Storsæter *et al*. has reported the characterization of Al_2O_3-, SiO_2- and TiO_2-supported cobalt catalysts as FT catalysts [37]. It was observed that the cobalt particle size and reducibility increased with increasing average pore diameter of the support. The pore structure of the support has a significant effect on the size, location, shape and appearance of the FT active metal catalysts.

Reuel and Bartholomew studied the catalytic activity of cobalt-based catalysts as a function of support and found it to decline in the following order: $Co/TiO_2 > Co/Al_2O_3 > Co/SiO_2 > 100\%$ Co > Co/MgO [34]. Iglesia *et al.* found that at pressures greater that 5 bar and at high conversions the influence of the support on the selectivity in methane and C_5+ formation could be insignificant [35]. One of the greatest functions of the support is to dissipate the heat released by the reaction and thus reduce the temperature gradient in fixed-bed reactors.

Mesostructured materials with adjustable porous networks have shown a great deal of promise for designing heterogeneous catalysts [32, 38, 39]. These materials can have a surface area that approaches 1000 m^2/g. The pore sizes ranging from 2 to 30 nm can be adjusted at the stage of synthesis using templates comprising different surfactants. Common mesoporous materials are MCM-41 and SB-15. Larger cobalt particles used in FTS have been prepared from large pore silicas [38]. High cobalt reducibilities and higher dispersion have generally been found in these large particles.

A few reports on the use of carbon as a support for FT catalysts have been written over the years [34, 40, 41]. Carbon-based materials are advantageous over the oxide supports because they do not react with the active metal to form inactive materials such as mixed oxides (aluminates, silicates or titanates) that are only reducible at high temperatures. Recently Bezemer *et al*. proposed cobalt and carbon nanofibers as model systems to study the effect of cobalt particle sizes on FT turnover frequency [42]. It was found that the turnover frequency was almost independent on cobalt particle size with sizes larger than 6-9 nm. The smaller cobalt particle size affected the FT reaction rates when catalyst particles have rates much lower and significant changes in hydrocarbon selectivities were observed. Despite all the advantages of carbon supports over inorganic oxides supports, they are less stable and can gasify in the presence of hydrogen.

Promotion of an active catalytic component with oxides has been one of the methods used to improve the activity, hydrocarbon selectivity to long-chain paraffins and low WGS activity of FT catalysts [1]. Oxide promoters such as ZrO_2, La_2O_3, MnO and CeO_2 have been the most employed. Jacobs *et al.* reported support effects on the reducibility of cobalt catalysts in FTS after examining different supports (SiO_2, TiO_2, Al_2O_3 and ZrO_2) [43]. These authors found that ZrO_2 addition increased the cobalt dispersion and decreased the reducibility of cobalt species in Al_2O_3 supported FT catalysts. A recent study by Enache *et al.* showed that the presence of ZrO_2 in supported cobalt catalysts promoted formation of the poorly crystallized hexagonal phase of cobalt [44]. This phase was found to be more active in FTS than the known cobalt cubic phase. Therefore, the use of ZrO_2 as promoter for cobalt FT catalysts could be due to the higher concentration of cobalt hexagonal phase in ZrO_2-promoted catalysts.

Promotion with noble metals (such as Ru, Rh, Pt and Pd) has a strong impact on the structure and dispersion of active FT species, reaction rates and selectivities. Introduction of noble metals on FT catalysts could result in the following phenomena: much easier reduction of metal oxide particles, formation of bimetallic particles and alloys, a lower fraction of barely reducible mixed oxides, enhancement of metal dispersion, inhibition of catalyst deactivation, appearance of additional sites for hydrogen activation and an increase in the intrinsic reactivity of surface sites [1].

1.7.3 Catalyst activation and deactivation

The three key properties of FT catalysts are activity, product selectivity and lifetime stability. In the last 5 decades optimization of these properties has been the focus for the use of catalysts in commercial applications. There is a variety of strategies which can be used to affect these properties and these include; the use of supports, promoters, catalyst preparation, pretreatment (drying and calcination) and reduction, selective poisoning and catalyst deactivation.

Studies by Reuel and Bartholomew indicated that activity/selectivity properties of cobalt and iron FT catalysts can be significantly altered by variations in calcination and reduction conditions [34]. They found that the average carbon number of the hydrocarbon product increased by 10 to 15% when the reduction temperature for Co/Al_2O_3 and Co/TiO_2 is increased from 650 or 675 to 800K.

FT catalysts are normally activated after preparation by calcining them at high temperatures (300-500 ^oC) to remove impurities and unwanted metal precursors, such as nitrates if metal nitrates were used. Calcination steps also allow the active metals to be redistributed evenly in the catalyst pores and chambers. After the catalysts have been calcined the active metals will be in the oxide form, e.g. Co_3O_4 in the case of cobalt. Before the FT reaction the catalysts are activated by reducing them to their metallic forms in pure hydrogen. Depending on the catalyst preparation and type of active metal support and promoter used the reduction temperatures can vary between 250 and 500 ^oC.

Figure 1.3 shows a schematic representation of the deactivation mechanisms involved during the FTS. These mechanisms are discussed below.

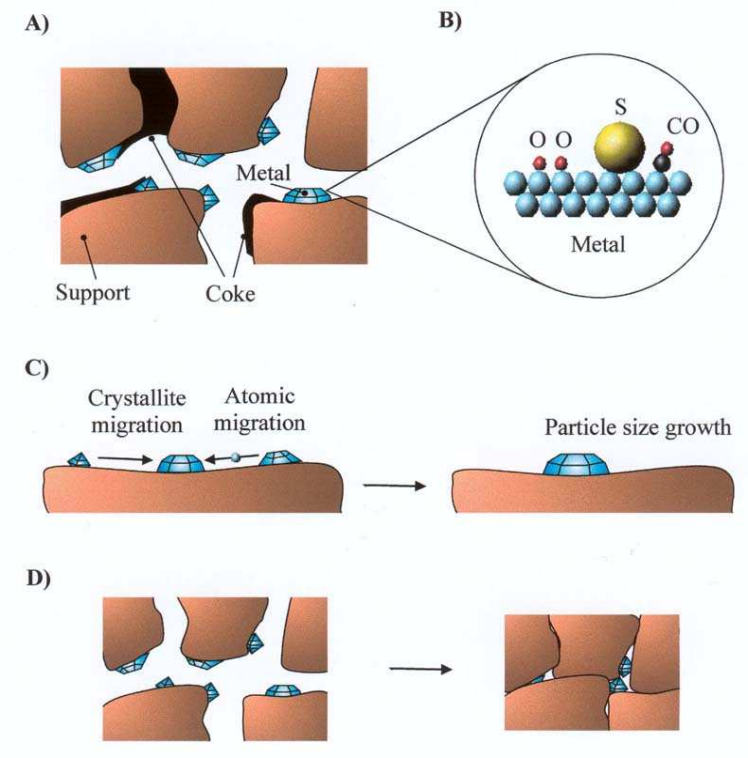

Figure 1.3 Deactivation mechanisms: (A) coke formation, (B) poisoning, (C) sintering of active metal particles and (D) sintering and solid-solid phase transitions and encapsulation of active metal particles [45]

Fouling and coke formation. Fouling due to formation of carbonaceous species during FTS may totally encapsulate a metal crystallite and render the crystallite inactive. The pores may be plugged such that access of reactants is denied to the catalyst crystallites found inside these pores [46].

Poisoning. Catalysts may loose their activity during FTS due to poisoning by contaminants such as sulphur in the feed. Irreversible adsorption of either reactants or products could also poison the catalyst by blocking the catalyst active sites.

Sintering. Sintering is probably the main cause of deactivation of FT catalysts. Agglomeration (crystallite growth) of smaller catalytic particles to larger particles takes

place at high temperatures. If this happens then the formation of FT products may either be minimal or may not be feasible. The sintering mechanism is directly related to the melting temperature and is defined by the so-called Hüttig and Tamman temperatures which indicate the temperature at which sintering starts. Equations 1.5 and 1.6 below are the semi-empirical relations that are commonly used to obtain the Hüttig and Tamman temperatures.

$$T_{Tamman} = 0.5\ T_{melting} \quad (1.5)$$

$$T_{Hüttig} = 0.3\ T_{melting} \quad (1.6)$$

Table 1.4 below gives T_{Tamman} and $T_{Hüttig}$ data for commonly used FT metals and support material similar to those used in this thesis study. Sintering of crystallites is irreversible and it is important to prevent this phenomenon.

Table 1.4 Temperature values of metals that are relevant for FTS and support material similar to those used in this work [47, 48]

Element/Compound	T_{Tamman} /K	$T_{melting}$ /K	$T_{Hüttig}$ /K
Co	877	1753	526
Fe	904	1808	542
Ni	863	1725	513
Ru	1362	2723	817
TiO_2[a]		1850	

[a] Melting point for the rutile phase

1.8 Synthesis of Fischer-Tropsch catalysts

Catalyst preparation methods are the most crucial steps because the catalytic performance is strongly dependent upon them. There are several steps that are involved in the preparation of FT catalysts. This includes the selection of appropriate catalyst supports, choice of method of deposition of the active phase on the support, catalyst promotion and oxidative and reductive treatments. The goal of active phase formation is to spread the active metal onto a porous support and provide a metal cluster precursor. The number of

metal sites, the catalyst properties, characteristics and localization on the support can be controlled by promotion with noble metals and oxides.

There are various ways of preparing FT catalysts and these include; incipient wetness impregnation, pH controlled precipitation, co-precipitation [49], deposition-precipitation [50], sol-gel [51], preparation of eggshells [52], monolithic catalyst preparation [53], colloidal [54], microemulsion [55], solvated metal atom dispersion [56], chemical vapor deposition [57] and plasma methods [58]. To be able to reproduce the catalyst, precautions must be taken during the preparation steps.

For the purpose of this work only two preparation methods are discussed; the incipient wetness impregnation and the pH controlled impregnation methods because these were the only methods used in the thesis study.

1.8.1 Incipient wetness impregnation method

The incipient wetness impregnation method, or the pore volume impregnation method, is a common method used to prepare FT catalysts and is normally described as being the simplest practical way to impregnate an active phase onto the support. However, this is not necessarily true because the fundamental phenomena underlying impregnation and drying are extremely complex.

In this method a salt solution, typically a metal-nitrate is added to a dry porous support, as demonstrated in Figure 1.4 below. After contact, the solution is drawn into the pores of a support by capillary forces. When all pores of the support are filled with the liquid and when there is no more excess liquid required to fill the pores then the incipient wetness process has occurred. The liquid is then removed in a drying or calcination step resulting in the preparation of the oxidic catalyst precursor. When the concentration of metal salt is high then large metal particles will be dispersed in the pores and when it is dilute then small metal particles will be dispersed in the support pores [59].

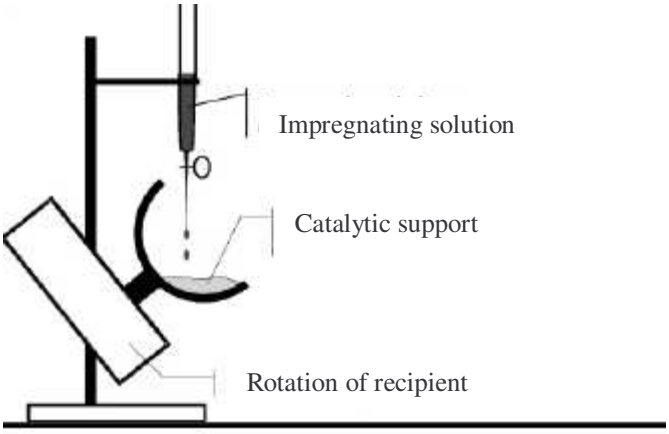

Figure 1.4 Schematic representation of experimental set up for incipient wetness impregnation [1]

In order to reproduce the catalyst synthesis careful control of all impregnation parameters are required. These include the rate of addition of impregnation solution, temperature and time of support drying, temperature and time of drying.

1.8.2 pH-controlled precipitation method

Classical impregnation techniques may result in a non-uniform catalyst distribution through the particles and pellets. Recently developed precipitation technique in which the pH is carefully controlled enables the uniform deposition of the active precursor material at practical loadings. The syntheses of well-dispersed low loaded ZSM-5-supported Fe/Cu/K catalyst by the pH-controlled precipitation method has been reported in a patent by Mobil [60]. Bartholomew *et al.* have also used pH-controlled precipitation to generate a series of nickel supported catalysts with higher specific activities than those obtained from an impregnation method [61].

Catalyst preparation by the pH-controlled precipitation method involves the dissolving of the precursors of the active components, usually in their salt forms, in water or another suitable medium to form a homogeneous solution. The corresponding solution is then subjected to pH adjustment so as to force the metal ions to precipitate. The support is

then impregnated with the corresponding precipitate. After drying and calcination, oxidic catalyst precursors are obtained.

1.9 Novel routes to the preparation of Fischer-Tropsch supports

1.9.1 Titanate nanotubes

The discovery of single walled carbon nanotubes with novel properties that are not found in conventional graphite or carbon fullerenes was first reported in 1991 by Iijima *et al* [62]. Theoretical and experimental results have shown that their properties depend significantly on the tube thickness, diameter, helicity and defect concentration [63, 64]. The hydrophobicity of the carbon nanotubes, however, limits their applications in catalysis. Since the discovery of carbon nanotubes a great deal of research has been conducted on developing other nanoscale non carbon tubular materials that have novel properties. In particular those that have relevant thermal, spectroscopic, electronic and the unusual mechanical properties have been synthesized and studied [65].

The idea of producing inorganic materials was inspired by the ability of graphitic sheets (with similar layered structures) to roll up into tubes and form the carbon nanotubes. These tubular materials are normally achieved by controlling the nanostructure. For instance ceramic oxides like Al_2O_3, SiO_2, V_2O_5 and MoO_3 with diameters of several tens of nanometers have been prepared by using carbon nanotubes as templates followed by removal of the template [66]. Chopre *et al.* has recently reported the production of pure boron nitride nanotubes with a length $\leq$ 200 nm and an inner diameter of 1-3 nm [67]. These were prepared from a carbon-free plasma discharge between boron nitride-packed tungsten rod and a cooled electrode.

Titanate nanotubes attracted wide attention as soon as they were discovered. This arises since titania is a highly catalytic active material and can also be used as catalytic support. These tubular materials are interesting because they have large surface areas which may enhance their photocatalytic activity, leading to a higher potential of applications for

environmental purification. Well-ordered structures with relatively simple compositions can be formed by these materials. Their structures and formation mechanism are still not well understood. Several authors claimed that titanate nanotubes did not exhibit a layered structure [68-70].

In the literature three main approaches have been reported for the preparation of these tubular materials in powdered form. These are the anodic oxidation method [71], the template method [72] and the wet chemical method [70]. Kasuga *et al.* has recently reported a new cost effective route for the synthesis of crystalline titanium oxide nanotubes that are layered [70]. They reported that their tubular material consisted of an anatase phase and had diameters ≈8 nm lengths of ≈100 nm and large specific surface area of ≈400 m^2/g. These materials were obtained by treating the sol-gel derived TiO_2 powders with NaOH aqueous solution and then the formation of tubular materials was made possible by acid (HCl) treatment. This method is supported by many researchers and is called an alkaline hydrothermal treatment. Even though it is recent [73], the materials produced have been intensely studied [74]. It has also been reported by many researchers that the titania nanotubes consisting of anatase phase can be obtained without an acid washing [75-79]. Materials prepared in this way are normally described as titanate nanotubes and can have different crystal structures [69, 76-78].

The titanate nanotubes in contrast to the carbon nanotubes are formed by rolling a single sheet of TiO_2 into a tube [80]. The formation mechanism of these tubular materials from anatase TiO_2 by basic treatment is not well understood. However Chen *et al.* proposed a morphological transformation of the anatase phase under chemical treatment [81]. They proposed that by treating TiO_2 with a concentrated base, i.e. concentrated NaOH, the dangling bonds on the surface of the TiO_2 react with hydroxide ions, making sheet of TiO_2 curl as demonstrated in Figure 1.5 (a), below. When the number of hydroxide ions increases, then the curliness of the TiO_2 sheet increases. They also proposed that the sheet of titanate normally rolls in the [001] direction of the overall titanate structure as depicted in Figure 1.5 (b) below. The overall model is shown is Figure 1.5 (c).

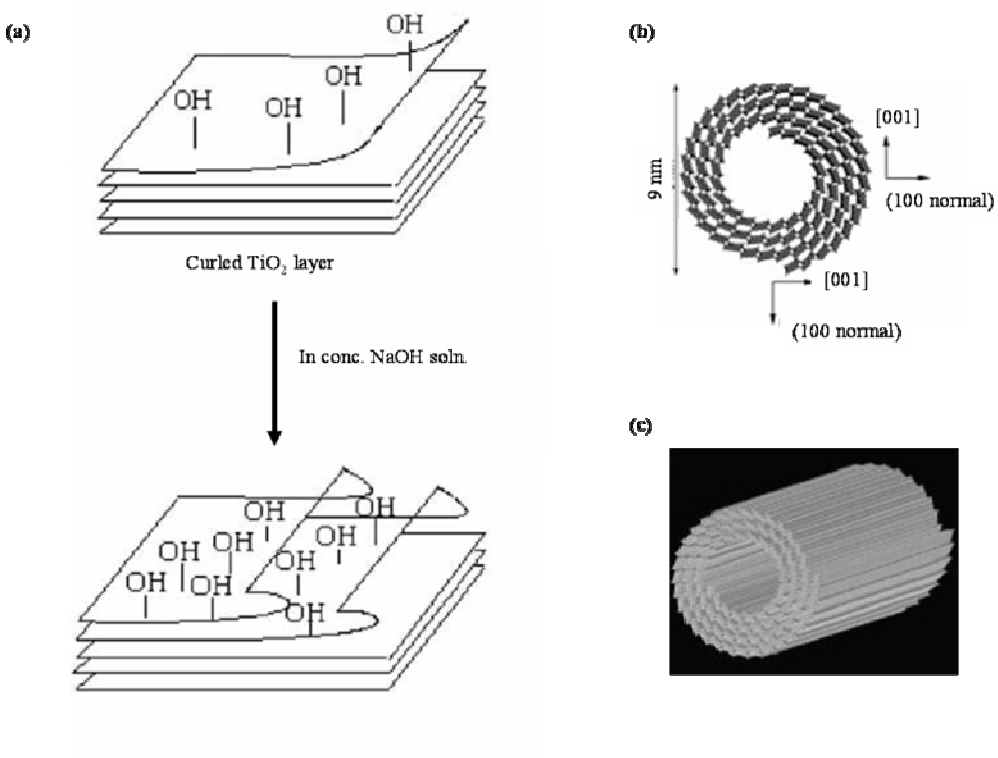

Figure 1.5 Schematic representation of (a) the formation pathway of titanate nanotubes [80], (b) the structure of the titanate nanotube and (c) the three-dimentional drawing of a titanate nanotube [81]

The catalytic application of the titanate nanotubes was studied by Sikhwivhilu [79]. He used these materials as supports for palladium in hydrogenation, oxidation and esterification reactions. These catalysts showed very high activities, viz. up to 97% in the hydrogenation of phenol and up to 100% activity in the hydrogenation of o-chloronitrobenzene. Ntho on the other hand employed these tubular materials as gold supports in the CO oxidation reaction [82]. His materials had a surface area of ≈148 m^2/g and were active for this reaction even though the CO conversions were kept at low levels, ≈5 %, for the purpose of the study.

1.9.2 Sol-gel and titania coating

In the last 20 years the sol-gel process has become one of the successful techniques for preparing nanocrystalline metallic oxide materials. In particular, the preparation of multi-component oxide materials by this method exhibits a number of advantages over conventional preparation methods [83, 84]. One of the advantages is that it has the ability to improve the surface area, the porosity, stability and homogeneity of the multi-component system [84, 85]. This method is normally used in catalysis for the preparation of oxide supports with high surface areas.

This multistage process involves the formation of a sol and then the transformation of a sol into a gel through hydrolysis and polycondensation reactions. The sol is formed when a gel of a metal alkoxide is dissolved in an alcohol. For the reaction to take place, water and a catalyst are added to the solution. Typical catalysts used are simple acids, e.g., hydrochloric acid, acetic acid and nitric acid. Acetylacetone can also be used as a modifier to moderate the reaction rate [86].

Many reports have shown that titania can be prepared using the sol-gel technique with the formation of only the anatase phase [83, 87-89]. In addition Jung *et al.* reported that the sol-gel technique can be used to prepare titania that can be used as a deep-coating agent for tubular materials in the preparation of new inorganic materials [90]. Figure 1.6 depicts a postulated schematic representation of a mechanism proposed by Jung *et al.* in their novel sol-gel creation of helical ribbon and double layered TiO_2 nanotube structures using an organogel template. They stated that the hydrogen interaction between the amide groups found in the organic material and the negatively charged TiO_2 precursors allowed the helical ribbon and nanotube structures to be transformed into the titania coated nanotube structures. Recently Wunderlich *et al.* reported the use of the sol-gel deep-coating method in the preparation of anatase titania coated nickel sheets that have been covered with amorphous carbon layers or carbon nanotubes [91]. Oki *et al.* recently reported a similar method to disperse functionalized carbon nanotubes in silica using sol-gel processing [92].

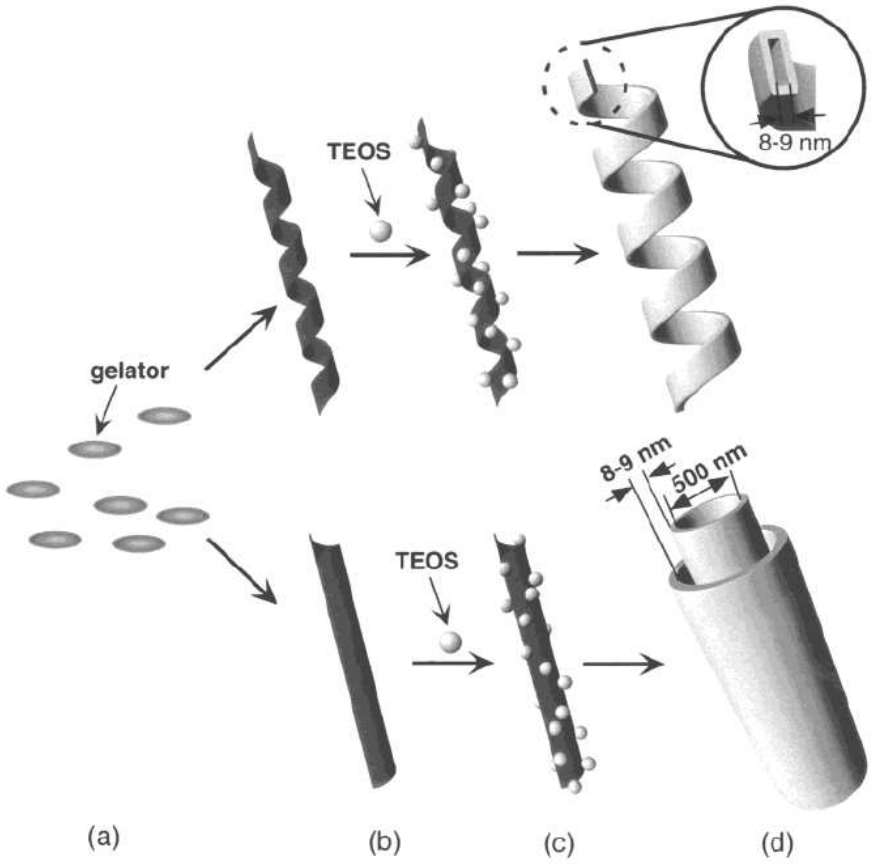

Figure 1.6 Postulated mechanism for the sol-gel polymerization of $Ti(O^iPr)_4$ using an organogel as a template: (a) gelator, (b) gelation, (c) sol-gel polymerization of TEOS and adsorption onto the gelator, (d) hollow helical-ribbon (upper) and hollow double-layered nanotube (low) of the TiO_2 formed after calcinations [90]

This method of incorporating nanotubular materials into an inorganic matrix is attractive because the properties of these materials can be maintained while only changing the surface properties of the coated materials. The fabrication of hollow nanotubes and the modification of the properties either by filling or by coating the tubes have been developed to fit particular application requirements.

1.10 References

1. A. Y. Khodakov, W. Chu, P. Fongarland, *Chem. Rev.*, **107**, 1692 (2007)
2. P. Sabatier, J. B. Sederens, *C. R. Acad. Sci.*, Paris, **134**, 514 (1902)
3. BASF: *German Pat.*, **293**, 787 (1913)
4. F. Fischer, H. Tropsch, *Brennst. Chem.,* **4**, 276 (1923)
5. M. E. Dry, The Fischer-Tropsch Synthesis*,* In: J. R. Anderson, M. Boudart (Eds.), *Catalysis Science and Technology*, Vol. **1**, Springer-Verlag, New York, 159 (1981)
6. G. Olive-Henrichi and S.Olive, In: Herley, Patai (Eds.), The *chemistry of the metal-carbon bond.* Vol. **3**, John Wiley and sons, New York (1985)
7. F. Fischer, H. Tropsch, *Ber. Dtsch. Chem. Ges.*, **59**, 830 (1926)
8. A. A. Adesina, *Appl. Catal. A: General*, **138**, 345 (1996)
9. J. Xu, C. H. Bartholomew, J. Sudweeks, D.L. Eggett, *Top. Catal.*, **26**, 55 (2003)
10. B. H. Davis, *Top. Catal.*, **32**, 143 (2005)
11. http://www.hydrocarbons-technology.com/project_printable.asp?ProjectID=3065
12. H. Storch, N. Golumbic, R. B. Anderson, *The Fischer-Tropsch and related Syntheses*, Wiley, New York (1951)
13. R. B. Anderson, *The Fischer-Tropsch Synthesis*, Academic Press, New York, (1984)
14. M. E. Dry, *Catal. Today*, **71**, 227 (2002)
15. M. E. Dry, *J. Appl. Catal. A: General*, **138**, 319 (1996)
16. M. E. Dry, *Catal. Today*, **6(3)**, 183 (1990)
17. H. Schulz, G. Schaub, M. Claeys, T. Riedel, *Appl. Catal. A: General*, **186**, 215 (1999)
18. H. A. J. van Dijk, *The Fischer-Tropsch Synthesis: A mechanistic study using transient isotopic tracing*, Proefschrift, Technische Universiteit Eindhoven (2001)
19. E. A. Van Schalkwyk, Msc. Dissertation, University of Cape Town, Rodenbosch (1998)
20. M. E. Dry, FT catalysts, In: A. Steynberg, M. E Dry (Eds.), *Fischer Tropsch Technology*, Vol. **152** of Stud. Surf. Sci. Catal. Elsevier, Amsterdam, 533 (2004)

21. M. M. G. Senden, S. T. Sie, M. F. M. Post, J. Ansorge, "*Engineering aspects of the conversion of natural gas into middle distillates"*, NATO ASI Series, Series E: *Applied Sciences*, **225**, 227 (1992)
22. W. L. Badger, *Ind. Eng. Chem.*, **36**, 397 (1944)
23. V. N. Ipatieff, *Catalytic reactions at High Pressures and Temperatures*, Macmillan, New York (1936)
24. H. Kölbel, M. Ralek, *Catal. Rev. Sci. Eng.*, **21**, 225 (1980)
25. J. Zhang, R. L. Espinoza, S. R. Mohedas, *WO 03/052335 A2* (2003)
26. D. S. van Vuuren, *CSIR CENG*, 432 (1982)
27. M. A. Vannice, *J. Catal.*, **37**, 449 (1975)
28. B. Jager, *Stud. Surf. Sci. Catal.*, **119**, 25 (1998)
29. R. L. Espinoza, A. P. Steynberg, B. Jager, A. C. Vosloo, *Appl. Catal. A.*, **186** (1-2), 13 (1999)
30. B. Jager, R. Espinoza, *Catal. Today*, **23**, 17 (1995)
31. M. Voβ, D. Borgmann, G. Wedler, *J. Catal.*, **212**, 10 (2004)
32. A. Y. Khodakov, A. Griboval-Constant, R. Bechara, V. L. Zholobenko, *J. Catal.*, **206**, 230 (2002)
33. B. Jongsomjit, C. Sakdamnuson, P. Praserthdam, *Mater. Chem. Phys.*, **89**, 395 (2004)
34. R. C. Ruel, C. H. Bartholomew, *J. Catal.*, **85**, 78 (1984)
35. E. Iglesia, S. L. Soled, R. A. Fiato, *J. Catal.*, **137**, 212 (1992)
36. A. Aaserud, A.-M. Hilmen, E. Bergene, S. Eri, D. Schanke, A. Holmen, *Catal. Lett.*, **94**, 171 (2004)
37. S. Storsæter, B. Tøtdal, J. C. Walmsley, B. S. Tanem, A. Holmen, *J. Catal.*, **236**, 139 (2005)
38. A. Corma, *Chem. Rev.*, **87**, 2373 (1997)
39. K. M. Ryan, N. R. B. Coleman, D. M. Lyons, J. P. Hanraham, T. R. Spalding, M. A. Morris, D. C. Steytler, R. K. Heenen, J. D. Holmes, *Langmuir*, **18**, 4996 (2002)
40. L. Fu, C.H. Bartholomew, *J. Catal.*, **92**, 367 (1985)
41. M. C. Bahome, L. L. Jewell, D. Hildebrandt, D. Glasser, N. J. Coville, *Appl. Catal. A: General*, **287**, 60 (2005)

42. G. L. Bezemer, J. H. Bitter, H. P. C. E. Kuipers, H. Oosterbeek, J. E. Holewijn, X. Xu, F. Kapteijn, A. J. van Dillen, K. P. de Jong, *J. Am. Chem. Soc.*, **128 (12)**, 3956 (2006)
43. G. Jacobs, T. K. Das, Y. Zhang, J. Li, G. Racoillet, B. H. Davis, *Appl. Catal. A: General*, **233**, 263 (2002)
44. D. I. Enache, B. Rebours, M. Roy-Auberger, R. Revel, *J. Catal.*, **205**, 346 (2002)
45. http://herkules.oulu.fi/isbn9514269543/html/x546.html
46. C. H. Bartholomew, *Appl. Catal. A: General*, **212**, 17 (2001)
47. J. A. Mouljin, E. van Diepen, F. Kapteijn, *Appl. Catal. A: General*, **212**, 3 (2001)
48. S. Matsuda, A. Kato, *Appl. Catal.*, **8**, 149 (1983)
49. A. A. Khassin, T. M. Yurieva, V. V. Kaichev, V. I. Bukhtiyarov, A. A. Budneva, E. A. Paukshtis, V. N. Parmon, *J. Mol. Catal. A*, **175**, 189 (2001)
50. C. J. G. van Der Grift, P. A. Elberse, A. Mulder, J. W. Geus, *Appl. Catal.*, **63**, 19 (1990)
51. K. Okabe, X. Li, M. Wei, H. Arakawa, *Catal. Today*, **89**, 431 (2004)
52. R. Baratti, V. Feckova, M. Morbidelli, A. Varma, *Ind. Eng. Chem. Res.*, **36**, 3416 (1997)
53. A. F. Pére-Cadenas, M. M. P. Zieverink, F. Kapteijn, J. A. Mouljin, *Catal. Today*, **105**, 623 (2005)
54. A. Roucoux, J.Schulz, H. Patin, *Chem. Rev.*, **102**, 3757 (2002)
55. I. Capek, *Adv. Colloid Interface Sci.*, **110**, 49 (2004)
56. D. H. Ralston, K. J. Klabunde, *Appl. Catal.*, **3**, 13 (1982)
57. M. Kurhinen, T. A. Pakkanen, *Langmuir*, **16**, 2658 (2000)
58. A. Rautiainen, M. Lindblad, L. B. Backman,R. L. Puurunen, *Phys. Chem. Chem. Phys.*, **4**, 2466 (2002)
59. G. C. Bond, In: P. W. Atkins, J. C. E Holker, A. K. Holliday (Eds.), *Heterogeneous Catalysis: Principles and applications*, Oxford University Press, New York, 70 (1990)
60. W. K. Bell, W. O. Haag, G. W. Keirkes, D. J. Klocke, *US Patent 4686313* (1987)
61. C. H., Bartholomew, R. B., Pannell, *J. Catal.*, **65**, 390 (1980)
62. S. Iijima, *Nature*, **354**, 56 (1991)

63. H. J. Dai, E. W. Wong, C.M. Liber, *Science*, **272**, 523 (1996)
64. T. W. Odam, J. L. Huang, P. Kim, C. M. Lieber, *Nature*, **391**, 62 (1999)
65. Q. Chen, G. H. Du, S. Zhang, L.-M. Peng, *Acta Cryst.*, **B58**, 587 (2002)
66. B. C. Satishkumar, A. Govindaraj, E. M. Voli, L. Basumallic, C. N. R. Rao, *J. Mater. Res.*, **12**, 604 (1997)
67. N. G. Chopra, R. J. Luyken, K. Cherry, V. H. Crespi, M. L. Cohen, S. G. Louie, A. Zettl, *Science*, **269**, 966 (1995)
68. P. Hoyer, *Langmuir*, **12**, 1411 (1996)
69. T. Kasuga, M. Hiramatsu, A. Hoson, T. Sekino, K. Niihara, *Adv. Mater.*, **11**, 1307 (1999)
70. T. Kasuga, M. Hiramatsu, A. Hoson, T. Sekino, K. Niihara, *Langmuir*, **14**, 3160 (1998)
71. D. Gong, C. A. Grimes, O. K. Varghese, W. Hu, R. S. Singh, Z. Chen, E. C. Dickey, *J. Mater. Res.*, **16**, 3331 (2001)
72. S. Kobayashi, K. Hanabusa, N. Hamasaki, M. Kimura, H. Shirai, S. Shinkai, *Chem. Mater.*, **12**, 1523 (2000)
73. V. D. Bavykin, A. A. Lapkin, P. K. Plucicinski, L. Torrente-Murciano, J. M. Friendrich, F. C. Walsh, *Top. Catal.*, **39**, 151 (2006)
74. C. C. Tsai, H. Teng, *Chem. Mater.*, **16**, 4352 (2004)
75. W. Wang, O. Varghese, M. Poulose, C. A. Grimes, *J. Mater. Res.*, **19**, 417 (2004)
76. G. H. Du, Q. Chen, R. C. Che, Z. Y. Yuan, L. M. Peng, *Appl. Phys. Lett.*, **79**, 3702 (2001)
77. X-Y. Liu, N. J. Coville, *S. Afr. J. Chem.*, **58**, 110 (2005)
78. M. Qamar, C. R. Yoon, H. J. Oh, D. H. Kim, J. H. Jho, K. S. Lee, W. J. Lee, H. G. Lee, S. J. Kim, *Nanotech.*, **17**, 5922 (2006)
79. L. M. Sikhwivhilu, PhD Thesis, University of the Witwatersrand, Johannesburg (2007)
80. Y.-F. Chen, C.Y. Lee, M.-Y. Yeng, H.-T. Chiu, *Mater. Chem. And Phys.*, **81**, 39 (2003)
81. Q. Chen, W. Zhou, G. Du, L.-M. Peng, *Adv. Mater.*, **14**, 1208 (2002)

82. T. A. Ntho, submitted PhD Thesis, University of the Witwatersrand, Johannesburg (2007)
83. X.-Z. Ding, X.-H. Liu, *Materials Science and Engineering*, **A224**, 210 (1997)
84. G. E. Dobler, K. S. Syslick, A. I. Ko, In: D. Helms (Ed.), *Novel Approaches to Catalyst Preparation*, Catalytica Studies Division (1993)
85. N. N. Madikizela-Mnqanqeni, N. J. Coville, *Appl. Catal. A: General*, **317**, 195 (2007)
86. Y. Nosaka, M. Jimbo, M. Aizawa, N. Fujii, R. Igarashi, *J. Mater. Sci. Lett.*, **10**, 406 (1991)
87. M. Schneider, A. Baiker, *Catal. Today*, **35**, 339 (1997)
88. I. A Montoya, T. Viveros, J. M. Domiguez, L. A. Canales, I. Schifter, *Catal. Lett.* **15**, 207 (1992)
89. T. Sugimoto, X. Zhou, A. Muramatsu, *J. Colloid Interface Sci.*, **259**, 43 (2003)
90. J. H. Jung, H. Kobayashi, K. J. C. van Bommel, S. Shinkai, T. Shimizu, *Chem. Mater.*, **14**, 1445 (2002)
91. W. Wunderlich, N. T. Hue, S. Tanemura, *AZojomo J. Mater online*, **2**, 1 (2006)
92. A. Oki, L. Adams, V. Khabashesku, Y. Edigin, P. Biney, Z. Luo, *Mater. Lett.*, Article in press, corrected proof (2007)

Chapter 2

2. Scope of this work

If the highest possible amount of metal atoms is targeted to be exposed to gaseous reactants during the Fischer-Tropsch synthesis (FTS), then the metal catalyst (i.e. cobalt or iron) must be deposited on a high-surface area support to obtain a high metal dispersion [1, 2]. When this high dispersion is achieved then an improvement of the catalyst activity is normally achieved due to an improved amount of active metal sites. However, strong metal support interactions (SMSI) between the active metal and the support can influence the reducibility of the active metal since high temperatures will be required to achieve reduction. Metal oxides such as TiO_2, SiO_2 and Al_2O_3 are normally used as high surface area supports for Fischer-Tropsch (FT) catalysts. Carbon has also been used as a high surface area support in FTS.

When high chain-growth probability and low branching are required during FTS then cobalt is a good choice of metal. Cobalt catalysts have been widely investigated in the FTS because of the high activity and selectivity to heavy hydrocarbon resulting from its use [2-4]. The activity of cobalt depends mainly on the density of surface metallic cobalt atoms, which is usually correlated with its dispersion and reducibility [5-7].

In this study the preparation of a novel high surface-area titanate nanotube support from a layered titanate structure by treating titania (TiO_2) with a base, KOH, prior to acid treatment was undertaken. Preparation of the high surface-area titania coated titanate nanotube support by means of a sol-gel derived titania from titanium butoxide, $Ti[O(CH_2)_3CH_3]_4$ was also undertaken. This procedure was utilized so that the high surface area could be maintained while using high potassium loadings of the titanate

nanotubes since potassium is known to poison the cobalt catalysts in FTS [8, 9]. Neither of these materials has been studied previously for this particular reaction. These materials were impregnated with cobalt and tested for activity in FTS. These materials were compared with that of the commercial titania (P25 Degussa) support. Figure 2.1 shows a diagrammatic representation of the morphologies for the three different titania supports and catalysts prepared and used in this work.

To be able to understand the catalytic properties, these catalysts were characterized using BET, H_2-chemisorption, H_2-TPR, TEM, TGA, XRD and XRF characterization techniques. The experimental approach, experimental set-up, result and data work-up used in this study are described in chapter 3.

2.1 Summary of the main aims of the study:

- To synthesise and study a high surface area titania support from a commercially available titania material (P25 Degussa) and use it as a support for a cobalt catalyst.
- To employ other forms of titania derived materials as supports, in particular titania derived tubular materials.
- To prepare cobalt based catalyst for the FTS using a pH-controlled precipitation method followed by impregnation onto a support.
- To study the change in the chemical interaction between the support and the metal precursor.
- To test the catalyst activity of the cobalt/support materials at 8 bar pressure.
- To compare three titania-derived supports, viz. titania nanoparticles, titanate nanotubes and titania coated titanate nanotubes to support cobalt as catalysts in FTS.
- To characterise the new materials by a range of techniques.

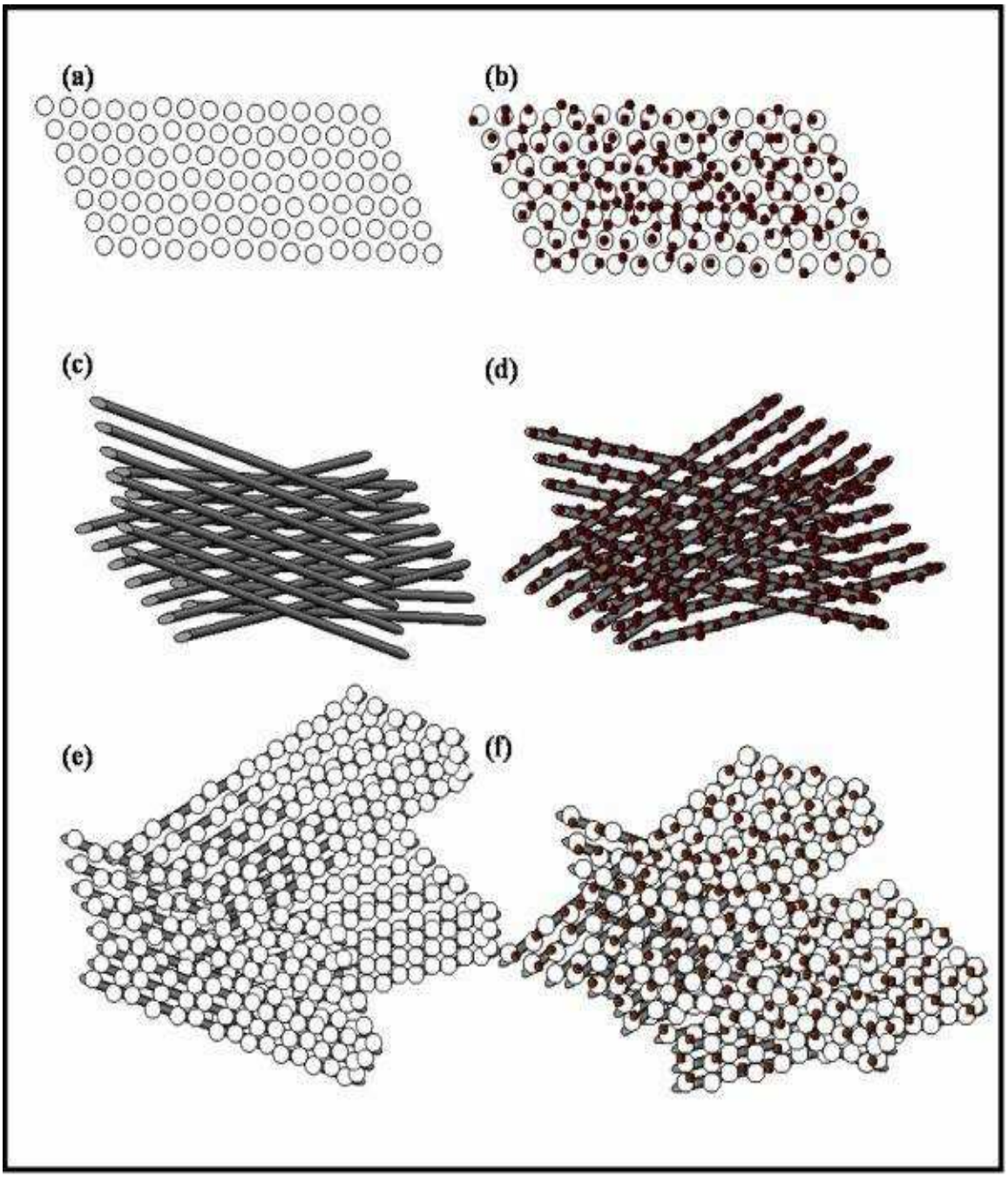

Figure 2.1 A diagrammatic representation of (a) TiO_2 nanoparticles (TN), (b) Co/TN, (c) Titanate nanotubes (TNT), (d) Co/TNT, (e) Titania coated titanate nanotubes (TC-TNT) and (f) Co/TC-TNT

2.2 References

1. E. van Steen, G. S. Sewell, R. A. Makhothe, C. Micklethwaite, H. Manstein, M. de Lange, C. T. O'Connor, *J. Catal.*, **162**, 220 (1996)
2. G. Jacobs, T. K. Das, Y. Zhang, J. Li, G. Racoillet, B. H. Davis, *Appl. Catal. A: General*, **233**, 263 (2002)
3. H. Schultz, *Appl. Catal. A*, **186**, 3 (1999)
4. B. Ernst, S. Libs, P. Chaumette, A. Kiennemann, *Appl. Catal. A*, **186**, 145 (1999)
5. R.C. Reuel, C. H. Bartholomew, *J. Catal.*, **85**, 63 (1984)
6. A. Barbier, A. Tuel, I. Arcon, A. Kodre, G. A. Martin, *J. Catal.*, **162**, 220 (1996)
7. E. Iglesia, S. L.Soled, R. A. Fiato, *J. Catal.*, **137**, 212 (1992)
8. J. Lahtinen, G. A. Somorjai, *J. Mol. Catal. A: Chemical*, **130**, 255 (1998)
9. W.-P. Ma, Y.-J. Ding, L.-W. Lin, *Ind. Eng. Chem. Res.*, **43**, 2391 (2004)

Chapter 3

3. Experimental Methods

3.1 Introduction

Methods of catalyst preparation determine the overall catalytic performance in Fischer-Tropsch Synthesis (FTS) [1]. This is affected by the support used to disperse the catalyst. It is critical to choose a catalyst support that will be suitable for enhancing the catalytic performance. The method of deposition of an active phase onto the appropriate support also plays a role in affecting the FTS activity. Control of the product distribution by controlling the reaction temperature, total pressure, H_2/CO ratio and the nature of the catalyst still remain a challenge [1]. In this chapter these aspects are discussed.

The experimental method section describes the choice and preparation of different catalytic supports and the deposition of an active phase into these supports to synthesise catalysts. Characterisation techniques and the information that can be obtained from them are outlined. Lastly the methods and experimental procedures for catalyst evaluation in FTS are also presented.

3.2 Preparation of catalyst and support materials

Catalyst preparations were conducted by two different methodologies; an incipient wetness impregnation method and a pH-controlled precipitation method. The corresponding metal solution precursors were then impregnated into a support.

Three different types of titania (TiO_2) derived supports were used. These are referred to as titania nanoparticles (TN), synthesized titanate nanotubes (TNT) and titania coated titanate nanotubes (TC-TNT). All of these supports were generated from a commercial TiO_2 powder (Degussa titania P25, containing a mixture of anatase and rutile phases). Even though all these supports were derived from a commercial TiO_2 powder their preparation procedures were different and the preparation methodologies are described below.

3.2.1 Preparation of titania nanoparticles support

In the case of the titania nanoparticles (TN) support, a commercial TiO_2 powder was mixed with deionised water and compressed into a moist paste. The solid material was dried in a conventional oven at 120 °C for 24 hours. After cooling, it was crushed and sieved to the desired size (500-850 µm).

3.2.2 Preparation of titanate nanotubes support

Titanate nanotubes (TNT) were prepared as described elsewhere [2, 3, 4]. About 25 g of TiO_2 powder was placed in a 1 L teflon container together with 300 g of KOH pellets. Deionised water (300 ml) was added to the mixture. The mixture was heated for 20 hours at 120 ^oC in an autoclave with constant stirring at the rate of 300 rpm. The solution was allowed to cool and then aged for 2 days before it was washed with deionised water. Subsequently the solid product was separated from the mixture by centrifugation at a stirring rate of 10 000 rpm for 30 minutes at -5 ^oC. The washing was repeated until the conductivity of the solution was constant and ≤ 100 µS/cm. The pH of the solution during washing was also monitored. Three different sample batches were prepared. The effect of

washing period was monitored by pH and the conductivity of the final washing solution. This data including that of the surface area, the pore volume and the pore diameter of these samples is given in Table 3.1 below. The removal of the basic ions is rather a lengthy process which may take many weeks to a month. The solid was dried in an oven at 120°C for 12 hours and then calcined at 300 ^{o}C for 5 hours at a heating rate of 5 ^{o}C/min. After cooling the sample was sieved to give particles with a size of 500-850 μm in diameter.

Table 3.1 The effect of washing by monitoring pH, conductivity and the surface area

Sample	pH	Conductivity /μS/cm	BET SA /m^2/g	Pore volume /cm^3/g	Pore diameter /nm
$TNT_{1\ 1/2\ weeks}$	9.95	159.8	187	0.49	6.3
$TNT_{2\ weeks}$	9.46	92.4	214	0.42	7.6
$TNT_{3\ weeks}$	9.32	89.3	231	0.37	10.2

3.2.3 Preparation of titania coated titanate nanotubes support

The titania coated titanate nanotubes (TC-TNT) were prepared by means of a sol-gel processing (deep coating) method. In Figure 3.1 a flow chart of the preparation of titania coated titanate nanotubes (TC-TNT) is shown. It is well known that through a sequence of hydrolysis and polycondensation reactions, the sol-to-gel transition of $Ti(OR)_4$ to TiO_x will gradually take place [5]. As this transition occurred, the titanate nanotubes dispersed in the ethanolic solution of the of butoxide became coated with the sol-gel derived titania coating (hence the name “titania coated titanate nanotubes”). The TNT acts as a template for the hydrolysed $Ti(OR)_4$ reactant.

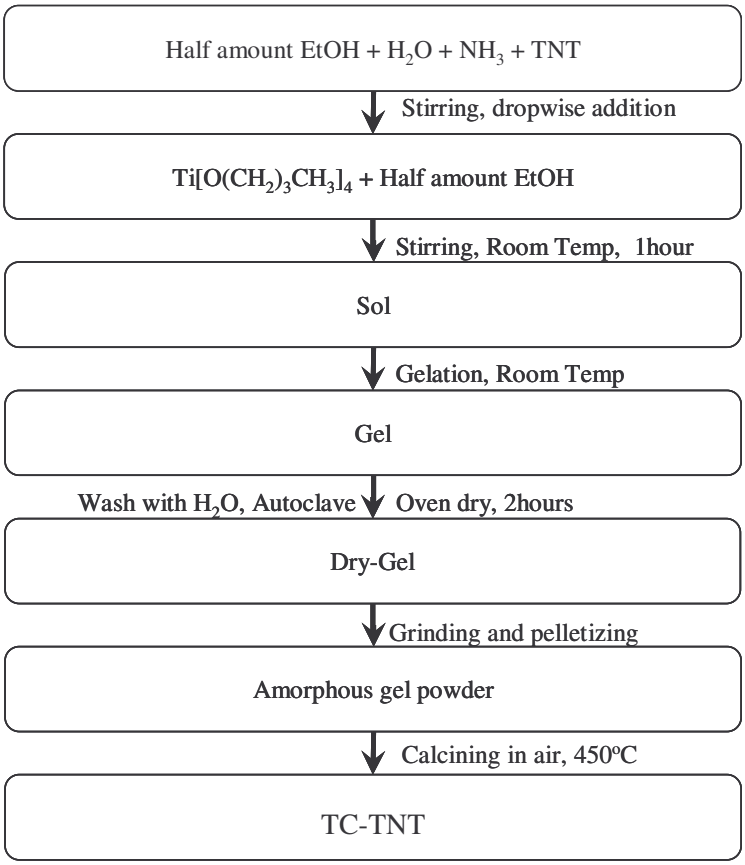

Figure 3.1 Flow chart of the preparation of titania coated titanate nanotubes by sol-gel method

Titanium(IV) butoxide (98%, Sigma Aldrich), $Ti[O(CH_2)_3CH_3]_4$, was used as the reactant. Nitric Acid (55%, Merck), HNO_3, was added to catalyze the hydrolysis reaction of $Ti[O(CH_2)_3CH_3]_4$ in water. A ratio of 1:5 (wt/wt) = TNT:$Ti[O(CH_2)_3CH_3]_4$ was used. The TNT material was dissolved in a mixture of $Ti[O(CH_2)_3CH_3]_4$ with half the prescribed amount of anhydrous ethanol (EtOH) in order to avoid the hydrolysis reactions. Water and HNO_3 dissolved in the remaining EtOH was added drop-wise to the ethanolic solution of butoxide while stirring continuously with a magnetic stirrer bar at ambient temperature as demonstrated in Figure 3.2. The molar ratio of the reactants used was: $Ti[O(CH_2)_3CH_3]_4$:H_2O:EtOH:HNO_3 = 1:4:15:0.3, as suggested in the literature by Ding *et al* [5].

During the addition of H_2O:EtOH:HNO_3 to $Ti[O(CH_2)_3CH_3]_4$ a sol formed. The sol was allowed to gelatize at room temperature until a clear solid gel was formed. The

corresponding gel was then washed with deionised water and centrifuged to remove excess butoxide. The wet gel was dried in an oven at 120 ^{o}C for 2 hours. This material was then ground and pelletized to the required particle size (500-850 μm). Calcination of this material was performed in air at 450 ^{o}C for 6.5 hours.

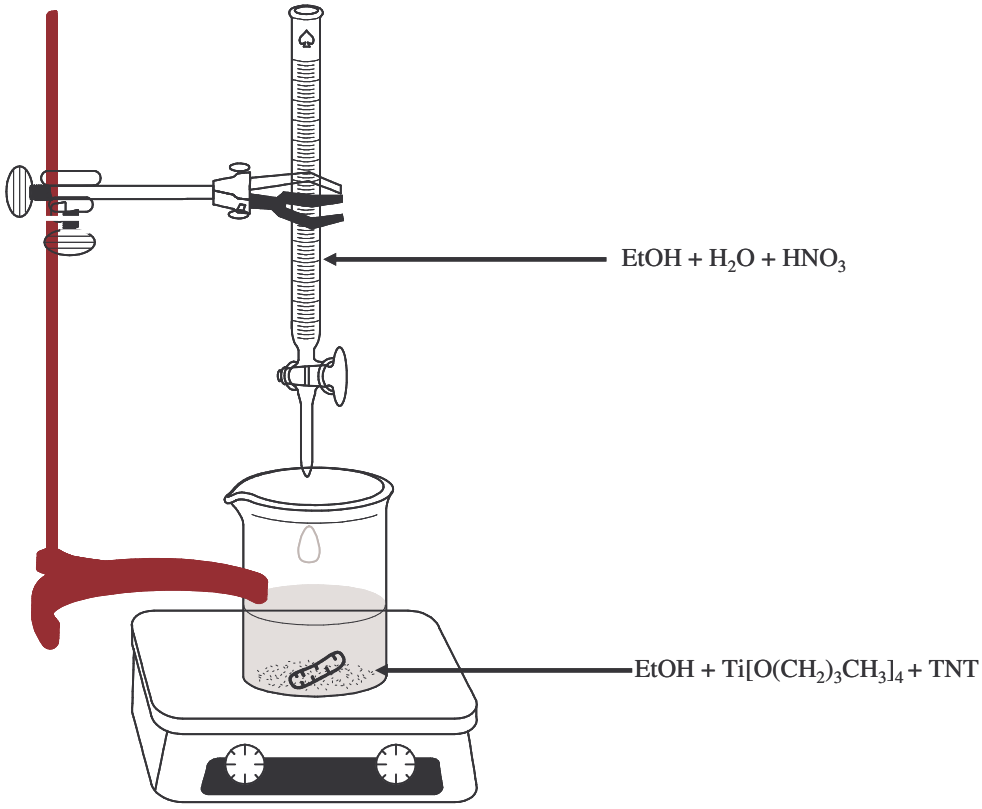

Figure 3.2 A schematic representation of the set up for the preparation of coated titanate nanotubes by the sol-gel method

3.2.4 Catalyzed preparation of 10%Co/support by a pH-controlled precipitation method

A 4M NH_4OH solution was added drop wise to a 0.2 M solution of cobalt nitrate, $Co[(NO_3)_2{\cdot}6H_2O$, in a beaker using a pipette until a required pH (7.8 ± 0.1) was achieved. Using a centrifuge the precipitate was separated from the liquid. This procedure was used to avoid agglomeration. The precipitate was re-slurried in 15 ml of ethanol and used to fill the pores of the support. The support was impregnated with the precipitate slurry. The

supported catalyst precursor was spread thinly on a plate and was dried overnight at 120°C in a static oven. The catalyst precursor was then calcined at 300 ^{o}C for 6.5 hours in air using a heating rate of 5 ^{o}C/minute. Three different catalysts were prepared by this method and these are hereby described to as 10%Co/TN, 10%Co/TNT and 10%Co/TC-TNT, these refer to 10% cobalt loaded on titania nanoparticles, titanate nanotubes, titania coated titanate nanotubes supports, respectively. These catalysts were then ready to be characterized and tested in order to understand their catalytic properties.

3.2.5 Catalyzed preparation of 20%Co/supports by an incipient wetness impregnation method

The incipient wetness impregnation (IWI) method was used to prepare a 20% cobalt loaded catalyst. Catalysts with 10% cobalt loadings that were previously prepared by a pH controlled precipitation method were further impregnated with a solution of cobalt nitrate by means of the IWI method to give a metal loading of 20% on the support. The supported precursors were oven dried overnight at 120 ^{o}C. The catalyst precursors were then calcined at 300 ^{o}C for 6.5 hours in air using a heating rate of 5 ^{o}C/minute. These catalysts were called 20%Co/TN, 20%Co/TNT and 20%Co/TC-TNT, respectively. These catalysts were also further characterized and tested in order to understand their catalytic properties.

3.3 Characterization of catalysts and supports

For a better understanding of the catalyst properties, both the supports and the catalysts were characterized by the following characterization techniques; Brunauer-Emmett-Teller surface area analysis method (BET), Thermogravimetric analysis (TGA), Transmission electron microscopy (TEM), X-ray diffraction spectroscopy (XRD), X-ray fluorescence (XRF) spectroscopy and Temperature programmed reduction (TPR). To determine the Co dispersion on supports a H_2-chemisorption analysis was conducted on all six catalysts. These catalysts were also evaluated in a Fischer-Tropsch synthesis (FTS) reaction.

3.3.1 Brunauer-Emmett-Teller method (BET)

About 0.2 g of samples were degassed in N_2 at 120 ^oC for 4 hours prior to analysis using a Micromeritics Flow Prep 060, sample degas system. The surface areas and pore size distributions were then obtained at 120 ^oC. The pore size distribution with specific surface areas of the calcined supports and supported catalysts, were determined via N_2 adsorption/desorption according to the BET method using a Micromeritics Tristar, surface area and porosity analyzer.

3.3.2 Thermogravimetric analysis (TGA)

A TGA study was performed on the supported catalysts and supports using a Perkin Elmer Pyris 1 TGA. The samples were purged with N_2 gas at a rate of 20 ml/minute. The samples were heated at a rate of 5 ^oC/minute from 25-800 ^oC and then the thermographs were collected from recorded PC equipment. The sample mass that was used varied between 0.1 and 0.3 g.

3.3.3 Transmission Electron Microscopy (TEM)

The morphologies of the calcined supports and catalysts were determined using a JEOL 100S transmission electron microscopy instrument operated at 80 kV. Samples were ultrasonically suspended in methanol and a drop of each sample was transferred onto a carbon coated copper grid placed on a filter paper. The samples were allowed to dry in air at room temperature before analysis. During analysis a magnification in the range 10 - 200 000 was used.

3.3.4 X-ray diffraction spectroscopy (XRD)

Average metal sizes, phase compositions of the support and catalysts were determined by means of XRD analysis technique. X-ray diffraction measurements were done on a Bruker AXS D8 machine with a primary beam Göbel mirror, a radial soller slit, a V Åntec-1 detector using Cu-Kα radiation at 40 kV and 40 mA. The scan range was $5^o < 2\theta$

< 90° in 0.021 steps, using a standard speed with an equivalent counting time of 14.7 seconds per step. The obtained diffraction peaks were then compared with those of standard compounds reported in the Diffrac^{plus} evaluation package using EVA (V11.0, rev .0, 2005) software package.

3.3.5 X-ray Fluorescence (XRF) spectroscopy

The XRF measurements were carried out on a PW 12404 Panalytical model instrument. Powder samples were mixed with 2% Mowiol binder before being pressed. The X-ray source used was a rhodium tube.

3.3.6 Temperature-Programmed Reduction (TPR)

Since catalyst reduction is a very critical step in FTS, it was necessary to study the reduction behaviors of the cobalt loaded-catalysts. The reduction temperatures required for the reduction of cobalt oxide to metallic cobalt before FTS reaction were determined. This confirmation is required since metallic cobalt is the active component for a successful FTS reaction.

Calcined samples, about 0.2 g and 0.1 g for 10% and 20% Co loaded catalysts, respectively, were placed in a U-shaped quartz reactor. Prior to analysis the samples were degassed in N_2 at 1 bar pressure and a temperature of 150 ^{o}C (10 ^{o}C/min) for 30 minutes. After cooling a reducing gas that contained 5% H_2 in argon was passed over the sample at a flow rate of 30 ml/min at 1 bar pressure while the temperature was raised to 800 ^{o}C at a heating rate of 7.5 ^{o}C/min. The resulting TPR profiles were then collected from recorded PC equipment.

3.3.7 H_2 chemisorption and O_2 titration analysis

Chemisorption analysis is a very useful technique that can be used to determine metal dispersion on a support, metal crystallite size, degree of reduction and the number of adsorption sites. This is achieved by adsorbing gaseous molecules onto catalyst samples.

The analysis procedure gives information on the number of active metal sites within the catalyst.

H_2 chemisorption analysis was performed with a Micromeritics ASAP 2020, surface area and porosity analyzer instrument. The calcined pre-weighed catalyst samples (about 0.5 g) were placed in a U-shaped quartz tube sample holder which was evacuated under vacuum. These samples were degassed using pure He at 150 ^{o}C. Evacuation of He molecules was then performed at 100 ^{o}C before reduction at 425 ^{o}C in pure H_2 for 8 hours took place. After the initial, reduction the catalysts were further reduced in pure H_2 at a temperature that was 25 ^{o}C below the reduction temperature (425 ^{o}C) for 1 hour prior to analysis. All physisorbed H_2 molecules were evacuated before measuring adsorption isotherms for H_2 at 100 ^{o}C. Detailed information of the analysis conditions procedure is given in Table 3.2. The conditions obtained from the TPR experiments were used as cobalt oxide reduction in the reactor. The total H_2 uptake was determined by extrapolating the straight-line portion of the adsorption isotherm to zero pressure.

After H_2 chemisorption was conducted for each sample, the same sample was evacuated using He at 100 ^{o}C to remove the adsorbed H_2. Evacuation of all weakly adsorbed He molecules was then performed at 400 ^{o}C after which O_2 titration was carried out using a stream of pure O_2 at 400 ^{o}C. Detailed information of the O_2 titration analysis conditions procedure is also given in Table 3.2. Extents of reduction were calculated using the O_2 uptake that was obtained by extrapolating the straight-line portion of the adsorption isotherm to zero pressure, this being the method that was proposed by Bartholomew and Farrauto [6]. The reaction of reduced cobalt with oxygen was considered to proceed to Co_3O_4 [7]. The adsorption measurements were reproducible and had an error bar of ± 5%.

Table 3.2 H_2 analysis and O_2 titration conditions for cobalt containing catalysts

Condition	Ramp rate /^{o}C/min	Temperature /^{o}C	Time /min
Analysis:			
Evacuate He	5	150	30
Evacuate	10	100	10
Flow H_2	2	425	480
Flow H_2	2	400	60
Evacuate	2	400	240
Leak	---	35	10
Evacuate	---	35	10
Analyze H_2[a]	1	100	---
O_2 titration:			
Evacuate He	10	100	30
Evacuate	10	400	30
Analyze O_2[b]	10	400	---

[a] Pressure points: 100,150, 200, 250, 300, 350, 400, 425, and 450 mmHg

[b] Pressure points: 100, 200, 300, 400 and 450 mmHg

Metal dispersions ($D\%$) and crystallite diameters (d_p) were calculated using the equations that were proposed by Bartholomew *et al.* [8, 9, 10]. These calculations were based on assumption that cobalt metal was present as spherical particles of uniform size and the assumptions that unreduced cobalt was present in a separate dispersed layer in intimate contact with the support [7]. Accordingly, percentage dispersion was calculated according to the following equation (3.1):

$$D\% = \frac{1.179X}{Wf} \tag{3.1}$$

where X is the total H_2 uptake in millimoles per gram of catalyst, W the weight percentage of cobalt and f the cobalt reduction extent determined from O_2 titration.

The average crystallite diameters (d_p) were calculated from $D\%$, assuming spherical metal crystallites with a site density (s) of 14.6 atoms/nm^2 and the following formula (3.2) was used:

$$d_p = \frac{6.59s}{D\%} \tag{3.2}$$

The number (N_s) of active cobalt metal sites was calculated using the same formula (3.3) that was used by Webb *et al.* [11]:

$$N_s = \frac{V_m \times N_A \times F_s}{V_{mol}} \tag{3.3}$$

where N_A is the Avagrado's number, V_m the quantity of H_2 irreversibly adsorbed on the sample (monolayer volume) and V_{mol} the molar volume of the adsorptive gas. F_s is the stoichiometry factor and was considered to be equal to 2 for H_2 on cobalt. The FT reaction turnover frequency (*TOF*) was evaluated by combining the number of active cobalt sites with the rate of CO conversion during the FT reaction [12].

The formula is as follows:

$$TOF = \frac{-r_{CO} \times N_A}{N_s} \tag{3.4}$$

where $-r_{CO}$ is the rate of CO consumption in (mol/s) and the *TOF* is therefore expressed in (s^{-1}).

3.4 Fischer-Tropsch Synthesis experiments

The rector system was constructed as part of the MSc study.

3.4.1 Reactor system and experimental setup

A schematic diagram for the reactor system is shown in Figure 3.3. All the gases that were used were supplied by AFROX (African Oxygen) Ltd. The gas cylinders were accompanied by a certificate that indicated the purity of the components available in a particular gas mixture. The gases used for the catalyst characterization and catalyst reduction prior to the FTS were Ultra High Purity (UHP) grade gases (99.997% purity). Gas cylinders that contained $H_2/CO/N_2$ mixtures (syn-gas) (0.60/0.30/0.1 vol. Purity: 99.99%) were used to supply the reactant gas stream to the catalyst. N_2 was used as an internal standard in order to ensure accurate mass balances. Ar gas was used as carrier gas for both the flame ionization detector (FID) and the thermal conductivity detector (TCD) gas chromatographs (GC). Pressure regulators on the cylinders were used to set the pressure on the system. The system was equipped with two pressure gauges, one installed between the gas cylinders and the reactor indicated the pressure of gas that entered the reactor, while the other one was installed between the cold trap and the TCD-GC, set at atmospheric pressure was used to allow consistent volumetric gas flow rates that were measured with the soap bubble meter connected to the FID-GC. All gas lines after the reactor were kept at 150 ^{o}C. Two product traps were installed below the reactor; a hot trap which was heated at 150 ^{o}C was used to collect wax while the cold trap (ambient temperature) was used to collect liquid products (oil and water). The gaseous products were directed to the GC's which were connected in series (on-line) for analysis. The reactor temperature and line temperatures were controlled electronically by using electronic temperature controllers connected to the system.

All the lines used in the system consisted of 1/4" and 1/8" stainless steel tubing and the fittings used were Swagelock stainless steel fittings. The on/off valves were SS Valco valves with viton seals and the needle valves were Whitey valves. The system was also equipped with an integrator (Varian Spectra-Physics, SP 4290) which was used to collect

all chromatograms from both the FID-GC and the TCD-GC. A dialog program as shown in Table 3.3 that entailed injection times, cooling times, chart speeds, attenuations (peak intensities) and noise levels was appropriately typed on the integrator before each FTS run.

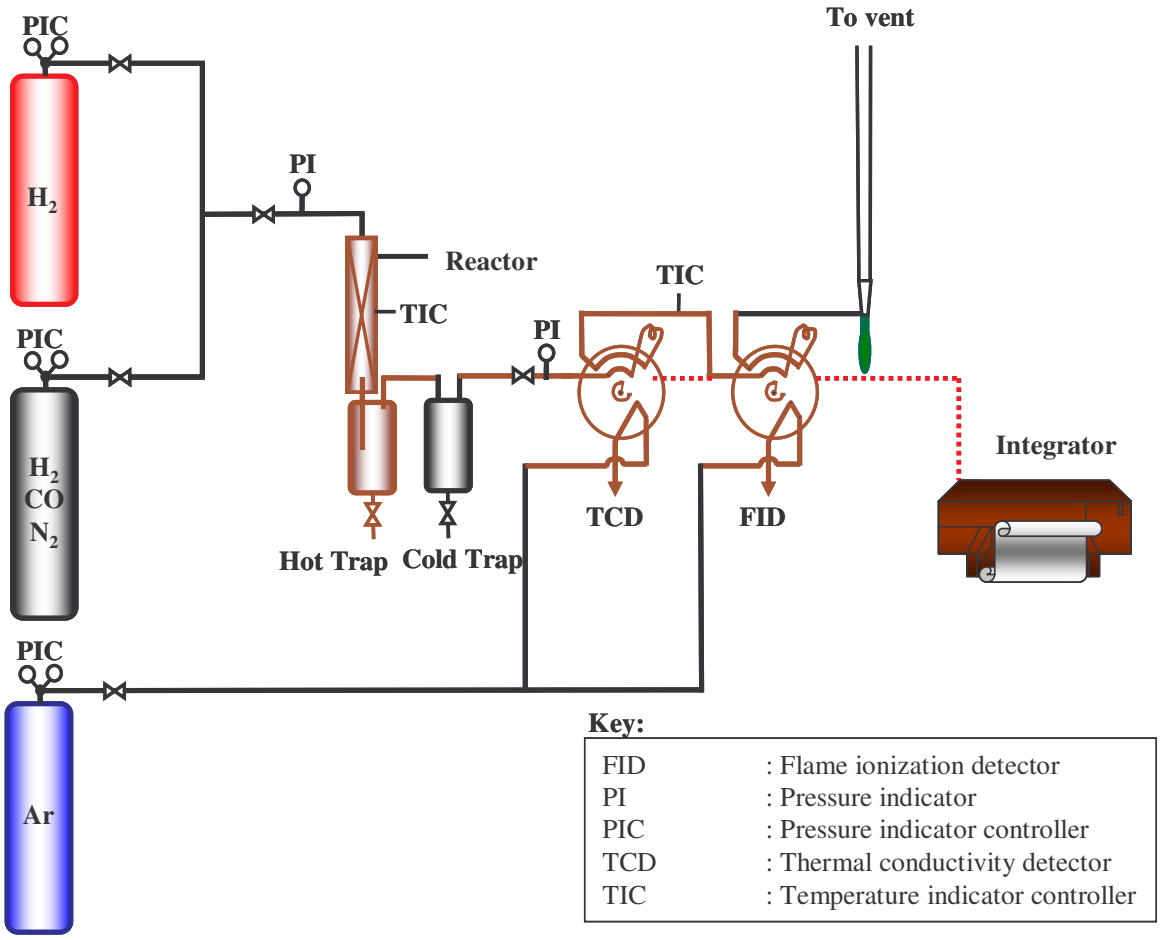

Figure 3.3 A schematic diagram for the reactor system

Table 3.3 A dialog program used in TCD and FID analysis

Dialog:
File Name = TCD (or FID)

RT	Function	Function Value
TV = 0.1	PF = AT	PV = 16
TV = 0.2	PF = PT	PV = 350
TV = 0.3	PF = CS	PV = 0.5
TV = 60	PF = ER	PV = 0

3.4.2 Reactor and catalyst packing

In Figure 3.4 a diagrammatic representation as well as a digital image of a stainless-steel fixed bed reactor (FBR) used is shown. The reactor comprised of three zones, the pre-heater zone where the gas entering is heated through a bed, the catalyst chamber where the reaction takes place in the catalyst bed and the reactor bottom, the region below the catalyst bed. The thermocouple was inserted into the thermocouple well touching the catalyst embedded on quartz wool. Gasses which emerged from the gas cylinders entered through the gas feed inlet of the reactor to the catalyst bed and the products were collected through the gas feed outlet which was connected to the two knockout ports (product traps). Catalyst mass loadings (1-2 g) were chosen to ensure that the gas would flow through the catalyst bed without any blockages. In essence the particle sizes (d_p) of the support and therefore that of the catalytic material were designed in such a way that they are smaller than a tenth of the inner diameter of the reactor ($ID_{reactor}$) as required by formula (3.5) below. This ensured ideal plug flow behavior with negligible wall effects [13], yet the flows were large enough to allow mobility of the gasses through the pores between packed catalytic particles in the reactor.

$$\frac{ID_{reactor}}{d_p} > 10 \qquad (3.5)$$

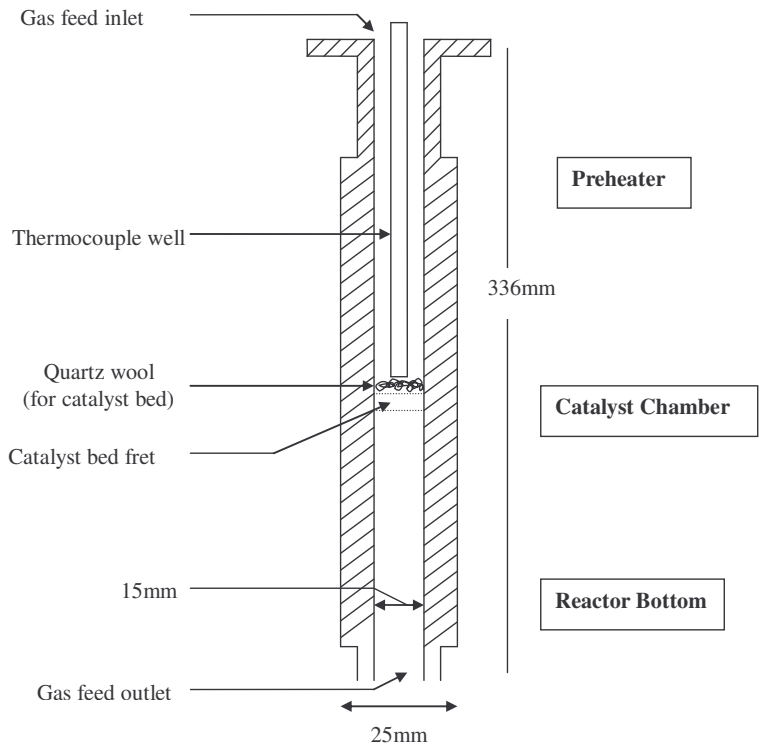

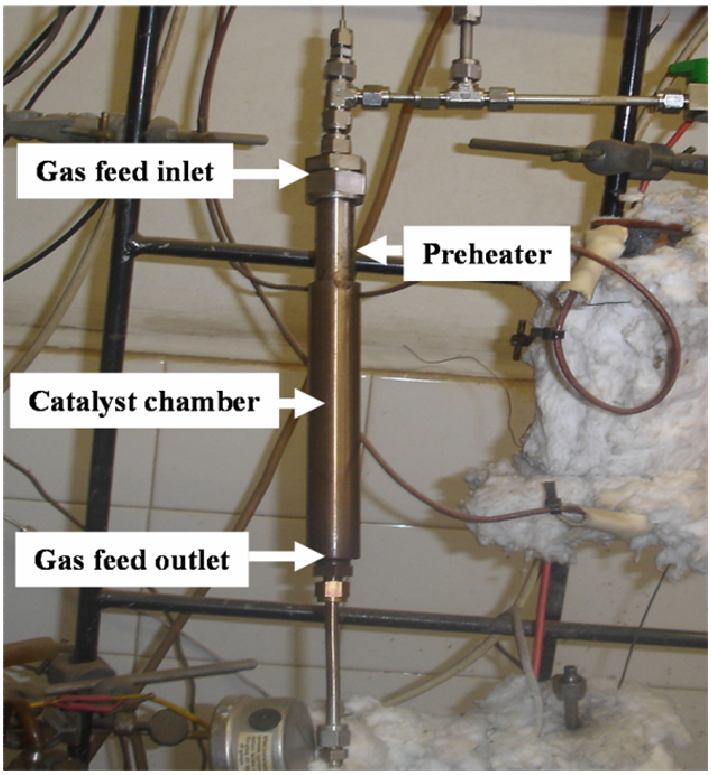

Figure 3.4 A diagrammatic representation (top) and a digital image (bottom) of a stainless-steel fixed bed reactor that has been used

3.4.3 Experimental procedure for catalyst evaluations

A catalyst sample (about 1 g to 2 g) was reduced *in-situ* in pure H_2 at 1 bar pressure with a flow rate of 45 ml/min/g for 16 hours at 300 ^oC using a heating rate of 5 ^oC/min. During the reduction step the shut-off valve for the syn-gas bottle was closed so as to stop syn-gas flow to the reactor. After cooling, the H_2 shut-off valve was closed while syn-gas valve was opened. The pressure on the syn-gas gauge was set to 1 bar and the TCD was calibrated with syn-gas with a standard concentration so as to determine the amount of syn-gas entering the reactor. This calibration was continued until consistent areas of H_2, N_2 and CO were obtained. The syn-gas pressure was then slowly adjusted to 8 bar at a volumetric flow rate of 12 ml/min/g while the temperature was ramped to the reaction temperature (230 ^oC, unless otherwise stated) at a heating rate of 5^oC/min.

3.5 Product analysis

3.5.1 Gas chromatographic analysis

Product analysis was divided into two segments. The first segment involved analysis of gaseous products on-line using two GC's; a thermal conductivity detector (TCD) and a flame ionization detector (FID). The second segment, an off-line FID-GC analysis, involved syringe injection (0.2 μl) of liquid (oil) and wax products that were collected from the knockout traps. The conditions used are given in Table 3.4. A typical GC trace of product gas analysis is shown in Figure 3.5. The analyses of oil and wax products were performed using different temperature programs on an off-line FID-GC.

Table 3.4 Conditions for gas chromatographic analyses

Gas chromtoraph	**PYE Unicam (Series 204)**
Detector	TCD, T = 220 ^{o}C
Column type	Packed, stainless steel, 2m x 2.2mm, O.D = 1/8"
Stationary phase	Carbosieve S-II, 60-80 mesh
Sample valve temperature	150 ^{o}C
Carrier gas	Argon
Flow rate	20 ml(NTP)/min
Oven temperature	250 ^{o}C (isothermal)
Products analysis	H_2, N_2, CO,CH_4, CO_2
Gas chromtoraph	**Hewlett Packard 5890**
Detector	FID, T = 220 ^{o}C
Column type	Packed, stainless steel, 1.5 m x 2.2 mm, O.D = 1/8"
Stationary phase	ZB-5, 80/100 mesh
Sample valve temperature	150 ^{o}C
Carrier gas	Argon
Flow rate	20 ml(NTP)/min
Oven temperature	250 ^{o}C (isothermal)
Products analysis	C_1 - C_8
Gas chromtoraph	**Varian 3700**
Detector	FID, T = 350 ^{o}C
Column type	30 m x 5 μFT, O.D.= 0.53 mm
Stationary phase	ZB-1
Sample valve temperature	250 ^{o}C
Carrier gas	Air
Flow rate	30 ml(NTP)/min
Oven temperature programme	
Oil:	Heat to 60 ^{o}C at 10 ^{o}C/min, heat to 300 ^{o}C at 12.5 ^{o}C/min, hold at 300 ^{o}C for 30 min
Wax:	Heat to 220 ^{o}C at 74 ^{o}C/min, heat to 300 ^{o}C at 10 ^{o}C/min, hold at 300 ^{o}C for 240 min
Products analysis	C_5 - C_{18}

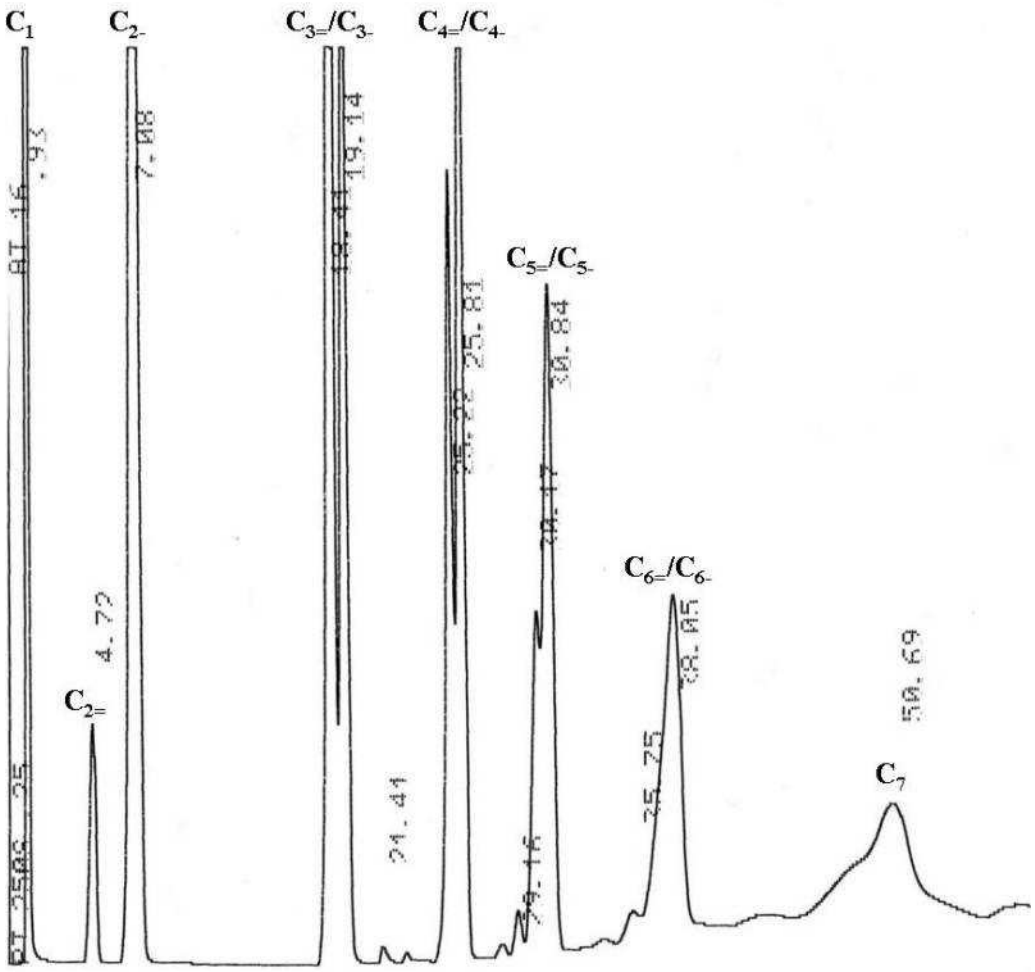

Figure 3.5 A typical FT spectrum for gaseous products obtained from an FID GC

3.5.2 Data work-up

The calculations that were used to compute the mass balance are similar to those used by, Nijs *et al*. [14], Mokoena [15], Duvenhage [16], Price [17] Mabaso [18] and Bahome [19]. Before every FTS reaction, the reactants, CO and H_2 are bypassed through the reactor and samples are analyzed. This then represents the amount of reactants fed into the reactor. The mass balance was performed on carbon and oxygen. Mass balance data of 100 ± 5% was accepted as adequate. The amount of carbon and oxygen entering the reactor equals the amount of carbon and oxygen reacted to form products plus the unreacted carbon and oxygen leaving the reactor.

The % Mass balance was calculated using equation (3.6) below:

$$\% \text{ Mass balance} = \frac{N_X + N_Y}{N_Z} \tag{3.6}$$

where N_x = moles of reacted carbon and oxygen

N_y = moles of unreacted carbon and oxygen

N_z = moles of carbon and oxygen entering the reactor to give products

A calibration gas containing a standard composition of CH_4, C_2H_6, C_2H_4, CO, CO_2, and N_2 was used to calibrate the FID and TCD data. This calibration was carried out once every six months. The hydrocarbon product areas obtained from the FID data were corrected for C_2H_4 (olefins) and C_2H_6 (paraffins) by using the response factors based on those reported by Dietz [20], and Scanlon *et al.* [21].

In all catalyst evaluations for FTS the reaction steady state was normally reached 24 hours after the reaction have been started. At that point the oil and wax traps were decanted and the mass balance calculations were commenced. The time recorded at the end of the mass balance period was used to calculate the rates of the reaction (i.e. FTS, CO conversion and CO_2 formation). The oil and water mixture from the cold trap and the wax from the hot trap were collected successively and weighed. The oil was separated from water before analysis on an offline GC.

The %CO conversion was calculated using equation (3.8) below:

$$\%CO = \left[\frac{CO_{in} - CO_{out} \times \frac{N_{2\,(in)}}{N_{2\,(out)}}}{CO_{in}} \right] \tag{3.7}$$

where CO_{in} and $N_{2\,(in)}$ are areas of CO and N_2 peaks obtained in the syngas, respectively. CO_{out} and $N_{2\,(out)}$ are areas of CO and N_2 peaks obtained from the gaseous products streams, respectively.

The product selectivity (S_i) for hydrocarbons was calculated for component x_i using equation (3.8) as follows:

$$S_i = \left[\frac{\text{mass component } x_i}{\sum x_i} \right] \times 100\% \tag{3.8}$$

The individual rates of reaction for FTS (r_{FTS}) and water gas shift WGS (r_{WGS}) were calculated from experimentally obtained quantities as:

$$r_{WGS} = r_{CO_2} \tag{3.9}$$

$$r_{FTS} = r_{CO} - r_{CO_2} \tag{3.10}$$

where r_{CO_2} is the rate of carbon dioxide formation and r_{CO} is rate of carbon monoxide conversion.

Since C_2H_4 and C_2H_6 were the only gaseous products that could be separated by the column, the olefin to paraffin ratio for C_2 could be determined (x_2) and was given as shown in equation (3.11):

$$\text{Olefin to Paraffin ratio } x_2 = \frac{\text{Mass olefin } x_2}{\text{Mass total hydrocarbon } x_2} \tag{3.11}$$

3.6 References

1. M. E. Dry, The Fischer-Tropsch Synthesis, In: J. R. Anderson, M. Boudart (Eds.), *Catalysis Science and Technology*, Vol. **1**, Springer-Verlag, New York, 159 (1981)
2. T. Kasuga, M. Hiramatsu, A. Hoson, T. Sekino, K. Niihara, *Langmuir*, **14**, 3160 (1998)
3. X-Y. Liu, N. J. Coville, *S. Afr. J. Chem*., **58**, 110 (2005)
4. L. M. Sikhwivhilu, PhD Thesis, University of the Witwatersrand, Johannesburg (2007)
5. X.-Z. Ding, X.-H. Liu, *Materials Science and Engineering*, **A224**, 210 (1997)
6. C. H., Bartholomew, R. J., Ferrauto, *J. Catal.*, **45**, 41 (1976)
7. R. L., Chin, D. M., Hercules, *J. Phys. Chem*., **86**, 360 (1982)
8. C. H., Bartholomew, R. B., Pannell, *J. Catal.*, **65**, 390 (1980)
9. C. H., Bartholomew, B. P. Richard, J. L. Butler, *J. Catal.*, **65**, 335 (1980)
10. D. G. Mustard, C. H. Bartholomew, *J. Catal.*, **46**, 340 (1981)
11. P. A. Webb, C. Orr, Analytical methods in fine particle technology, *Micromeritics* 229 (1997)
12. K. Jalama, N. J. Coville, D. Hildebrandt, D. Glasser, L. L. Jewell, *Appl. Catal. A: General*, **326**, 164 (2007)
13. G. Ertl, H. Knözinger, J. Weitkamp, In: G. Ertl, H. Knözinger and J. Weitkamp (Eds.): *Handbook of heterogeneous catalysis.* VCH, Weiheim, Federal Republic of Germany, 439 (1997)
14. H. H. Nijs, P. A. Jacobs, *J. Chrom. Sci*., **19**, 40 (1981)
15. E. M. Mokoena, PhD Thesis, University of the Witwatersrand, Johannesburg (2005)
16. D. J. Duvenhage, PhD Thesis, University of the Witwatersrand, Johannesburg (1992)
17. J. G. Price, PhD Thesis, University of the Witwatersrand, Johannesburg (1994)
18. E. I. Mabaso, PhD Thesis, University of Cape Town, Rodenbosch (2005)
19. M. C. Bahome, PhD Thesis, University of the Witwatersrand, Johannesburg (2007)

20. A. W. Dietz, *J. Gas Chrom.*, **62** (1967)

21. J. T. Scanlon, D.E. Willis, *J. Chrom. Sci.*, **23**, 33 (1985)

Chapter 4

4. Results and discussion

It this chapter the results obtained in this study are discussed. The results for discussion purposes are subdivided into three parts, viz. the characterization of supports materials, the characterization of the catalysts and finally evaluation of the reactor studies using the new catalysts in the Fischer-Tropsch synthesis.

4.1 Characterization of support materials

4.1.1 TEM analysis of support materials

Figures 4.1 and 4.2 compare the low magnification transmission electron microscopy (TEM) micrographs of the three calcined supports; titania nanomaterials (TN), titanate nanotubes (TNT) and titania coated titanate nanotubes (TC-TNT). The particles and tubes are relatively small and are scaled in the nano-range. It is apparent that the resulting three differently derived powdered supports have different structural and morphological properties.

The TN consisted of an amorphous cluster of TiO_2 nanoparticles, as depicted in Figure 4.1. The particles ranged from tens to hundreds of nanometers in size. This powdered material was prepared by simply mixing commercial TiO_2 powder with deionised water, followed by drying and calcination (350 ^{o}C).

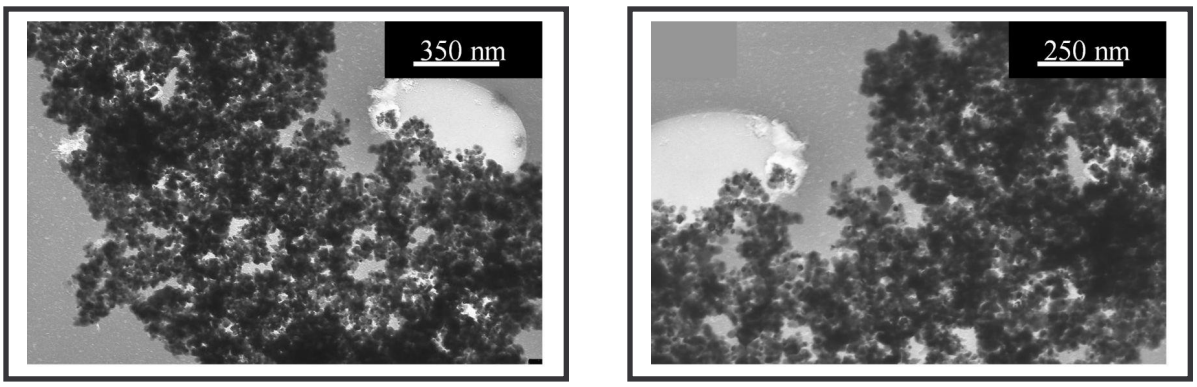

Figure 4.1 Low resolution TEM micrographs of titania nanoparticles (TN)

Preparation of the high surface area potassium titanate nanotubes (TNT) was successful, as depicted in Figure 4.2 (a-d). The effect of the washing period (used in order to remove excess KOH that was used to prepare this material) on the morphological and structural properties was varied by preparing three different sample batches. This washing effect is illustrated in Figure 4.2 wherein the TEM images of the three different samples washed for 1½, 2 and 3 weeks are shown. In all cases the TNTs were prepared by reaction in an autoclave for 24 hours followed by aging for 24 hours at room temperature. When the samples were washed for short time periods some of the unreacted TiO_2 materials were observed (Figure 4.2 (a) and (b)). These unreacted TiO_2 particles are identical to those of TN as seen in Figure 4.1 above. It was realized that the samples needed to be washed for at least 3 weeks to achieve complete formation of tubes (Figure 4.2 (c) and (d)). It appears that further reaction occur during the washing procedure used. This is possible as the washing process is laborious and requires allowing the product to be stirred in water for long period of time. When the sample was washed for about 3 weeks the observed TNT material consisted of clean tubular materials made up of coiled TiO_2 sheets. These tubular materials were randomly distributed in different directions. The diameters of the tubes ranged from tens to hundreds of nanometers, while the lengths of these tubes varied from 60 to about 200 nm. The $TNT_{3\ weeks}$ material is the one that will be referred to as TNT in this dissertation and is the one that was fully characterized and employed in the Fischer-Tropsch synthesis.



(a) Tinanate nanotubes ($TNT_{1\ 1/2\ weeks}$)

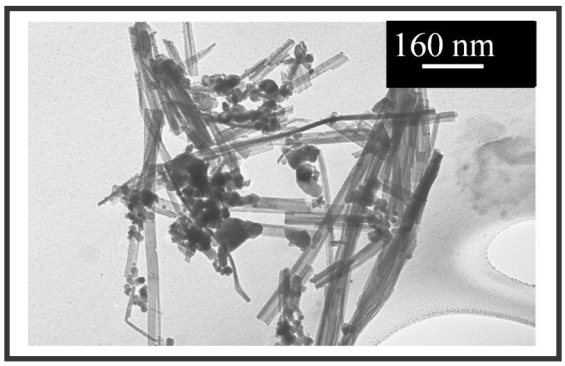

(b) Tinanate nanotubes ($TNT_{2\ weeks}$)

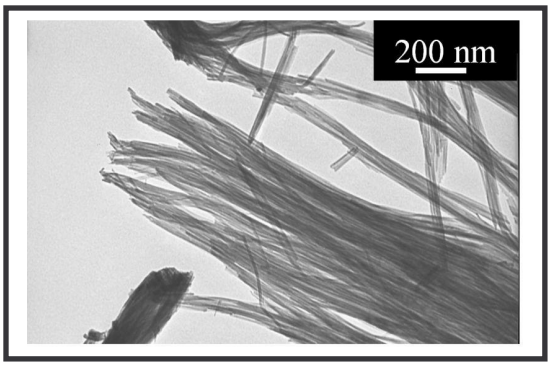

(c) Tinanate nanotubes ($TNT_{3\ weeks}$)

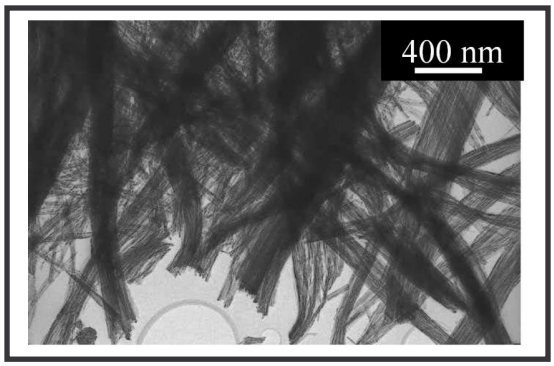

(d) Tinanate nanotubes ($TNT_{3\ weeks}$)

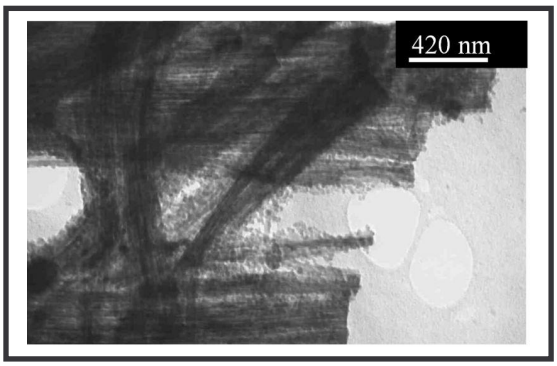

(e) Titania coated tinanate nanotubes (TC-TNT)

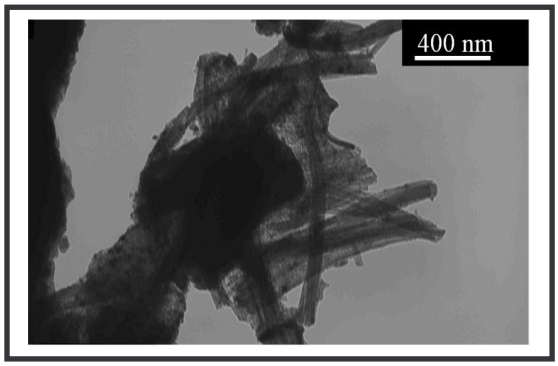

(f) Titania coated tinanate nanotubes (TC-TNT)

Figure 4.2 Low resolution TEM micrographs of tinanate nanotubes (TNT) and titania coated titanate nanotubes (TC-TNT) prepared by different methodologies

Coating of this tubular material (TNT) with TiO_2 by the sol-gel method to form the titania coated potassium titanate nanotubes (TC-TNT), as shown in Figures 4.2 (e) and (f) was successful. This was confirmed by the appearance of a TiO_2 coating and the formation of small black coating of particles representing the sol-gel derived TiO_2 over the surface of the TNT. This is more readily seen in an expanded TEM micrograph of the TCNT (Figure 4.3).

The sizes of these TiO_2 particles ranged between tens to hundreds of nanometers in size. The coating can also be readily seen (compare Figures 4.2(f) and 4.2(c). The particles also acted as a coating for the tubes. However, it is necessary to mention that the TNTs prepared in this work may not have been fully coated since some layers of the tubes appeared uncoated under the microscope (not shown in this case). This suggests that the ratio of butoxide to titanate (5:1) used to prepare these material was insufficient to achieve maximum TiO_2 coating.

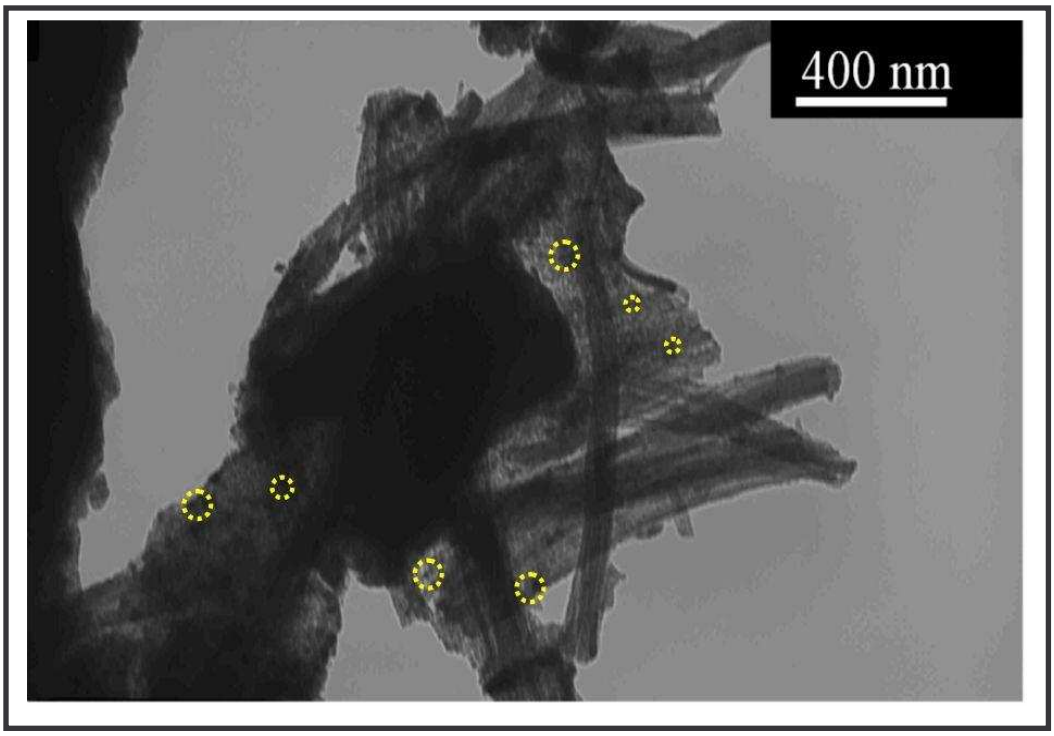

Figure 4.3 Low resolution TEM micrograph of titania coated titanate nanotubes (TC-TNT) (The dashed circles show that the sol-gel derived TiO_2 particle sizes are not uniform)

4.1.2 Porosity and surface area analysis of support materials

The surface area and porosity measurements of the support materials are tabulated in Table 4.1. The TN support had a measured surface area of 47.2 m^2/g. This is a typical TiO_2 surface area since the commercial material is reported to have a surface area of ≈50 m^2/g [1]. BET measurements confirmed that a high surface area TNT support was achieved. The highest surface area for the TNT material was achieved when the preparation solution was washed

for a long period of time with deionised water during the preparation steps (to see the effect of washing on pH, conductivity and the surface area of the TNTs see Table 3.1 in Chapter 3). The highest measured surface area obtained for this material ($TNT_{3\ weeks}$) was 231 m^2/g.

The coating of this material (TNT) with TiO_2 at ambient temperature (25 ^oC) to form TC-TNT reduced the surface area to 166 m^2/g. However, when the TCNT was prepared at 35 ^oC, a higher surface area was obtained (222 m^2/g). This surface area is comparable to that obtained on ($TNT_{3\ weeks}$). The reason for the decrease in the surface area of TC-TNT when prepared at ambient temperature could be that the sol-gel reaction forming a TiO_2 coat on the TNT support was not yet complete since it was a slow reaction. However, when the reaction temperature was increased to 35 ^oC then the reaction rate was also increased and thus the higher surface area was achieved.

Table 4.1 Porosity measurements of support materials

Support	BET SA (S_{BET}) /m^2/g	Pore volume (p_v) /cm^3/g	Pore diameter (p_d) /nm
TN	47.2	0.42	35.5
$TNT_{1\ 1/2\ weeks}$	187	0.49	6.3
$TNT_{2\ weeks}$	214	0.42	7.6
$TNT_{3\ weeks}$	231	0.37	10.2
TC-TNT	166	0.14	3.3
$TC\text{-}TNT_{35°C}$	222	0.25	4.3

The average pore volume, p_v (0.42 cm^3/g), and the pore diameter, p_d (35.5 nm) of TN were larger than those obtained for TNT (with p_v = 0.37 cm^3/g, p_d = 10.2 nm), TC-TNT (with p_v = 0.14 cm^3/g, p_d = 3.3 nm) and $TC\text{-}TNT_{35°C}$ (with p_v = 0.25 cm^3/g, p_d = 4.3 nm) materials as shown in Table 4.1 above. The pore diameter of the uncoated tubular material (TNT) was larger than those of the coated tubular materials (TC-TNT and $TC\text{-}TNT_{35°C}$).

In general, the smaller pore diameter correlates with the larger BET surface area. Also the surface area increased when tubular materials were produced. This is associated with the expectation that the average BET surface areas of the tubes (TNT, TC-TNT and $TC\text{-}TNT_{35°C}$) will include both the outer and the inner surface areas of the curled tubular materials. In the case of TN the surface area is achieved from only the external average surface area of the

spherical particles. The results for the surface area of TC-TNT show that the average surface area obtained between the curled tubular materials (inner and outer surface area) is slightly lower than that of TNT since the pores were blocked by TiO_2 (i.e. note the lower pore diameters and pore volumes of TC-TNTs than for TNT).

4.1.3 A thermal analysis of support materials using TPR and TGA

The reducibility behavior of TN, TNT and TC-TNT support materials was characterized by temperature programmed reduction (TPR) analysis in a 5% hydrogen/argon mixture. Figure 4.4 shows the TPR profiles obtained from calcined (350 ^{o}C) TN and uncalcined TNT and TC-TNT support materials. The TPR profiles of all supports did not show any hydrogen consumption peaks. These results agree with the work published by Jung *et al.* and by Ho *et al.* from their TiO_2 reduction studies [2, 3].

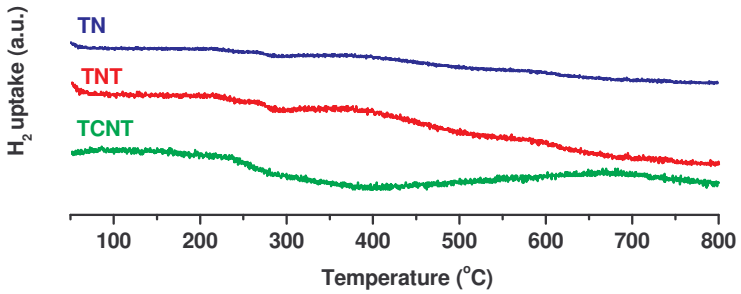

Figure 4.4 TPR profiles of calcined TN, uncalcined TNT and uncalcined TC-TNT support materials

The TPR profile of TC-TNT showed a broad trough in hydrogen uptake when the sample was heated between 240 and 680 ^{o}C. However, this behavior is not clearly understood.

A thermogravimetric analysis (TGA) study was performed on both calcined (450 ^{o}C) and uncalcined TC-TNT support materials. This study was performed only for the TC-TNT support in order to obtain the calcination temperature since the correct calcination temperature of this material was unknown. TGA studies of TN and TNT supports are well known [4-7]. Figure 4.5 shows the TGA traces of the calcined and the uncalcined TC-TNT

supports. It can be seen from the TGA trace of uncalcined TC-TNT that there are three weight-loss stages. The first stage was due to the removal of moisture (≈14%) when the sample was heated from 100 to 200 ^{o}C. The second stage (from 200 to 230 ^{o}C) might have been due to the removal of the nitrate ions (from HNO_3 source which was used as a catalyst for the sol-gel reaction), since this temperature range correlates to that of the loss of nitrate ions. The third stage might have been due to structure rearrangement and condensation reactions of the sol-gel material (from 230 to 280 ^{o}C). When this material was calcined at 450 ^{o}C then all the adsorbed nitrates and moisture had been removed. This is clearly seen in the blue curve (on top) of Figure 4.5.

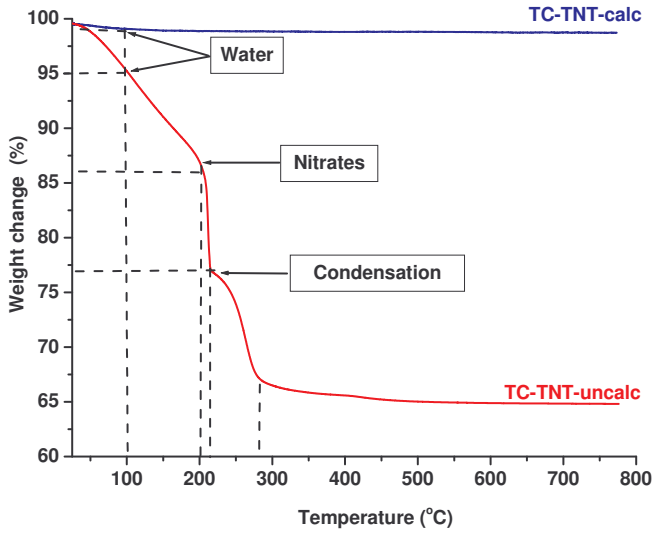

Figure 4.5 TGA plots of calcined and uncalcined TC-TNT support

4.1.4 XRD analysis of support materials

XRD patterns of the calcined support materials are shown in Figure 4.6, where A and R represents anatase and rutile phases, respectively that were present in the TN material. The XRD pattern of TN suggests that the material was crystalline and consisted of 80% anatase and 20% rutile phases. This material's phases compares to that reported by Weng *et al.* [8].

The broad peak (2θ = 25-30°) for TNT and the low intensities of other peaks (2θ = 25, 38, 58 and 64°) revealed that the material was not as crystalline as TN. These broad peaks appeared

broad because these materials are X-ray amorphous. The TNT material also contained a rutile phase ($2\theta = 25, 38, 54^{o}$). This pattern is similar to those reported in literature [7, 9, 10]. Chen *et al.* recently reported that this profile cannot be attributed to the known crystal structures [9]. They also suggested that the broadening of the XRD peaks were due to the nanometer size of the tubes and the bending of some atom planes on the tube.

The broad peaks noted in the XRD pattern of TC-TNT show that the material was less crystalline than those obtained for TN and the uncoated TNT material. It is apparent that the most intense anatase peak (at $2\theta = 25^{o}$) and the rutile peaks (at $2\theta = 28$ and 38°) that were found in the XRD pattern of TN appears in the TC-TNT XRD pattern. This confirms that sol-gel derived TiO_2 was formed on the surface of the tubes. The anatase phase appears to dominate.

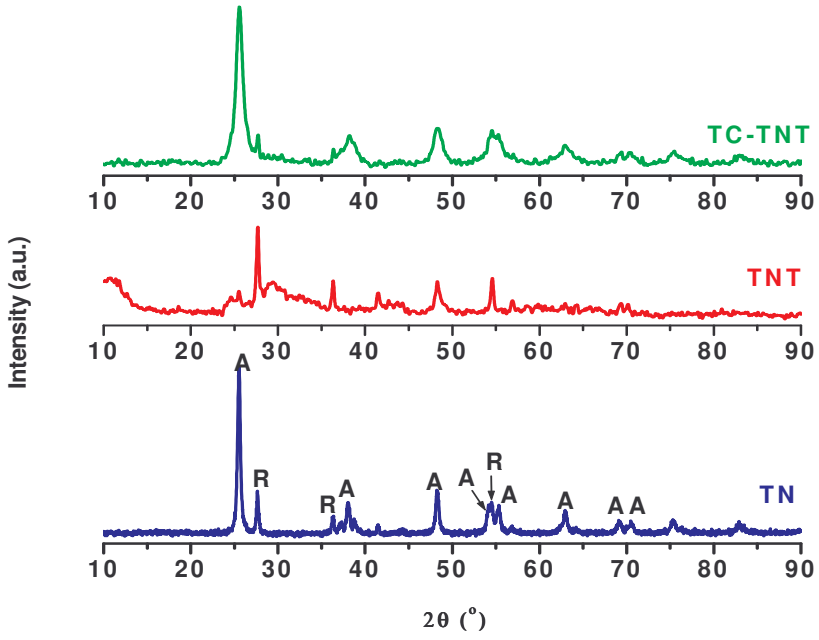

Figure 4.6 Powder XRD patterns of calcined support materials (TN, TNT and TC-TNT), where A = anatase phase and R = rutile phase

Table 4.2 below summarizes the intense planes of the calcined supports and the angels at which they occur. These are similar to those reported in literature.

Table 4.2 XRD data of the most intense planes for the calcined support materials (TN, TNT and TC-TNT)

Sample	2θ (exp)	2θ (lit)	hkl
TC-TNT	26	26	110
TNT	28 (49)	28 (49)	211 (020)
TN	26	26	110

4.2 Catalyst characterization

4.2.1 Porosity and surface area analysis of catalyst

Table 4.3 gives a summary of the measured BET surface area and porosity measurements for the calcined (350 ^{o}C) catalysts prepared in this work. The surface area (S_{BET}) of the calcined unsupported Co_3O_4 was measured as 48.1 m^2/g. This value of the surface area is similar to that reported elsewhere [11]. The surface area of unsupported cobalt oxide is said to range from 30 to 70 m^2/g [11]. The pore (p_v) volume and pore diameter (p_d) values of this material were measured as 0.14 cm^3/g and 11.7 nm, respectively.

Table 4.3 Porosity measurements of catalysts

Catalyst	BET SA (S_{BET}) /m^2/g	Pore volume (p_v) /cm^3/g	Pore diameter (p_d) /nm
Co_3O_4	48.1	0.14	11.7
10%Co/TN	44.2	0.36	32.9
20%Co/TN	39.4	0.30	30.9
10%Co/TNT	103	0.27	10.4
20%Co/TNT	73.7	0.22	10.9
10%Co/TC-TNT	101	0.14	4.4
20%Co/TC-TNT	71.4	0.10	4.4

Calcination temperature = 350°C in air for 6 hours

The measured surface areas of the catalysts were smaller than those of the supports. When 10% cobalt was loaded on all supports the surface areas were decreased (see S_{BET} of supports in Table 4.1). These values decreased even further when 20% cobalt was loaded on to the supports. The pore volume for TN was measured as 0.42 cm^3/g while for 10%Co/TN and 20%Co/TN catalysts the pore volumes were measured as 0.36 and 0.30 cm^3/g, respectively.

These decreases in the surface areas are due to the material blockage of the support pores by the cobalt crystallites.

The surface areas of the 20% cobalt loaded catalysts are smaller than their 10% cobalt loaded catalyst counterparts. The 20% cobalt loaded catalysts possess more and larger cobalt crystallites than the 10% cobalt loaded catalysts. Their surface areas would be smaller that those of the 10% cobalt loaded catalysts since they have smaller total pore volumes, i.e. more pores were blocked and filled. The pore diameters of the supports were unaffected by cobalt loading (for comparison see p_d values of supports in Table 4.1 and p_d values of catalysts in Table 4.3). The measured surface areas of 10%Co/TNT and 10%Co/TC-TNT were comparable and were 103 and 101 m^2/g, respectively. The measured surface areas of 20%Co/TNT and 20%Co/TC-TNT were also found to be comparable and these were 73.7 and 71.4 m^2/g, respectively.

4.2.2 Metal loading by XRF spectroscopy

The cobalt loading was evaluated by X-ray fluorescence (XRF) spectroscopy. In Table 4.4 the actual cobalt loading percentages on the supports are given.

Table 4.4 XRF analysis for the %Co loading on support materials

Catalyst sample	Co loading /%
10%Co/TN	10.7
20%Co/TN	17.3
10%Co/TNT	8.6
20%Co/TNT	21.9
10%Co/TC-TNT	6.9
20%Co/TC-TNT	20.1

Note: An error bar of ± 5% was carried in the measurements

It is apparent that only two catalyst samples were prepared with exactly the desired % cobalt loading. These were the 10%Co/TN and 20%Co/TC-TNT catalyst samples. The other catalyst samples, viz. 20%Co/TN, 10%Co/TNT and 10%Co/TC-TNT were under-loaded and cobalt loading percentages of 17.3, 8.6 and 6.9 were obtained, respectively.

4.2.3 XRD analysis of catalysts

The effect of cobalt on the supports is shown in the XRD patterns of calcined (350 ^{o}C) 10% cobalt loaded catalyst samples in Figure 4.7 below. An XRD pattern of a calcined (350 ^{o}C) unsupported Co_3O_4 is also shown so that the peak positions of Co_3O_4 can be established. The patterns indicated that all the cobalt contained in the calcined samples was in the form of Co_3O_4. Loading of 10% cobalt on TN did not change the anatase/rutile phase ratio of 80/20 of TiO_2. This implies that loading of cobalt on the TN support and calcination of the catalyst under the reaction conditions employed (i.e. see reaction conditions in Chapter 3 section 3.4) had no significant effect on this support. The most intense Co_3O_4 peak overlaps with TN and TC-TNT peaks (anatase and rutile phases) in the region between 2θ = 35-39°.

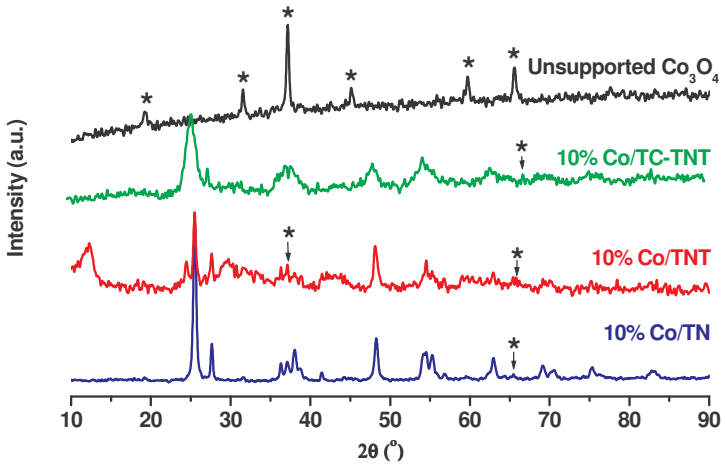

Figure 4.7 XRD patterns of calcined unsupported Co_3O_4 and 10% cobalt loaded catalysts, where * = Co_3O_4 phase

Table 4.5 below summarizes the intense planes of the calcined unsupported Co_3O_4 and 10% cobalt loaded catalysts and the angels at which they occur. These are similar to those reported in literature.

Table 4.5 XRD data of the most intense planes for calcined unsupported Co_3O_4 and 10% cobalt loaded catalysts

Sample	2θ (exp)	2θ (lit)	hkl
Unsupported Co_3O_4	37	37	311
10%Co/TC-TNT	37	37	311
10%Co/TNT	37	37	311
10%Co/TN	37	37	311

Loading of cobalt on TNT and TC-TNT supports was successful since small Co_3O_4 peaks can be observed. This can be seen by comparing Figures 4.6 and 4.7. When cobalt was loaded on TNT and the catalyst was calcined then the intensity of some of the TNT peaks decreased (i.e. $2\theta = 28, 54^o$). Cobalt loading on TC-TNT had no significant effect on the broadness of the peaks, but had a significant effect on the peak intensities. They became less intense after cobalt addition.

Figure 4.8 shows the effect of an increase in cobalt loading on the XRD patterns. XRD patterns for calcined 20%Co/TN and 20%Co/TNT are shown. The XRD pattern for 20%Co/TC-TNT was not available for characterization since there was insufficient sample for XRD characterization. It is immediately apparent that by increasing the amount of cobalt on the both TN and TNT supports that the Co_3O_4 peaks became easily visible, i.e. their intensity increased. Similar to the behavior on 10%Co/TN, an increase in cobalt loading did not have a significant effect on the anatase/rutile phase ratio of 80/20 of TiO_2. The intensity of some of the TNT peaks (i.e. $2\theta = 28, 54^o$) in the 20%Co/TC-TNT pattern were similar to those for 10%Co/TC-TNT. So by extrapolating the results obtained in the XRD patterns in Figure 4.8 it can be assumed that the intensity of Co_3O_4 peaks would also be increased with cobalt loading. The peak breaths would not be affected as shown by the 10%Co/TC-TNT sample (Figure 4.7).

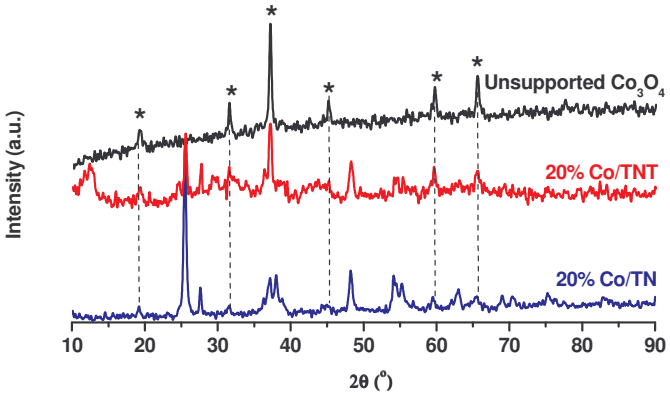

Figure 4.8 XRD patterns of calcined unsupported Co_3O_4, 20%Co/TN and 20%Co/TNT, where * = Co_3O_4 phase

Table 4.6 below summarizes the intense planes of the calcined unsupported Co_3O_4, 20%Co/TN and 20%Co/TNTand the angels at which they occur. These are similar to those reported in literature.

Table 4.6 XRD data of the most intense planes for calcined unsupported Co_3O_4, 20%Co/TN and 20%Co/TNT

Sample	2θ (exp)	2θ (lit)	hkl
Unsupported Co_3O_4	37	37	311
10%Co/TNT	37	37	311
10%Co/TN	37	37	311

4.2.4 A thermal analysis of catalysts using TPR and TGA

The reduction behavior of the supported catalysts was characterized by means of TPR analysis. Figure 4.9 shows the recorded hydrogen consumption TPR profile of a calcined (350 ^{o}C) unsupported cobalt oxide sample. This curve show three peaks, indicative of the reduction of nitrate ions (at 200 ^{o}C) remaining after calcination and the two step reduction of Co_3O_4 to CoO (at 306 ^{o}C) and CoO to metallic cobalt (at 360 ^{o}C) occurring as mentioned by

Sexton *et al.* [12]. The two reduction peaks of cobalt oxide to metallic cobalt are said to correspond to the chemical reactions shown in equations 4.1 and 4.2 below [13].

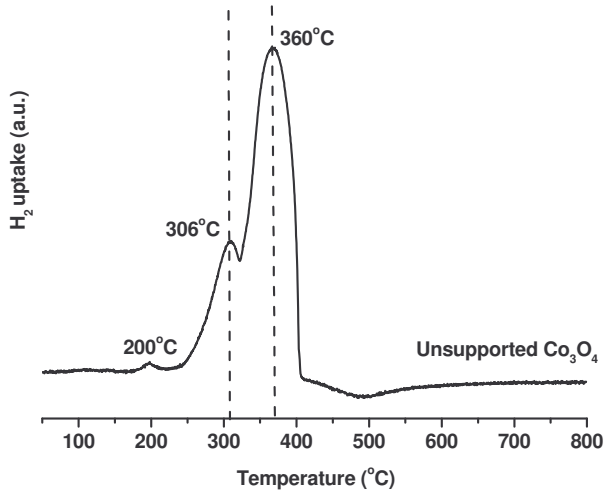

Figure 4.9 TPR of calcined unsupported cobalt oxide precursor

$$Co_3O_4 + H_2 \rightarrow 3CoO + H_2O \quad (4.1)$$

$$3CoO + 3H_2 \rightarrow 3Co + 3H_2O \quad (4.2)$$

The reduction behavior of the calcined (350 ^oC) 10 and 20% cobalt loaded catalysts are compared in the TPR profiles shown in Figures 4.10 and 4.11, respectively. In all catalysts the two cobalt reduction peaks were observed even though they occurred at different temperatures. These reduction temperatures occurred at temperatures higher that those found in unsupported Co_3O_4 sample. This was due to the strong metal support interactions (SMSI) between the support and the metal [14]. This observation implies that when cobalt was impregnated on the supports then the rate of reduction of cobalt was hampered.

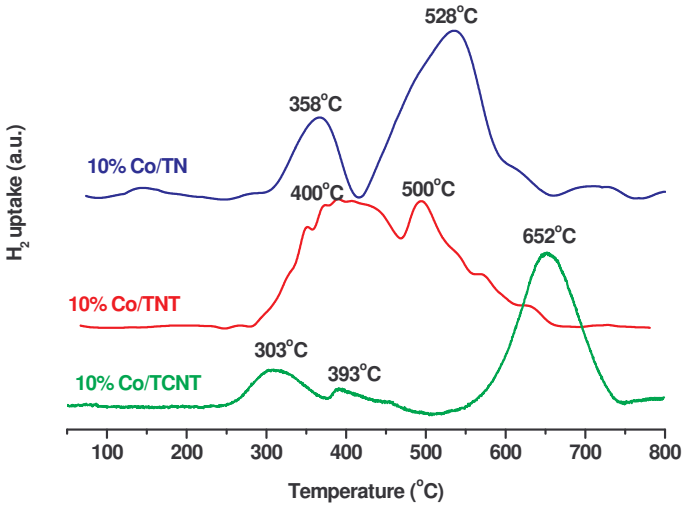

Figure 4.10 TPR profiles of calcined 10% cobalt loaded catalysts

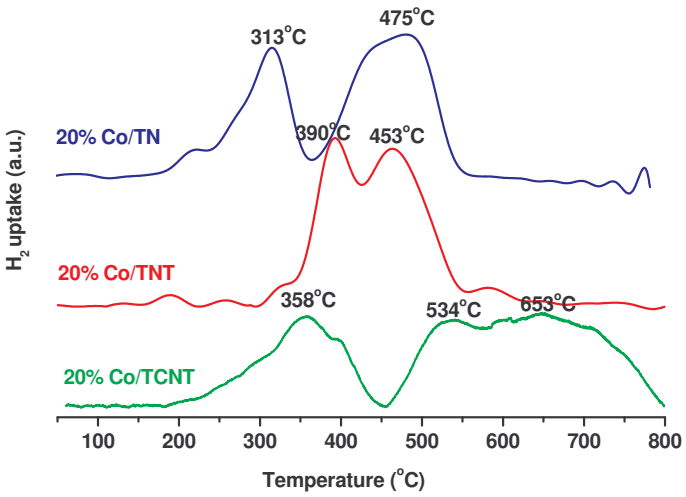

Figure 4.11 TPR of calcined 20% cobalt loaded catalysts

In the profile of 10%Co/TN sample two reduction peaks occurred at 358 and 528 °C. The two reduction peaks in 10%Co/TNT sample occurred at 400 and 500 °C, while these same two reduction peaks in the 10%Co/TC-TNT sample occurred at 303 and 393 °C. In addition to these two reduction peaks observed in the profile of 10%Co/TC-TNT sample a high

temperature reduction peak was noticed at 652 ^{o}C. The assignment to this peak is not straightforward. It may be due to the SMSI between cobalt and the support to form cobalt-titanates ($CoTiO_3$) species which are more difficult to reduce than Co_3O_4 [3, 15] or it may be due to the reduction of the fraction of cobalt that is contained in the inner cavities of TC-TNT support whose reducibility is limited by the dispersion of the H_2O (through the pores) formed during the reaction [16].

In terms of reducibility the TPR profiles suggests that 10%Co/TN sample was easier to reduce than 10%Co/TNT. This is because the first reduction peak of 10%Co/TN occurred at 358 ^{o}C while that of 10%Co/TNT occurred at a higher temperature, i.e. 400 ^{o}C. However, the second reduction peak of 10%Co/TN was obtained at higher temperature (528 ^{o}C) than that of 10%Co/TNT (500 ^{o}C). The higher reduction temperatures might be due to cobalt active sites being poisoned by the potassium ions which might have migrated from the TNT support to the cobalt surface [17, 18].

The formation of two reduction peaks that occurred in the 10%Co/TC-TNT sample, suggest that it is an easier catalyst to reduce than either the 10%Co/TN or 10%Co/TNT samples since these peaks occurred at low temperatures, i.e. 303 ^{o}C and 393 ^{o}C, respectively. However, this was not completely true since there is a third peak which is observed at high temperature, i.e. 652 ^{o}C.

When 20% of cobalt was loaded on to the supports all the reduction peaks shifted to temperatures lower than those found in their 10% cobalt loaded counterparts (i.e. see TPR profiles in Figure 4.10 and 4.11). This behavior is not surprising because one would expect a catalyst sample with more cobalt atoms to be easier to reduce because cobalt is readily available on the catalyst surface. The reducibility trend for the three 20% cobalt loaded samples was similar to that found in the 10% cobalt loaded samples. The difference is that for 20%Co/TC-TNT, the first and second reduction peaks occurred as one broad peak at temperatures between 220 and 400 ^{o}C. In addition to this difference, two broad peaks at high temperatures, i.e. 534 and 653 ^{o}C were seen in the TPR profile of this sample.

The TGA profile of a calcined (350 °C) and uncalcined 10%Co/TNT sample is shown in Figure 4.12. For the uncalcined 10%Co/TNT sample an initial weight loss of ≈5%, which is attributed to the removal of physisorbed water, occurs between 100 and 150 °C. A second weight loss (≈20%) is attributed to the removal of nitrate ions and these occurred at temperatures between 150 and 250 °C. These nitrate ions were adsorbed on the support during the catalyst preparation. The TGA profile of a calcined 10%Co/TNT sample confirms that the calcination of this catalyst at 350 °C for 6 hours was enough to remove both moisture and the nitrate ions.

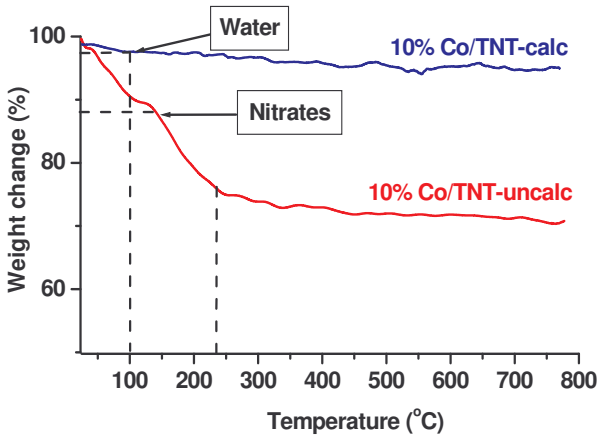

Figure 4.12 TGA plots of calcined and uncalcined 10%Co/TCNT catalyst sample

4.2.5 Chemisorption analysis for catalysts

The results of the H_2-chemisorption study for all catalysts are listed in Table 4.7. Prior to the H_2-chemisorption the calcined (350 °C) catalysts were reduced in pure hydrogen at 425 °C for 8 hours. Several interesting trends, similar to those obtained by Reuel *et al.* [19], are apparent from our chemisorption data obtained for all catalysts and these are:

1) The average crystallite diameter increased with increasing cobalt loading.
2) The percentage dispersion decreased with increasing cobalt loading.

Table 4.7 H_2-Chemisorption results for all calcined catalysts

Catalyst sample	Degree of reduction /%	Dispersion /%	Average crystallite diameter /nm
10%Co/TN	92.7	1.74	55.3
20%Co/TN	67.5	1.32	72.5
10%Co/TNT	90.8	0.61	157.3
20%Co/TNT	61.3	0.47	202.4
10%Co/TC-TNT	83.5	0.07	-
20%Co/TC-TNT	42.4	0.30	316.8

Calcination T = 350 ^oC in air for 6 hours, Reduction T = 425 ^oC for 8 hours in pure H_2

The average crystallite diameters obtained for cobalt were large, but for 10%Co/TN (55.3 nm) a comparable crystallite diameter of 56.9 nm (dispersion 1.69%) was reported by Riedel *et al.* for their 10%Co/SiO_2 prepared by a precipitation methodology [20]. The percentage dispersion of these catalysts was low. However, with the values still allow a ranking of the catalysts regarding their cobalt dispersion and crystallite size, with the highest values found in this study for 10%Co/TN and 20%Co/TN catalysts and the lowest values found for 10%Co/TC-TNT and 20%Co/TC-TNT.

The reasons for the small dispersions obtained for cobalt loaded on both TNT and TC-TNT supports might have been contributed by their relatively low extents of reductions (as compared to their TN counterparts). These lower extents of reduction might be due to the same reasons as used to describe the TPR results (in section 4.2.4), i.e. SMSI between cobalt and TC-TNT in the case of 10%Co/TC-TNT and 20%Co/TC-TNT, while in the case of 10%Co/TNT and 20%Co/TNT this was caused by cobalt poisoning by potassium on the support surface [17, 18].

The degree of reduction calculations were measured by O_2-titration (at 400 ^oC) of the pre-reduced catalysts. The reduction degree decreased with an increase in cobalt loading. This observed relationship appears as a surprise because one would expect the reduction degree to increase with cobalt loading since the average cluster size was increased [20]. These measurements are different to those obtained by Reuel *et al.* [19] and by Jacobs *et al.* [21] whereby the percentage reduction of their catalysts increased with cobalt loadings. The course of this obscure observation is not known.

4.3 Reactor studies for catalyst evaluation

The catalytic performance for all cobalt loaded catalysts was tested in a stainless-steel fixed bed reactor with catalyst loadings of 1 to 2 grams. Prior to FTS runs catalysts were activated following the same reduction procedure as previously listed in chapter 3 section 3.4.3 (in pure H_2 at 300 ^oC for 16 h). Mass balance calculations were performed when the reactions reached a steady state %conversion (i.e. about 24 h after syn-gas addition). However, in the case of the 10%Co/TNT tested at 230 ^oC the mass balance calculations were only performed after 16 hours since the reaction was discontinued at that time because of a low %CO conversion. All catalyst tests were performed at three different temperatures (i.e. 230, 250 and 280 ^oC) with a total pressure of 8 bar. Some of the reported data for the specific reactions are listed in tables and figures found in sections 4.3.1, 4.3.2 and 4.3.3.

4.3.1 FTS for 10% cobalt loaded catalysts

The changes in the syn-gas conversion or catalyst activity (expressed as %CO conversion) with time-on-stream (TOS) at three different temperatures with three different 10% cobalt loaded catalysts (viz. 10%Co/TN, 10%Co/TNT and 10%Co/TC-TNT) are shown in Figures 4.13, 4.14 and 4.15. It is evident that for all sets of catalysts the %CO conversion increased with temperature. However, the increase in %CO conversion was different for every catalyst. For 10%Co/TN the %CO conversions were 22.4, 40.4 and 40.7% at 230, 250 and 280 ^oC, respectively. For 10%Co/TNT %CO conversions at 230, 250 and 280 ^oC were 2.2, 3.5 and 17.2%, respectively; while for 10%Co/TC-TNT the %CO conversions of 9.4, 17.9 and 33.8% were obtained at those temperatures, respectively. In terms of CO conversion, the overall activity of these catalysts at all temperatures decreased in the following array:

10%Co/TN > 10%Co/TC-TNT > 10%Co/TNT

In general the tubular material (TNT) did not form a better support for cobalt in FTS. The reason for this poor catalytic activity exhibited by 10%Co/TNT might be due to the presence of the potassium ions in the TNT sample. These ions can poison cobalt active sites. It has been reported that when potassium was used as a potential promoter for cobalt catalysts in

FTS the activity decreased due to poisoning of cobalt active sites [17, 18]. However, when the TNT material was coated with TiO_2 to form TC-TNT and used as a support for cobalt catalysts in FTS the catalytic activity was improved. Despite the improved activity, 10%Co/TC-TNT did not perform as well as the 10%Co/TN at all reaction temperatures. This might be due to the higher percentage of unreduced cobalt species or due to the presence of excess potassium ions. The interactions between cobalt and the support suggest that the support can only be reduced at high temperatures (i.e. 652 ^{o}C as suggested by a TPR study).

Catalytic testing of 10%Co/TN at 280 ^{o}C revealed that the reaction does not reach steady state activity as the %CO conversion continued to decrease until the reaction was stopped after 66 hours. At other temperatures (i.e. 230 and 250 ^{o}C) the reaction showed steady activity (Figure 4.13). Even though 10%Co/TNT was the least active catalyst, the reaction reached steady state after 10 hours at all temperatures (Figure 4.14). In the case of 10%Co/TC-TNT it can be seen that FT reaction at all temperatures reached steady state quickly and the catalyst was still active even after 90 hours of reactions (Figure 4.15).

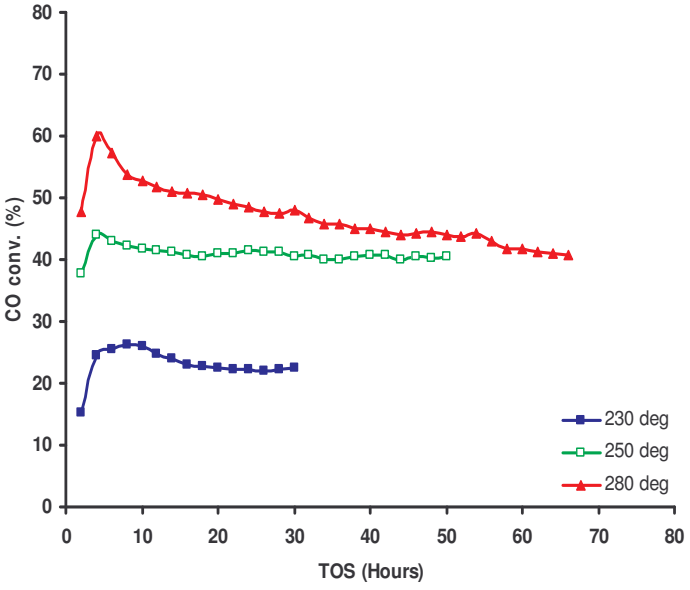

Figure 4.13 Effect of temperature on CO conversion in the Fischer-Tropsch synthesis as a function of time on stream for 10%Co/TN

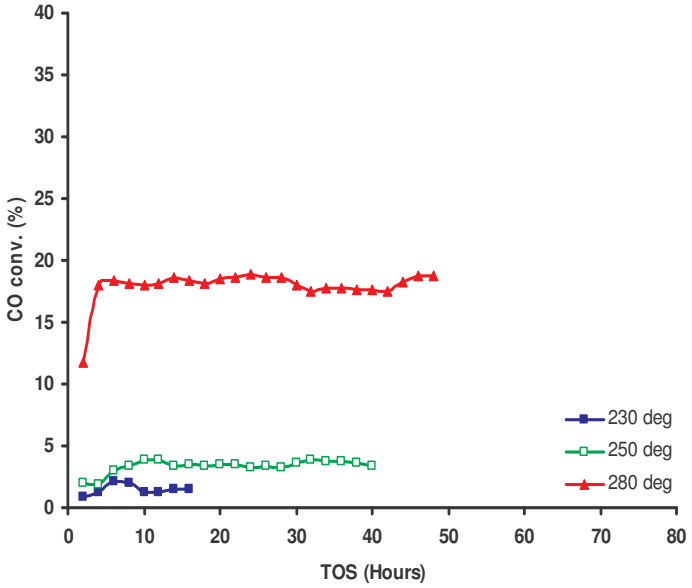

Figure 4.14 Effect of temperature on CO conversion in the Fischer-Tropsch synthesis as a function of time on stream for 10%Co/TNT

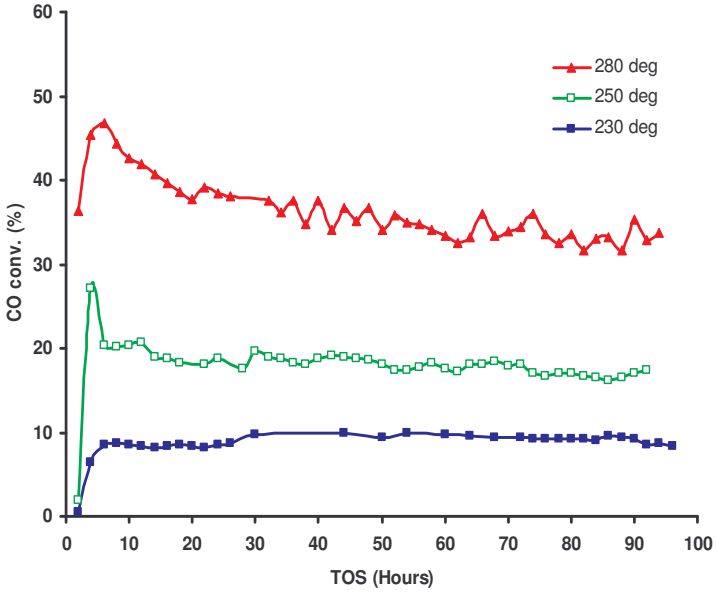

Figure 4.15 Effect of temperature on CO conversion in the Fischer-Tropsch synthesis as a function of time on stream for 10%Co/TCNT

The product selectivity, which is defined as the mass of a single component produced per total mass of other products, for 10%Co/TN, 10%Co/TNT and 10%Co/TC-TNT at various temperatures are listed in Tables 4.8, 4.9 and 4.10, respectively. A similar trend for CO

conversion and CH_4 selectivity is apparent for all these catalysts. It can be seen that both CO conversion and CH_4 selectivity increased with an increase in temperature. These results are normal because it is well known that at high temperature cobalt produces an excessive amount of CH_4 [22, 23]. However, a decrease in CH_4 selectivity for 10%Co/TNT when the temperature was increased from 250 to 280 ^oC is unusual. This might have been due to the large ±10% error associated with low CO conversion (≈3%). For all catalysts the highest C_2 olefin selectivity was achieved at 250 ^oC. CO_2 formation was absent for all catalysts tested at low temperatures (i.e. 230 and 250 ^oC) and was only detected at 280 ^oC. This presence of CO_2 was due to the WGS reaction that is known to occur at high temperatures over cobalt based FT catalysts [23, 24]. The highest selectivity to long chain products (C_{12+}) was achieved at 230^oC for 10%Co/TN and at 250 ^oC for 10%Co/TC-TNT. In the case of 10%Co/TNT it was difficult to collect long chain products due to the low conversion as only small amounts of oil and wax were trapped in the product knockout pots at all reaction temperatures.

Table 4.8 FTS data for the catalytic performance of 10%Co/TN catalyst

Temp/^oC	**230**	**250**	**280**
CO conv./%	22.4	40.4	40.7
H_2 conv./%	27.7	46.7	43.1
Rate CO	-4.8×10^{-07}	-1.2×10^{-06}	-1.1×10^{-06}
Rate CO_2	0.0	0.00	1.5×10^{-07}
Rate FT	4.8×10^{-07}	1.2×10^{-06}	9.2×10^{-07}
Activity/ µmol/sec.g_{Co}	16.1	40.2	35.7
α1	0.67	0.82	0.71
α2	0.98	0.92	0.83
C_1	37.2	42.9	50.2
C_2 - C_4	21.8	22.7	20.5
C_5 - C_{11}	26.9	25.1	22.6
C_{12+}	14.2	9.5	6.6
C_2 olefin/%	4.7	4.9	3.3
CO_2/%	0.0	0.0	2.2

Data consist of ± 5% experimental error. **Reduction**: 300 ^oC in pure H_2, 45 ml/min.g_{cat} (16hrs)
Reaction conditions: H_2/CO = 2, 12 ml/min.g_{cat}, P_{tot} = 8 bar

Table 4.9 FTS data for the catalytic performance of 10%Co/TNT catalyst

Temp/^{o}C	**230**	**250**	**280**
CO conv./%	2.2	3.5	17.7
H_2 conv./%	2.3	3.4	11.3
Rate CO	4.6×10^{-09}	1.4×10^{-08}	-3.1×10^{-07}
Rate CO_2	0.00	0.00	1.7×10^{-07}
Rate FT	-4.6×10^{-09}	-1.4×10^{-08}	1.4×10^{-07}
Activity/ µmol/sec.g_{Co}	-0.2	-0.5	10.4
α1	0.43	0.51	0.30
α2	-	-	-
C_1	44.5	52.0	45.8
C_2 - C_4	49.6	38.7	49.9
C_5 - C_{11}	5.9	9.3	4.4
C_{12+}	≈0.0	≈0.0	≈0.0
C_2 olefin/%	4.3	6.0	3.8
CO_2/%	0.00	0.00	2.4

Data consist of ± 5% experimental error. **Reduction**: 300 ^{o}C in pure H_2, 45 ml/min.g_{cat} (16hrs)
Reaction conditions: H_2/CO = 2, 12 ml/min.g_{cat}, P_{tot} = 8 bar

Table 4.10 FTS data for the catalytic performance of 10%Co/TC-TNT catalyst

Temp/^{o}C	**230**	**250**	**280**
CO conv./%	9.4	17.9	33.8
H_2 conv./%	10.8	19.6	31.5
Rate CO	-3.6×10^{-07}	-5.7×10^{-07}	-9.8×10^{-07}
Rate CO_2	0.0	0.0	1.8×10^{-07}
Rate FT	3.6×10^{-07}	5.7×10^{-07}	8.0×10^{-07}
Activity/ µmol/sec.g_{Co}	12.1	19.1	32.8
α1	0.56	0.62	0.54
α2	0.95	≈1.0	0.83
C_1	42.6	43.6	55.0
C_2 - C_4	37.5	20.0	25.6
C_5 - C_{11}	16.4	24.0	15.2
C_{12+}	7.5	13.0	10.6
C_2 olefin/%	2.1	4.7	3.2
CO_2/%	0.0	0.0	2.6

Data consist of ± 5% experimental error. **Reduction**: 300 ^{o}C in pure H_2, 45 ml/min.g_{cat} (16hrs)
Reaction conditions: H_2/CO = 2, 12 ml/min.g_{cat}, P_{tot} = 8 bar

4.3.2 FTS for 20% cobalt loaded catalysts

To study the effect of cobalt loading on the three different supports (TN, TNT and TC-TNT), the same studies as those performed for 10% cobalt loading were done for the 20% cobalt loaded catalysts. Figures 4.16, 4.17 and 4.18 show the %CO conversion with time-on-stream plots for 20%Co/TN, 20%Co/TNT and 20%Co/TC-TNT, respectively. It is apparent that, in general, for all these catalysts that the overall %CO conversions increased with the cobalt loading. In the FT reaction for 20%Co/TNT at 230 ^{o}C a low %CO conversion of 2.6% was obtained and this was comparable to that obtained at 230°C for 10%Co/TNT (2.2%).

The effect of temperature on these catalysts followed similar trends as found for the 10% cobalt loaded catalysts, i.e. %CO conversion increased with temperature. However, in the case of 20%Co/TN a high and constant %CO conversion was maintained at all reaction temperatures, i.e. approximately the same CO conversions were obtained and calculated as 52.4, 52.4 and 54.9% at 230, 250 and 280 ^{o}C, respectively. This unusual behavior might have arisen because the reaction equilibrium was already reached at that syn-gas flow-rate (i.e. 12 mL/min); therefore the temperature did not have any effect on the %CO conversion, but had affected the product distribution (see below). The same activity trend as followed by 10% cobalt loaded catalysts were followed by 20% cobalt loaded catalysts and was as follows:

20%Co/TN > 20%Co/TC-TNT > 20%Co/TNT

This activity trend behavior is due to the same reasons as explained in section 4.3.1 for the 10% cobalt catalysts.

In terms of catalyst stability, it is evident that 20%Co/TN and 20%Co/TNT catalysts are stable at all reaction temperatures. The stability of 20%Co/TC-TNT for FT reaction at 280 ^{o}C did not reach equilibrium for the first 70 hours. This catalyst only reached steady state after 78 hours. However, for the FT reactions at lower temperatures (i.e. at 230 and 250 ^{o}C) the reaction steady state was achieved throughout the catalyst run.

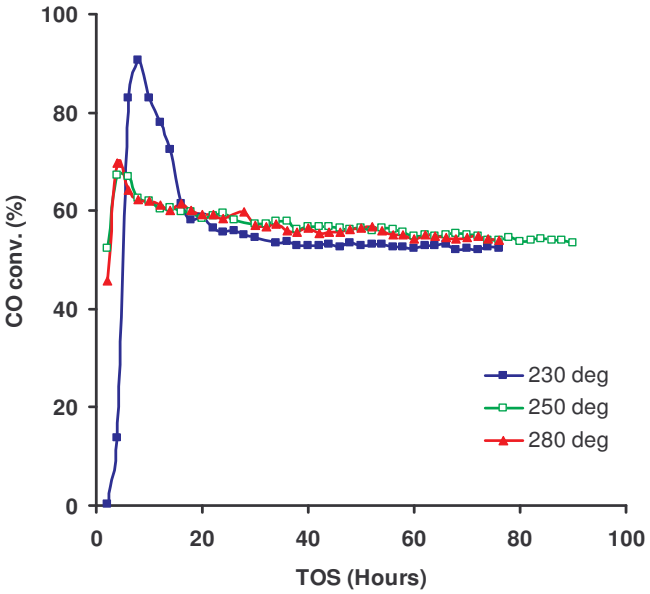

Figure 4.16 Effect of temperature in %CO conversion in the Fischer-Tropsch synthesis as a function of time on stream for 20%Co/TN

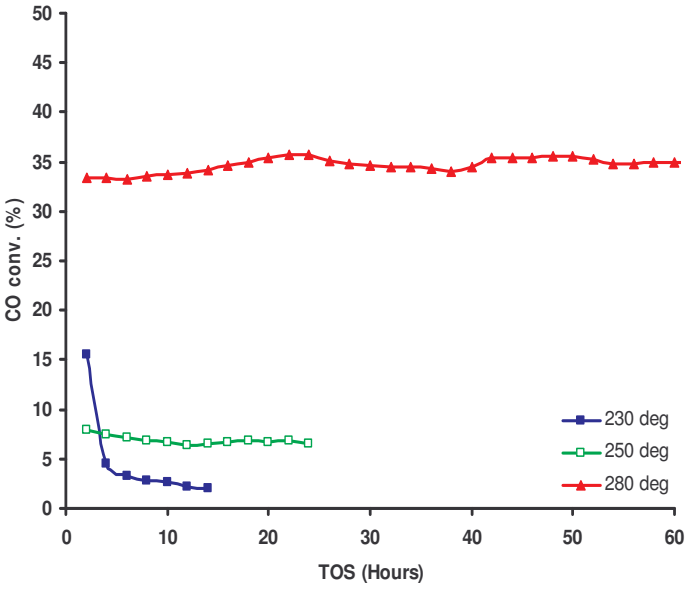

Figure 4.17 Effect of temperature in CO conversion in the Fischer-Tropsch synthesis as a function of time on stream for 20%Co/TNT

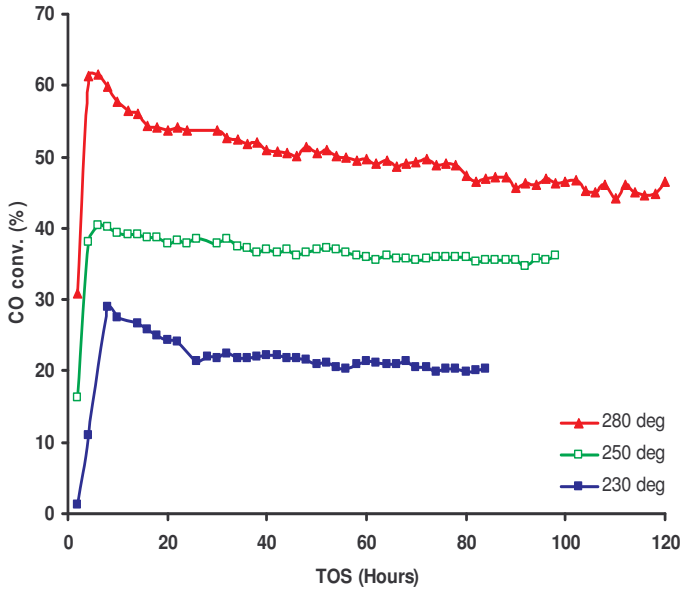

Figure 4.18 Effect of temperature in CO conversion in the Fischer-Tropsch synthesis as a function of time on stream for 20%Co/TC-TNT

Tables 4.11-4.13, illustrate the results for the catalytic performance and product selectivities of 20%Co/TN, 20%Co/TNT and 20%Co/TC-TNT at various temperatures. It is evident that both %CO conversion and CH_4 selectivity increased with temperature for all 20% cobalt loaded catalysts. Similarly as with the 10% cobalt loaded catalysts, CO_2 was only formed at 280 ^oC, but in this case a much higher % of CO_2 was formed compared to the10% cobalt loaded catalysts. The maximum C_2 olefin selectivity was obtained at 250 ^oC for all 20% cobalt loaded catalysts. All these catalysts seem to be more selective towards the formation of short chain hydrocarbons.

A similar general trend in the product selectivity that was observed in the 10% cobalt loaded catalysts was observed in the 20% cobalt loaded catalysts. However, minor changes were observed in some of the 20% cobalt loaded catalysts. For instance in the FT reaction of 20%Co/TNT at 280 ^oC the formation of 2.5% C_2 olefin selectivity was noticed in contrast to about 0% for the 10%Co/TNT tested at the same temperature.

Table 4.11 FTS data for the catalytic performance of 20%Co/TN catalyst

Temp/^{o}C	**230**	**250**	**280**
CO conv./%	52.4	52.4	54.9
H_2 conv./%	58.0	61.6	58.3
Rate CO	-2.1×10^{-06}	-2.1×10^{-06}	-1.9×10^{-06}
Rate CO_2	0.0	0.0	2.8×10^{-07}
Rate FT	2.1×10^{-06}	2.1×10^{-06}	1.6×10^{-06}
Activity/ µmol/sec.g_{Co}	71.4	70.7	63.8
α1	0.78	0.69	0.53
α2	0.86	0.80	≈1
C_1	31.5	45.3	68.3
C_2 - C_4	18.9	23.1	20.5
C_5 - C_{11}	37.9	24.4	6.9
C_{12+}	23.8	8.2	4.9
C_2 olefin/%	4.9	4.1	4.5
CO_2/%	0.0	0.0	4.1

Data consist of ± 5% experimental error. **Reduction**: 300 ^{o}C in pure H_2, 45 ml/min.g_{cat} (16hrs)
Reaction conditions: H_2/CO = 2, 12 ml/min.g_{cat}, P_{tot} = 8 bar

Table 4.12 FTS data for the catalytic performance of 20%Co/TNT catalyst

Temp/^{o}C	**230**	**250**	**280**
CO conv./%	2.6	6.8	35.4
H_2 conv./%	2.7	5.2	19.8
Rate CO	2.8×10^{-08}	-7.2×10^{-08}	-8.5×10^{-07}
Rate CO_2	0.0	0.0	3.7×10^{-07}
Rate FT	-2.8×10^{-08}	7.2×10^{-08}	4.8×10^{-07}
Activity/ µmol/sec.g_{Co}	-0.9	2.4	28.5
α1	0.48	0.54	0.58
α2	-	-	0.86
C_1	43.5	47.4	57.9
C_2 - C_4	49.8	43.9	29.0
C_5 - C_{11}	6.7	8.7	9.3
C_{12+}	≈0.0	≈0.0	4.2
C_2 olefin/%	3.2	4.2	2.5
CO_2/%	0.0	0.0	5.4

Data consist of ± 5% experimental error. **Reduction**: 300 ^{o}C in pure H_2, 45 ml/min.g_{cat} (16hrs)
Reaction conditions: H_2/CO = 2, 12 ml/min.g_{cat}, P_{tot} = 8 bar

Table 4.13 FTS data for the catalytic performance of 20%Co/TC-TNT catalyst

Temp/^{o}C	**230**	**250**	**280**
CO conv./%	20.2	36.1	46.1
H_2 conv./%	20.6	36.0	41.7
Rate CO	-6.6×10^{-07}	-1.2×10^{-06}	-1.4×10^{-06}
Rate CO_2	0.0	0.0	2.3×10^{-07}
Rate FT	6.6×10^{-07}	1.2×10^{-06}	1.2×10^{-06}
Activity/ µmol/sec.g_{Co}	22.1	41.3	46.9
α1	0.73	0.55	0.53
α2	0.98	0.91	0.94
C_1	28.3	30.8	48.8
C_2 - C_4	14.9	18.9	22.0
C_5 - C_{11}	32.5	30.2	18.3
C_{12+}	34.0	30.3	11.8
C_2 olefin/%	3.8	4.5	4.3
CO_2/%	0.0	0.0	3.3

Data consist of ± 5% experimental error. **Reduction**: 300 ^{o}C in pure H_2, 45 ml/min.g_{cat} (16hrs)
Reaction conditions: H_2/CO = 2, 12 ml/min.g_{cat}, P_{tot} = 8 bar

4.3.3 Schulz-Flory distribution on the cobalt loaded catalysts

Figure 4.19 represents the entire hydrocarbon distributions ($\log(W_n/n)$) versus carbon number for the 10%Co/TN, 20%Co/TN, 10%Co/TNT, 20%Co/TNT, 10%Co/TC-TNT and 20%Co/TC-TNT catalysts. It is to be noted that the hydrocarbon distribution plots for the 10%Co/TNT and 20%Co/TNT catalyst did not indicate contributions from the liquid phase as there was too little liquid to analyze. No oil or wax products were produced during the reaction (see Tables 4.9 and 4.12).

The hydrocarbon distributions after C_3 almost obey the ideal ASF law (i.e. $\text{Log}(W_n/n) = n\log\alpha + \log((1 - \alpha)^2/ \alpha)$); whereas expected deviations occur at C_1 and C_2, which show an excess weight percentage at C_1 and a lower percentage at C_2. The high methane percentage may be due to higher concentration of methyl species on the catalyst surface, whereas lower C_2 weight percentages in the hydrocarbon products might have been caused by higher rate of ethene secondary reaction, which takes place during the FTS reaction [21, 24-27].

Despite the approximate ideal ASF behavior for all the catalysts shown in Figure 4.19, two catalysts, viz. 20%Co/TN and 10%Co/TC-TNT portray peculiar behavior for reactions performed at 280 and 230 ^{o}C, respectively. In the hydrocarbon distribution plot of 20%Co/TN for the reaction performed at 280 ^{o}C the selectivities for C_4-C_{11} hydrocarbons seems to be low and are outside the ideal and normal ASF predictions. The hydrocarbon distribution plot of 10%Co/TC-TNT for the reaction performed at 230 ^{o}C shows high selectivities for C_9-C_{15} and these were outside the ideal and normal ASF predictions. However, all data for hydrocarbon selectivities obtained in Tables 4.5-4.10 are in agreement to the hydrocarbon distribution curves in Figure 4.19.

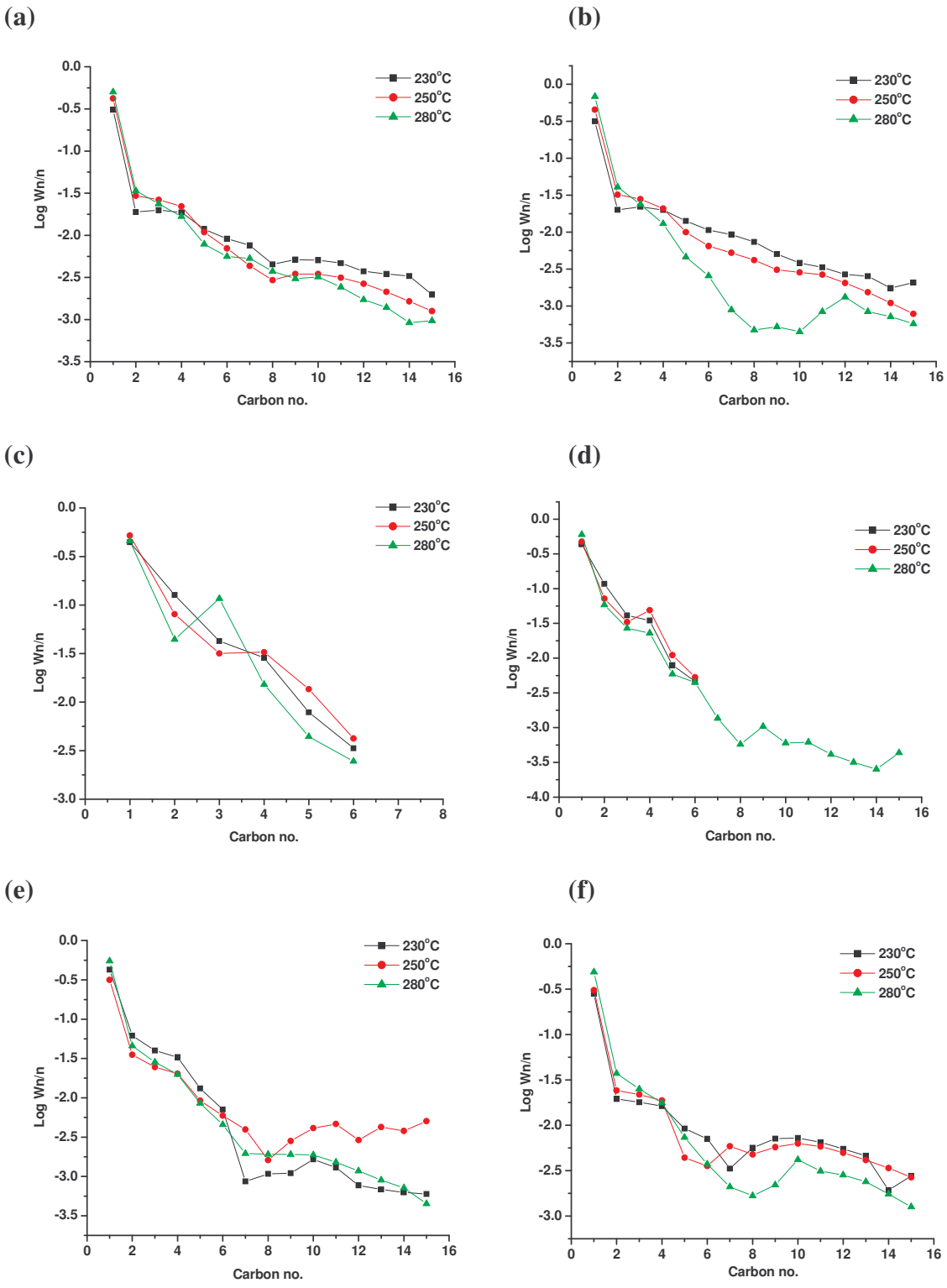

Figure 4.19 Typical overall hydrocarbon distribution on (a) 10%Co/TN, (b) 20%Co/TN, (c) 10%Co/TNT, (d) 20%Co/TNT, (e) 10%Co/TC-TNT and (f) 20%Co/TC-TNT catalysts

4.3.4 Comparison of catalyst activities at *iso*-conversions

In order to judge as to which catalyst support system is the most active and gives the better selectivity for FTS it was necessary to obtain activity and selectivity results of these catalysts at similar CO conversions. To achieve this, the same CO conversions were obtained at different cobalt loadings for the different supports. Tables 4.14-4.16 give the activity and selectivity data of various cobalt catalysts that were obtained at similar CO conversions.

Table 4.14 below illustrates the activity and selectivity results for cobalt loaded on TN and TNT supports. It is immediately apparent that for the CO conversion of cobalt loaded on TNT supports (40.4%) to be comparable to that obtained for cobalt loaded on the TN support (35.4%) two variables needed to be changed. These were the temperature (280 ^{o}C in contrast to 250 ^{o}C) and the cobalt loading (i.e. 20%Co/TNT in contrast to 10%/TN). In terms of product selectivity it is evident that the CH_4 and CO_2 selectivities of 20%Co/TNT were higher than that those obtained for 10%Co/TN. A 10%Co/TN catalyst did not produce any CO_2 at 250 ^{o}C. However, the data do not necessarily mean that the 20%Co/TNT catalyst is a better methanation catalyst than 10%Co/TN since it is well known that at high temperatures cobalt catalysts produce large amounts of CH_4. Also the WGS side reaction to produce CO_2 will increase with temperature. Rather it can be concluded that 10%Co/TN was a better FT catalyst than 20%Co/TNT since the same activities were obtained at a lower temperature for the TN support and better chain growth was also obtained.

Table 4.14 Comparison of product selectivity data for Co/TN and Co/TNT at *iso*-conversion

Catalysts (Temp./^{o}C)	**10%Co/TN (250)**	**20%Co/TNT (280)**
CO conv./%	40.4	35.4
α1	0.82	0.58
α2	0.92	0.86
C_1	40.2	59.9
C_2 - C_4	22.6	29.0
C_5 - C_{11}	25.1	9.3
C_{12+}	9.5	4.2
C_2 olefin/%	4.9	2.5
CO_2/%	0.0	5.4

The product selectivities were also compared when the same amount of cobalt (10%) was impregnated on the TNT and TC-TNT supports (Table 4.15). It can be seen that in order for 10%Co/TC-TNT to achieve the same CO conversion of about 17% obtained by 10%Co/TNT at 250 ^{o}C the reaction temperature had to be raised to 280 ^{o}C. Despite a similar conversion and comparable CH_4 selectivity of approximately 45%, other product selectivities were not identical. For the 10%Co/TC-TNT catalyst more long chain hydrocarbons were produced while 10%Co/TNT produced very small amounts of long chain hydrocarbons with ≈50% of other products being short chain hydrocarbons (C_2-C_4). The other advantage associated with this catalyst is that it did not produce any CO_2 at this conversion level; due to the WGS reaction.

It can be inferred that 10%Co/TC-TNT was a better catalyst than 10%Co/TNT since it was able to achieve similar CO conversion at a lower temperature, produced more long chain hydrocarbons and there was no evidence of a WGS side reaction. All of these points imply that the TC-TNT support was a better support to use for FTS that TNT.

Table 4.15 Comparison of product selectivity data for Co/TNT and Co/TC-TNT at *iso*-conversion

Catalysts (Temp./^{o}C)	**10%Co/TNT (280)**	**10%Co/TC-TNT (250)**
CO conv./%	17.7	17.9
α1	0.30	0.62
α2	-	≈1.0
C_1	45.8	43.6
C_2 - C_4	49.9	20.0
C_5 - C_{11}	4.4	24.0
C_{12+}	≈0.0	13.0
C_2 olefin/%	3.8	4.7
CO_2/%	2.5	0.0

Finally, a comparison of the activity and product selectivity that were achieved by utilizing TN and TC-TNT cobalt based catalysts was performed. Table 4.16 illustrates the product selectivity data obtained by cobalt based TN and TC-TNT catalysts at near *iso*-CO conversions in the FT reactions performed at the same temperature (i.e. 280 ^{o}C). It is apparent that for these supports to achieve similar conversions (≈40%); higher cobalt loading (i.e. 20%) on TC-TNT was needed relative to the TN support (10% of cobalt loading). Since

for both catalysts the FT reactions were performed at high temperature it is evident that high CH_4 and CO_2 (by WGS reaction) yields were produced. CH_4 selectivities of 10%Co/TN and 20%Co/TC-TNT were identical and were approximately 50% while CO_2 selectivities produced were 2.2 and 3.3% for 10%Co/TN and 20%Co/TC-TNT, respectively. For the 20%Co/TC-TNT catalyst a higher selectivity for long chain hydrocarbons and more C_2 olefins were obtained.

Table 4.16 Comparison of product selectivity data for Co/TN and Co/TC-TNT at *iso*-conversion

Catalysts (Temp./^{o}C)	**10%Co/TN (280)**	**20%Co/ TC-TNT (280)**
CO conv./%	40.7	46.1
α1	0.71	0.53
α2	0.83	0.94
C_1	50.2	48.8
C_2 - C_4	20.5	22.0
C_5 - C_{11}	22.6	18.3
C_{12+}	6.6	11.8
C_2 olefin %	3.3	4.3
CO_2/%	2.2	3.3

In conclusion, when product selectivity data was compared at *iso*-conversions so as to determine which support was the best to employ for FTS the following trend was observed:

TN > TC-TNT > TNT

This trend simply means that tinania nanomaterial (TN) support was to be preferred over a titanate nanotube (TNT) catalyst even though the latter has the higher surface area. Coating this TNT material with TiO_2 (to form TC-TNT) improved the FT activity, but the improved activity was still lower than that obtained when TN was used as a support. Hence this material/support was still not better than TN.

It is apparent that the objective of enhancing the surface area of titania support has been achieved by use of the TC-TNT support. However a number of issues still need to be addressed with this support:

i) the effect of potassium in the TC-TNT support and

ii) the enhanced coverage of the TC-TNT support by use of more $Ti(OR)_4$ in the sol-gel process used to cover the TNT.

These issues will need to be addressed in future studies.

4.4 References

1. J. Keränen, C. Guimon, E. Iiskola, A. Auroux, L. Niinistö, *Catal. Today*, **78**, 149 (2003)
2. K. Jung, O. Joo, S. Han, *Catal. Lett.*, **68**, 49 (2000)
3. S. Ho, J. M. Cruz, M. Houalla, D. Hercules, *J. Catal.*, **135**, 173 (1992)
4. D. J. Duvenhage, PhD Thesis, University of the Witwatersrand, Johannesburg (1992)
5. N. N. Madikizela, PhD Thesis, University of the Witwatersrand, Johannesburg (2002)
6. X-Y. Liu, N. J. Coville, *S. Afr. J. Chem*., **58**, 110 (2005)
7. L. M. Sikhwivhilu, PhD Thesis, University of the Witwatersrand, Johannesburg (2007)
8. L.-Q. Weng, S.-H Song, S. Hodgson, A. Baker, J. Yu, *J. Euro. Cer. Soc.*, **26**, 1405 (2006)
9. Q. Chen, G. H. Du, S. Zhang, L.-M. Peng, *Acta Cryst.*, **B58**, 587 (2002)
10. M. Qamar, C. R. Yoon, H. J. Oh, D. H. Kim, J. H. Jho, K. S. Lee, W. J. Lee, H. G. Lee, S. J. Kim, *Nanotech.*, **17**, 5922 (2006)
11. http://www.matweb.com/search/SpecificMaterialText.asp?bassnum=EJAMER23, 12 November 2007
12. B. A. Sexton, A. E. Hughes, T.W. Turney, *J. Catal.*, **97**, 390 (1986)
13. A. M. Hilmen, D. Schanke, A. Holman, *Catal. Lett.*, **38**, 143 (1996)
14. X.S. Li, W.Z. Li, Y. X. Chen, H. L. Wang, *Catal. Lett*., **32**, 31 (1995)
15. R. Riva, H. Miessner, R. Vitali, G. Del Piero, *Appl. Catal. A: General*, **196**, 111 (2000)
16. D. G. Castner, P. R. Watson, I. Y. Chan, *Phys. Chem.*, **94**, 819 (1990)
17. J. Lahtinen, G. A. Somorjai, *J. Mol. Catal. A: Chemical*, **130**, 255 (1998)
18. W.-P. Ma, Y.-J. Ding, L.-W. Lin, *Ind. Eng. Chem. Res.*, **43**, 2391 (2004)
19. C. R. Reuel, C. H. Bartholomew, *J. Catal.*, **85**, 63 (1983)
20. T. Riedel, G. Schaub, *Top. Catal.*, **26**, 145 (2003)
21. G. Jacobs, T. K. Das, Y. Zhang, J. Li, G. Racoillet, B. H. Davis, *Appl. Catal. A: General*, **233**, 263 (2002)
22. M. E. Dry, *Catal. Today*, **71**, 227 (2002)
23. A. Y. Khodakov, W. Chu, P. Fongarland, *Chem. Rev.*, **107**, 1692 (2007)

24. M. J. Keyser, R.C. Everson, R. L. Espinoza, *Appl. Catal. A: General*, **171**, 9 (1998)

25. H. Schulz, M. Claeys, *Appl. Catal. A*, **186**, 71 (1999)

26. H. Schulz, M. Claeys, *Appl. Catal. A*, **186**, 91 (1999)

27. E. Iglesia, *Appl. Catal. A*, **161**, 59 (1997)

Chapter 5

5. Conclusions and Recommendations

The major target of this study was to prepare a novel tubular high surface area support without any acid treatment. This was successfully achieved by treating TiO_2 with a high concentration (≈18 M) of KOH. Characterization of this material showed that a tubular potassium titanate (TNT) material with a surface area of 231 m^2/g was produced. This was achieved by prolonged washing of the material with water. This surface area was about five times higher than that of the TiO_2 starting material (47 m^2/g).

This material was then used as a cobalt support. Different cobalt loadings (10 and 20%) were impregnated on to this support using a pH controlled precipitation methodology. These catalysts were employed in Fischer-Tropsch synthesis. Different operating conditions were used in the reaction. Regardless of the large surface area, this material did not portray good FT results.

Since this material contained a high concentration of potassium ions (from KOH) it was believed that the presence of potassium on the surface poisoned the cobalt active sites, leading to the poor FT activity. During the time of printing of this dissertation the XPS results were still not available to confirm this claim. Even though the XPS results were not yet available it was decided to coat this tubular material with sol-gel derived TiO_2 so as to create a "protective" TiO_2 layer over the potassium without significantly changing the morphology and the surface area. By coating this material a new material was created and this was named titania coated potassium titanate (TC-TNT). This material was then used as a support and was impregnated with cobalt at different loadings (10 and 20%).

These catalysts were used in the Fischer-Tropsch synthesis. Similar characterization procedures and Fischer-Tropsch reactions as performed on TNT based catalysts were made on this material. The Fischer-Tropsch activity improved when this material was employed.

After cobalt addition the Fischer-Tropsch activity and product selectivity obtained by the coated and the uncoated tubular potassium titanate materials was compared with that obtained when the commercial TiO_2 (referred to as TN) support. It was expected that high surface area supports would give high metal dispersion and hence better FT activity. It was discovered that despite the high surface area these materials possessed a lower FT activity than that obtained when the low surface area material (TN) was used as a support. The reasons for these low activities were explained from information obtained from different characterization techniques. It was discovered from TPR that the reducibility of cobalt loaded TNT was more difficult than when cobalt was loaded on TN since the reduction peaks occurred at higher temperatures. The poor activity may also have been caused by the presence of potassium ions leading to surface poisoning of the cobalt active sites. When the TNT support was coated with TiO_2 so as to create a protective layer around high concentration of potassium from TNT to form TC-TNT it was realized from TPR profiles that the reducibility behavior of the cobalt had improved. However the FT activity was still low. The reason for the lower FT activity was believed to be due to new SMSI between cobalt and the support (TC-TNT) which made the cobalt more difficult to reduce.

The following recommendations will be necessary for future studies:

- It will be necessary that the reducibility of Co/TNT be studied in detail and the effect of higher reduction temperatures (i.e. 350-400 ^{o}C) on FTS be undertaken since chemisorption studies showed a poor reduction for cobalt loaded on TNT.

- XPS studies will be necessary to give a better understanding on the role of potassium on the surface chemistry of the cobalt.

- The effect of an increase in the titanium alkoxide to TNT ratio during the sol-gel TiO_2 coating of TNT so as to form TC-TNT will provide both catalysts.

- The strong metal support interactions that occur between cobalt and TCNT and their role in the low catalytic activity.

- The role of potassium addition on TN sample and its behavior on FTS when the same mass % or the same potassium is added on TN.